Superradiant lasing, optical forces and collective interaction in active optical atomic clocks

Dissertation

zur Erlangung des akademischen Grades

Doctor of Philosophy

eingereicht an der

Fakultät für Mathematik, Informatik und Physik

der Leopold-Franzens-Universität Innsbruck

von

Anna Bychek M.Sc.

Betreuer: Univ.-Prof. Dr. Helmut Ritsch
Institut für Theoretische Physik

Innsbruck, September 2024

Abstract

Most atomic clocks existing up to date are passive clocks, where a frequency generated by some local oscillator is compared with a reference frequency provided by a narrow clock transition in atoms or ions. After interrogation, a new sample of atoms has to be prepared, which results in the dead time when the laser must be stabilized by locking it to a mode of a high finesse ultrastable reference cavity. Such clocks have demonstrated an excellent level of accuracy and stability. However, on short timescales this stability remains limited by environmental and thermal fluctuations impacting the reference cavity length. Here active optical atomic clocks can be an opportunity to overcome this limitation. Superradiant lasers based on collective superradiant emission of coherent light emitted by atoms placed inside an optical cavity are a viable option providing an intrinsically precise and accurate frequency reference. At the moment the experimental realization of continuous superradiant lasing on optical clock transitions still remains challenging as it requires continuous loading, cooling, and pumping of atoms within an optical cavity.

As efforts for the experimental realization of continuous superradiant lasing are growing, this thesis focuses on theoretical studies investigating realistic models and new ideas for superradiant narrowband lasing closely related to experimental configurations. In the first part of this work, we investigate a superradiant laser model where, unlike many identical atoms, the focus is on inhomogeneity among the ensemble of atoms. The inhomogeneity is primarily associated with a distribution of the atomic resonance frequencies leading to stimulated emission into the cavity at a range of different frequencies. These processes are an inherent part of any laboratory experiment and capable of disrupting the collective interaction between the atoms and the cavity field. We show the conditions required to reach the buildup of collective atomic coherence as well as scaling and limitations for the achievable laser linewidth. Here, we developed an extensive numerical model of clusters with different atomic parameters using a cumulant expansion method, which allows us to simulate realistic systems with a large number of atoms beyond the mean-field approach. To this end, we investigate the ultimate stability of such active clocks, both under homogeneous and inhomogeneous broadening effects present in a large atomic ensemble.

A challenging part of building a superradiant laser is to find a mechanism, that achieves population inversion. The primary obstacle is the destructive nature of superradiant lasing to a cold atomic ensemble, where one needs to have an efficient procedure of incoherent pumping in the system or a continuous supply of excited atoms. We propose a new scenario for creating an intrinsic light force generated inversion by studying optical light forces acting on the atoms due to interaction with laser light. Inspired by maser models, where ground and excited state atoms are separated in space by means of the magnetic field, we investigate the ways to manipulate the atoms with zero magnetic moment by optical forces. Finally, we extend the developed framework to study self-organization, cooling and lasing in an ensemble of clock atoms. This allows us to investigate the conditions for the laser-like emission in the vicinity of the self-organization threshold.

Zusammenfassung

Die meisten der bisher existierenden Atomuhren sind passive Uhren, in welchen eine Frequenz, generiert durch einen lokalen Oszillator, verglichen wird mit einer Referenzfrequenz eines schmalbandigen Überganges in Atomen oder Ionen. Nach einem Experiment muss ein neues Ensemble von Atomen prepariert werden, was in eine Wartezeit resultiert, da der Laser stabilisiert werden muss durch Eichung auf eine hochstabile optische Resonatormode. Diese Uhren weißen eine herausragende Präzision und Stabilität auf. Dennoch, auf kurzen Zeitskalen bleibt diese Stabilität begrenzt durch umweltbedingte und thermische Fluktuationen, welche wiederum die Dimensionen der optischen Resonators beeinflusst, der als Referenz dient. Hierbei bieten aktive optische Atomuhren eine Möglichkeit, diese Limitationen zu überwinden. Sogenannte superradiante Laser, basierend auf kollektiver superradianter Emission von kohärentem Licht, emittiert von Atomen welche sich innerhalb eines optischen Resonators befinden, bieten eine Möglichkeit, als präzise und akurate Frequenzstandards. Derzeit bleibt die experimentelle Realisierung von kontinuierlichen superradianten Lasern auf einer optischen Frequenz eine Herausforderung, da es eine kontinuierliche Beladung, Kühlung und Anregung von Atomen in einem optischen Resonator erfordert.

Da die Bemühungen zur experimentellen Realisierung von kontinuierlichen superradianten Lasern zunehmen, konzentriert sich diese Arbeit auf theoretische Studien, die realistische Modelle und neue Ideen für superradianten, schmalbandigen Lasern untersuchen, die eng mit Experimenten verbunden sind. Im ersten Teil dieser Arbeit untersuchen wir ein superradiantes Lasermodell, bei dem im Gegensatz zu vielen identischen Atomen der Schwerpunkt auf der Inhomogenität innerhalb des atomaren Ensembles liegt. Die Inhomogenität ist hauptsächlich mit einer Verteilung der atomaren Resonanzfrequenzen verbunden, was zu stimulierter Emission in den Resonator bei verschiedenen Frequenzen führt. Diese Prozesse sind ein fester Bestandteil jedes Laborexperimentes und können die kollektive Wechselwirkung zwischen den Atomen und dem Hohlraumfeld stören. Wir zeigen die Bedingungen, die erforderlich sind, um den Aufbau kollektiver atomarer Kohärenz zu erreichen, sowie die Skalierung

und Einschränkungen für die erreichbare Laserlinienbreite. Hier haben wir mithilfe einer Kumulantenentwicklung ein umfangreiches numerisches Modell von Clustern mit unterschiedlichen Atomparametern entwickelt, das es uns ermöglicht, realistische Systeme mit einer großen Anzahl von Atomen über den sogenannten Mean-Field Ansatz hinaus zu simulieren. Zu diesem Zweck untersuchen wir die ultimative Stabilität solcher aktiven Atomuhren, sowohl unter homogenen als auch inhomogenen Verbreiterungseffekten, die in einem großen Atomensemble vorhanden sind.

Ein herausfordernder Teil bei der Entwicklung eines superradianten Lasers ist ein Mechanismus zur Erzielung einer Besetzungsinversion. Das Haupthindernis ist die destruktive Natur der superradianten Emission auf ein gekühltes atomares Ensemble, wo ein effizienter Mechanismus des inkohärenten Pumpens im System oder eine kontinuierliche Versorgung mit angeregten Atomen erforderlich ist. Wir schlagen ein neues Szenario zur Erzeugung einer intrinsischen, durch Lichtkraft erzeugten Inversion vor, indem wir optische Lichtkräfte untersuchen, die aufgrund der Wechselwirkung mit Laserlicht auf die Atome wirken. Inspiriert von Maser-Modellen, bei denen Atome im Grund- und angeregten Zustand durch das Magnetfeld im Raum getrennt werden, untersuchen wir die Möglichkeiten, die Atome mit null magnetischem Moment durch optische Kräfte zu manipulieren. Schließlich erweitern wir das entwickelte Framework, um Selbstorganisation, Kühlung und Laserwirkung in einem Ensemble von Atomen zu untersuchen. Dies ermöglicht es uns, die Bedingungen für die laserartige Emission in der Nähe der Selbstorganisationsschwelle zu untersuchen.

Acknowledgements

I would like to take this opportunity to sincerely thank all those people who have accompanied and supported me during the years dedicated to this work.

First of all I would like to thank my supervisor Helmut Ritsch for giving me the opportunity to work in his group, his incredible enthusiasm and passion for physics, open mindset, pleasant and healthy environment in the group.

I would also like to thank all the collaborators of the past years, Swadheen Dubey, Christoph Hotter, Georgy Kazakov, Laurin Ostermann, David Plankensteiner, and all the group members, Elvia Colella, Martin Fasser, Karol Gietka, Raphael Holzinger, Daniela Holzmann, Nicole Jorda, Arkadiusz Kosior, Natalia Masalaeva, Farokh Mivehvar, Mariona Moreno-Cardoner, Arpita Pal, Verena Scheil and Matthias Sonnleitner for their companionship throughout my PhD. A big thanks to all the ESRs and members of the MoSaiQC European Innovative Training Network with whom I learned a lot about clock experiments during the consortium meetings and conferences.

During the first two years of my PhD, I had the pleasure of doing my secondments at the University of Amsterdam and the TU Wien Atominstitut. I would like to thank Florian Schreck, Georgy Kazakov and all the group members for sharing their knowledge and making me feel welcomed in a new environment. I am also very greatful to my colleagues from Krasnoyarsk, D.N. Maksimov, I.V. Timofeev, and my undergraduate research supervisor A.R. Kolovsky for the knowledge they shared with me that helped me a lot throughout my research.

A special thanks to my mother, Svetlana, for always supporting me and letting me follow my path, and to my husband, Raphael, for believing in me and standing by my side through all these years. Finally, I would like to thank my friends and family for all the support.

Contents

1 Introduction

The properties of an atom are not only determined by its internal structure but also by its interaction with the surrounding environment. The quantized energy levels of an atom introduced by Bohr in 1913 are the central idea in quantum physics [1]. Later in 1916, Einstein described the fundamental interaction processes between light and matter in his work on emission and absorption of radiation in quantum theory [2, 3]. However, the interaction of particles with photons was still not sufficiently understood. The formulation of quantum mechanics in its relatively modern form in 1925-1928 by de Broglie, Dirac, Schrödinger, Heisenberg, Pauli and others [4–9], together with the later works of Schwinger, Feynman, Tomonaga and Dyson [10], who solved the electron self-energy problem by the late 1940's, have led to the success of quantum electrodynamics and quantum optics in describing light-matter interactions.

1.1 Cavity quantum electrodynamics

Many atoms placed close to one another start to interact strongly with each other and exhibit collective behavior. However, coupling light to atoms in free space such that it couples equally to all of them can be challenging.

One way to strongly modify the interaction of an atom or a quantum emitter with the electromagnetic field is to place it between highly reflecting mirrors of a cavity. This allows the light in the cavity to bounce back and forth many times before escaping through the cavity mirrors, therefore greatly increasing the coherent coupling between light and matter. This field of research, known as cavity quantum electrodynamics (cavity QED) has rapidly developed in the past decades and has become one of the most important areas of research in modern quantum optics. Today, cavity QED is studied in a wide variety of contexts including the demonstration of fundamental effects in light-matter interaction processes [11], cavity-assisted cooling [12–14], self-organization [15–17], collective effects with light-induced interactions [18, 19], single-photon light sources [20], micromasers [21], superradiant lasing [22, 23] and many more. These effects are investigated among different types of quantum emitters, such as cold atoms, ions, molecules, nitrogen-vacancy centers in diamonds, quantum dots and other systems with discrete energy levels, which exhibit a nonvanishing dipole coupling to the electromagnetic field.

1.2 Atomic clocks

Throughout the years our definition of the best clocks for measuring time has vastly changed, see Fig. 1.1. From a simplest shadow or sundial clock to complex atomic clocks, time and frequency became the most precise physical quantities available to us to explore the laws of nature. Applications of accurate and transportable atomic clocks vary from navigation and geopositioning to low-frequency gravitational wave detectors and tests of general relativity [24–26], as well as radio telescope synchronization for astronomical research [27], search for dark matter [28] and variations in fundamental

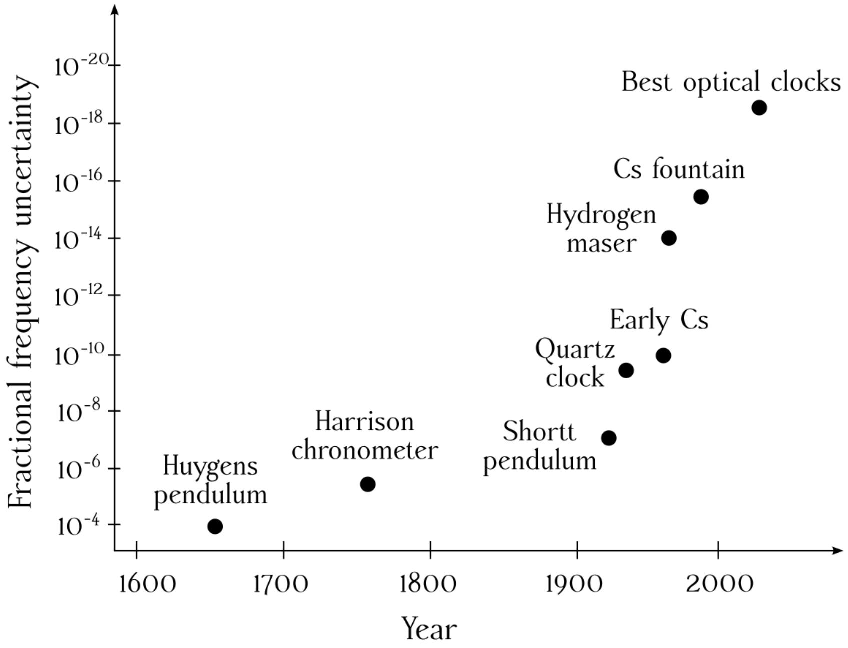

Figure 1.1: Evolution of time and frequency standards: relative uncertainty of different clocks over the years.

constants [26,29]. Further applications can be found in geodesy, monitoring of volcanic activity and underground exploration of natural resources without drilling [30,31].

A clock needs a stable and accurate oscillator to calculate time by counting the number of oscillations in a given time interval. The oscillator provides a signal of the period T (or frequency $\nu_0 = 1/T$) and can be characterized by its fractional uncertainty $\Delta\nu/\nu_0 = 1/Q$, where Q is the oscillator's quality factor given by the ratio of the oscillation frequency ν_0 to its uncertainty $\Delta\nu$. In atomic clocks, the oscillation frequency is given by the frequency of a particular atomic transition $\hbar\omega_0 = E_e - E_g$, where E_g and E_e denote the ground and excited energies of the clock transition. Therefore, working with atomic clocks operating at optical frequencies, which is five orders of magnitude higher than those of microwave clocks led to much higher precision in measuring time. At the same time, atomic clocks have enabled the development of universal frequency standards based on atoms or ions, where the identical isotopes placed in the same environment feature the same internal structure and behavior, which holds everywhere in the world unless influenced by external perturbations.

The choice of an atomic clock transition for ultra-stable clocks requires having a narrow linewidth transition in the optical domain preferably insensitive to external perturbations. Typically these are long-lived metastable excited states, where the transition to the ground state is forbidden in the electric dipole approximation and only higher-order multipole transitions are allowed. It is expected that in the foreseeable future the definition of a second by the International System of Units (SI) will be redefined by an optical transition in atoms or ions, replacing the existing definition based on a microwave transition in Cs atoms [32]. Furthermore, atomic clocks can be characterized as active or passive frequency standards, and by their frequency stability and accuracy [33].

1.2.1 Frequency stability and accuracy

Today's best atomic clocks reach an unprecedented level of accuracy and stability, as shown in Fig. 1.1. Progress in theoretical and experimental science opened a way to operate with higher frequencies, thus increasing clock precision. Mechanical clocks with the resonant frequency (ν_0) of the order of 1 Hz were followed by quartz clocks ($10^3 \lesssim \nu_0 \lesssim 10^7$ Hz), microwave atomic clocks ($10^8 \lesssim \nu_0 \lesssim 10^{10}$ Hz) and optical atomic clocks ($\nu_0 \lesssim 10^{15}$ Hz).

The figures of merit to characterize the performance of a clock or a frequency standard are its stability and accuracy. In Fig. 1.2 one can see the examples of a frequency measurement that is: (a) accurate and stable, (b) accurate but not stable, (c) stable but not accurate, (d) both not accurate and unstable. A frequency source that gives an accurate and stable measurement outcome (Fig. 1.2(a)) can be used as a frequency standard. However, most of the time such a precise clock can not be completely isolated from different systematic effects coming from the environment. These systematic shifts would result in a frequency shift presented in Fig. 1.2(c). If this shift is carefully calculated and calibrated accordingly, this in turn can also be used as a frequency standard.

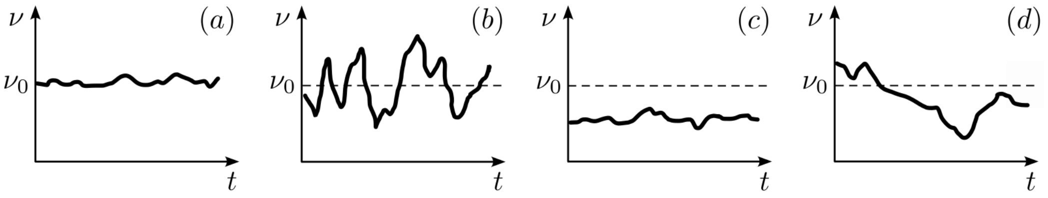

Figure 1.2: Examples of frequency measurements representing: (a) accurate and stable; (b) accurate but not stable; (c) stable but not accurate; (d) not accurate and unstable output.

1.2.2 Passive clocks

Passive optical atomic clocks are the most precise scientific instruments available to humanity, reaching an unprecedented level in measuring time and frequency. A schematic representation of a passive clock based on neutral atoms, where the frequency generated by a laser is regularly compared with the frequency of a narrow clock transition, is shown in Fig. 1.3(a). The clock consists of three key components: a reference oscillator, a local oscillator and a frequency counter. The role of the reference oscillator plays an atomic medium with a narrow clock transition, where atoms are contained in the ultra-high vacuum chamber and isolated from the environment. Typically neutral atoms are cooled down to ultracold temperatures and trapped in a magic wavelength optical lattice, which ensures no Doppler broadening and zero light shifts on the clock transition [34]. The local oscillator is a laser, which is locked with the Pound-Drever-Hall method [35] to the resonance frequency of an ultra-low expansion (ULE) cavity. The output signal from the local oscillator can be tuned by

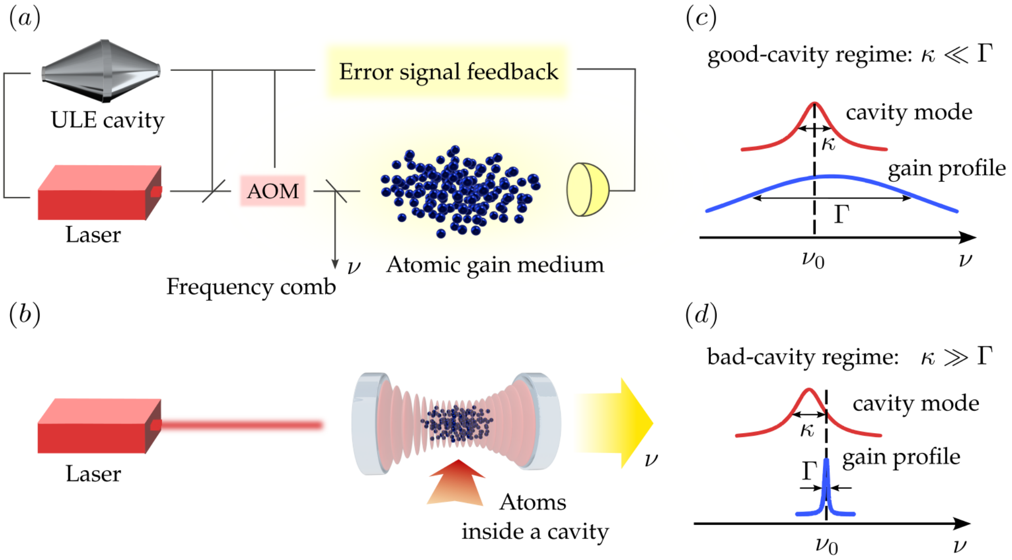

Figure 1.3: Optical atomic clocks: passive vs active. (a) Schematic representation of a passive clock operating in a good-cavity regime (c) on a clock transition in neutral atoms. (b) Schematics of an active clock based on collective superradiant emission of coherent light by atoms inside an optical cavity operating in a bad-cavity regime (d).

an acousto-optic modulator (AOM) before it interrogates the atomic medium. After interrogation a new sample of atoms has to be prepared, which results in the dead time when the short-term stability of the clock is limited by the stability of the ULE cavity. The signal from the probed transition is sent to a feedback loop, which generates an error signal back to the laser to tune its frequency with respect to the atomic transition frequency. Finally, the light is sent to a frequency counter, where a very fast oscillating optical frequency is converted into a measurable electronic signal by means of a frequency comb [36].

Such clocks have demonstrated excellent frequency stability of the order of 10^{-19} after one hour of averaging [37]. In other words, this means that in the lifetime of our Universe such a clock would be off by less than a second. However, on short timescales this stability remains limited by environmental and thermal fluctuations of the cavity mirrors [22, 38]. Here, active optical atomic clocks can be an opportunity to overcome this limitation and become a robust and transportable alternative. This would be especially beneficial to the measurement precision of clocks operating on moving vehicles, such as satellites and boats.

1.2.3 Active superradiant clocks

The best atomic clocks up to date are passive clocks. However, the development of active clocks can provide a valuable alternative to its passive counterparts. In this case, such an active clock alone continuously generates highly stable narrow-linewidth laser radiation, using an ensemble of excited atoms that emit light directly at a frequency of an atomic clock transition. In the microwave domain, such an active clock has existed for many decades in a hydrogen maser setup [39], where population inversion is created by coherent pumping of atoms followed by magneto-mechanical separation of ground- and excited-state atoms in the mode volume. Unfortunately, this solution is not possible at optical frequencies, because the magnetic gradients for a sufficient state separation are very difficult to achieve as the length scales are several orders of magnitude smaller in this case. At the moment, many interesting methods for generating a continuous gain from the clock atoms are being explored with the goal of developing active optical clocks, also known as superradiant clocks [40–45].

A superradiant clock is based on the phenomenon of collective superradiant emission of light by atoms inside an optical cavity [22, 46]. In the superradiant regime, the atoms constructively synchronize their photon emission in the cavity and produce a highly coherent and stable output light at the frequency of the atomic clock transition. A superradiant clock is schematically illustrated in Fig. 1.3(b). The atomic medium is confined inside a single-mode optical cavity with resonance frequency ω_c. Each atom has a ground and an excited state associated with the clock transition with frequency ω_a. The system dynamics is governed by the atom-cavity coupling strength (g), atomic spontaneous emission rate (Γ), and cavity losses (κ). Additionally, the atoms are externally driven by a pumping mechanism (red arrow) to provide the population inversion in the atomic medium and support the continuous gain to the cavity mode.

The implementation of the superradiant clock is predicted to provide far better short-term stability and robustness to thermal and mechanical fluctuations compared to modern-day passive optical clocks [40]. Theoretical studies show that superradiant lasing on optical clock transitions can as well give an intrinsically precise and accurate frequency reference [22,23,40]. The superradiant clock typically operates in the limit of low photon number operation or the so-called bad-cavity regime shown in Fig. 1.3(d), where the coherence necessary for frequency stability is stored in the atoms rather than the cavity field, making it robust to cavity fluctuations.

In view of establishing a new outstanding and robust optical time and frequency standard, the quest to build a continuous clock operating on a very narrow atomic transition has been the subject of intense theoretical and experimental studies in the past decade. In recent years, pulsed superradiance has been experimentally demonstrated [40,47,48]. However, despite significant recent progress, the experimental realization of a continuously operating superradiant clock still remains a challenging task and requires continuous loading, cooling and pumping of atoms. As efforts for the experimental realization of continuous superradiant lasing are growing, this thesis constitutes a theoretical study of such superradiant clocks, which focuses on developing and investigating realistic models and new ideas for continuous superradiance closely related to experimental configurations.

1.3 Outline of the Thesis

The content of the Thesis focuses on three distinct parts. Part I provides an introduction into the fundamental aspects of light-matter interactions in the absence and presence of an optical cavity. Part II dives into cavity-mediated collective interactions in a large atomic ensemble to investigate continuous superradiant lasing under realistic conditions. Lastly, part III investigates optical light forces and the emergence of self-ordering, cooling and lasing of atoms in the superradiant regime. These parts are complemented by an introductory chapter that reviews several theoretical concepts, useful to understand the main body of the Thesis. Readers familiar with these topics can skip the introduction and directly select an individual chapter for reading. Below is a compact summary of each chapter,

- Chapter 2 introduces basic concepts of light-matter interactions and cavity electrodynamics. First, we introduce a two-level quantum system interacting with an electromagnetic field, in particular a mode of an optical cavity, leading to the well-known Jaynes-Cummings model. We proceed by describing dissipative open quantum systems and derive the Master equation for many quantum emitters coupled individually to a Markovian reservoir.
- Chapter 3 presents how superradiance emerges when two-level emitters are positioned at small distances in free space in the absence of an optical cavity. We then proceed by including a single-mode optical cavity and provide a basic understanding of the superradiant laser and the bad-cavity regime. This is

supplemented by showing the methods used to calculate the dynamics and light spectrum of the system.

- Chapter 4 investigates collective superradiant emission of light in the inhomogeneously broadened ensemble of two-level emitters in a cavity. Here the inhomogeneity is in the atomic resonance frequencies and the dynamics is calculated using a second-order cumulant expansion, which is described in Chapter 3. We show that for sufficiently large atom numbers under strong continuous incoherent pumping, superradiant lasing can emerge and the laser linewidth can be orders of magnitude smaller than the cavity linewidth while being more resilient to cavity frequency noise.
- In Chapter 5 we explore the ultimate limit for the frequency stability in an active optical atomic clock as opposed to a passive clock. We investigate the spectral properties and the stability of such active clocks, both under homogeneous and inhomogeneous broadening effects for the atomic transition frequencies. We find that for short averaging times, the stability is limited by photon shot noise from the limited emitted laser power and at long averaging times by phase diffusion of the laser output. Lastly, we identify operational parameters for best long-term stability utilizing ^{87}Sr (Strontium) atoms as the active gain medium.
- Chapter 6 studies a continuous population inversion mechanism for superradiant lasing. At the moment of writing, it remains an open challenge as it requires continuous loading, cooling, and pumping of active atoms within an optical resonator. In this chapter, we propose a new scheme for creating continuous gain by using optical forces acting on the states of a two-level atom via bichromatic coherent pumping of a cold atomic gas trapped inside a single-mode cavity. To tackle the numerical treatment, we describe the atomic motion in a semi-classical approximation with position-dependent light shifts which induce optical gradient forces along the cavity axis. Finally, we identify a parameter regime of a continuous narrow-band laser operation close to the bare atomic frequency, which is insensitive to cavity noise as well.
- In Chapter 7 we look into spatial self-organization in a coherently driven ensemble of clock atoms inside an optical cavity and coherent light emission from the cavity. We focus on the spectral properties of the emitted light in the narrow atomic linewidth regime and identify a self-organization regime where atoms align themselves in a checkerboard pattern thus maximizing light scattering

into the cavity which simultaneously induces cooling. We calculate the spectra of the cavity light field and investigate the conditions for the laser-like emission near the self-organization threshold.

Lastly, we summarize the main conclusions of this Thesis and give an outlook for future research directions and open questions in the context of superradiant clocks.

2 Fundamental aspects of light-matter interactions

This chapter aims to provide a compact overview of the most important theoretical foundations and concepts that are used in the main part of the Thesis.

2.1 Two-level atom interacting with a classical field

Let us consider the interaction of an atom with a classical field, provided that the field is monochromatic with the angular frequency $\omega = c|\mathbf{k}|$ and the field amplitude E_0,

$$\mathbf{E}(\mathbf{r}, t) = E_0 \cos(\omega t) f_{\mathbf{k}}(\mathbf{r}) \mathbf{e}_{\mathbf{k}} = \frac{E_0}{2}(e^{-i\omega t} + e^{i\omega t}) f_{\mathbf{k}}(\mathbf{r}) \mathbf{e}_{\mathbf{k}}, \tag{2.1}$$

where $f_{\mathbf{k}}(\mathbf{r})$ is the spatial function of the field and $\mathbf{e}_{\mathbf{k}}$ is the unit length polarization vector. Later we use the dipole approximation and neglect the spatial variation of the electromagnetic field over an atom, which is valid when the wavelength of the field is much longer than the size of the atom. In our case, this is a good approximation, since the optical wavelengths are of the order of hundreds of nm, while the atomic size is of the order of angstrom.

Throughout the manuscript we will treat the atom as a two-level atom whose relevant internal degrees of freedom constitute a dipolar, two-level transition with the ground and excited states $|g\rangle$ and $|e\rangle$, respectively, separated by the transition energy $\hbar\omega_a$. Here, we do not take into account the atomic motion, which will be discussed in the next section. Thus, the free energy Hamiltonian of the two-level atom reads

$$H_A = \hbar\omega_a |e\rangle\langle e| \tag{2.2}$$

and the atom-field interaction Hamiltonian in the dipole approximation is given by

$$H_{AF} = -\mathbf{d} \cdot \mathbf{E}. \tag{2.3}$$

Here, $\mathbf{d}$ is the atomic dipole operator written in terms of the distance operator $\mathbf{r_e}$ between the electron and the nucleus as

$$\mathbf{d} = -e\mathbf{r_e}, \tag{2.4}$$

or in terms of the atomic operators

$$\mathbf{d} = \langle g|\mathbf{d}|e\rangle(\sigma^+ + \sigma^-), \tag{2.5}$$

where $\sigma^+ = |e\rangle\langle g|$ and $\sigma^- = |g\rangle\langle e|$ is the atomic raising and lowering and operators, respectively, and $\langle g|\mathbf{d}|e\rangle := \mathbf{d}_{eg}$ is the dipole matrix element associated with the electronic transition, which can be chosen to be real.

2.2 Interaction of an atom with a quantized field

In order to describe the interaction of a two-level atom with light in a full quantum picture we make use of the quantized electromagnetic field operator derived from Maxwell's equations [49] and written in the second quantization formalism via the bosonic creation and annihilation operators $a^\dagger_{\mathbf{k},\lambda}$ and $a_{\mathbf{k},\lambda}$, where the sum runs over all possible wave vectors $\mathbf{k}$ and two orthogonal polarizations $\lambda = 1, 2$ of the field modes,

$$\mathbf{E}(\mathbf{r}, t) = \sum_{\mathbf{k},\lambda} \mathbf{e}_{\mathbf{k},\lambda} E_k \Big(f_{\mathbf{k},\lambda}(\mathbf{r}) a_{\mathbf{k},\lambda}(t) + f^*_{\mathbf{k},\lambda}(\mathbf{r}) a^\dagger_{\mathbf{k},\lambda}(t) \Big). \tag{2.6}$$

The electromagnetic field is quantized by introducing the quantization volume V and imposing periodic boundary conditions, which determine the field amplitude for each mode $E_k = \sqrt{\hbar\omega_k/(2\epsilon_0 V)}$ with the frequency $\omega_k = c|\mathbf{k}|$, and the normalized spatial mode function $f_{\mathbf{k},\lambda}(\mathbf{r})$, where $\mathbf{e}_{\mathbf{k},\lambda}$ is the unit length polarization vector of the field.

Here, the different states of the each field mode can be treated as the states of a quantum harmonic oscillator and represented in a Fock space, where the Fock state $|n\rangle$ with $n \in \mathbb{N}$ describes a field with n photons in a particular field mode given by its wave vector and polarization. In the second quantization picture, the field annihilation and creation operators are defined as

$$\begin{aligned} a_{\mathbf{k},\lambda}|n\rangle &= \sqrt{n}|n-1\rangle \\ a^{\dagger}_{\mathbf{k},\lambda}|n\rangle &= \sqrt{n+1}|n+1\rangle, \end{aligned} \tag{2.7}$$

which obey the bosonic commutation relation

$$[a_{\mathbf{k},\lambda}, a^{\dagger}_{\mathbf{k}',\lambda'}] = \delta_{\mathbf{k},\mathbf{k}'}\delta_{\lambda,\lambda'}\mathbb{1}. \tag{2.8}$$

Thus, the Hamiltonian describing the combined system of a two-level atom and the free radiation field can be written as

$$H = H_A + H_F + H_{AF}, \tag{2.9}$$

where

$$H_A = \hbar\omega_a \sigma^+\sigma^- \text{ and } H_F = \sum_{\mathbf{k},\lambda} \hbar\omega_k a^{\dagger}_{\mathbf{k},\lambda} a_{\mathbf{k},\lambda}. \tag{2.10}$$

This does not include the energy of the vacuum field $\hbar\omega_k/2$, since the constant terms in the Hamiltonian only lead to the energy shift and do not contribute to the dynamics of the system. The dipole form of the atom-field interaction Hamiltonian in Eq. (2.3) with the quantized electric field can be expressed as

$$H_{AF} = \sum_{\mathbf{k},\lambda} \hbar g_{\mathbf{k},\lambda}(\sigma^+ + \sigma^-)(f_{\mathbf{k},\lambda}(\mathbf{r})a_{\mathbf{k},\lambda} + f^*_{\mathbf{k},\lambda}(\mathbf{r})a^{\dagger}_{\mathbf{k},\lambda}), \tag{2.11}$$

where the strength of the dipole coupling is given by

$$g_{\mathbf{k},\lambda} = \sqrt{\frac{\omega_k}{2\hbar\epsilon_0 V}}\mathbf{e}_{\mathbf{k},\lambda} \cdot \mathbf{d}_{eg}. \tag{2.12}$$

The spatial mode function $f(\mathbf{r})$ is determined by the boundary conditions. In free space, the mode function is a running plane wave $f(\mathbf{r}) = e^{i\mathbf{kr}}$. However, inside a cavity the electric field needs to vanish at the surface of the cavity mirrors. In the case of a linear cavity, these boundary conditions lead to standing waves along the cavity axis $f(\mathbf{r}) = \cos(\mathbf{kr})$, where only an integer number n of the half-wavelengths of the field fit within a distance L between the mirrors of a high-finesse cavity, such that $k = n\pi/L$.

2.3 Jaynes-Cummings model

Next, for the sake of simplicity we will consider an atom placed inside a single-mode optical cavity, such that the interaction Hamiltonian in Eq. (2.11) can be written as

$$H_{AF} = \hbar g \cos(kr)(\sigma^+ a + \sigma^- a^\dagger + \sigma^+ a^\dagger + \sigma^- a). \tag{2.13}$$

Let us simplify the atom-field interaction using the rotating wave approximation as follows. From the free energy Hamiltonian of the atom (ω_a) and the cavity mode (ω_c) described as $H = \hbar\omega_a \sigma^+\sigma^- + \hbar\omega_c a^\dagger a$ one can write down the following time dependence for the operators of the uncoupled system in the Heisenberg picture: $\sigma^-(t) = \sigma^-(0)e^{-i\omega_a t}$, $a(t) = a(0)e^{-i\omega_c t}$. Thus, the first two terms in Eq. (2.13) rotate at a slow frequency $\omega^- = \omega_a - \omega_c$, while the last two terms rotate at a very high frequency $\omega^+ = \omega_a + \omega_c$. The fast oscillation terms would quickly average to zero during the dynamics, therefore we can neglect these terms in the rotating wave approximation [49], which is valid when the condition $\omega_a + \omega_c \gg |\omega_a - \omega_c|$ is fulfilled. This leads us to the well-known Jaynes-Cummings model [50],

$$H_{JC} = \hbar\omega_a \sigma^+\sigma^- + \hbar\omega_c a^\dagger a + \hbar g(r)(\sigma^+ a + \sigma^- a^\dagger), \tag{2.14}$$

which Hamiltonian captures the interaction between a two-level atom and a quantized mode of an optical cavity.

2.4 Dissipative dynamics in open quantum systems

Spontaneous atomic decay and cavity losses play an important role in the dynamics of combined atom-cavity systems. Below we will introduce the master equation in the Lindblad form, which is generally used in open quantum systems to describe irreversible and non-unitary processes, from dissipation to decoherence and quantum measurement processes [51].

In this section, we will go through the derivation of the master equation in the Lindblad form largely based upon the more general description provided in Ref. [52]. The approach is to find the dynamics of the system by tracing out the degrees of freedom of the environment. In order to do this we assume that the Born-Markov approximation is valid, therefore the resulting master equation is often called the

Born-Markov master equation.

First, the full Hamiltonian of the system and the environment (called bath) is

$$H = H_S + H_B + H_{SB}, \tag{2.15}$$

where H_{SB} denotes the interaction term between the system and the bath. In the Schrödinger picture, the evolution of the total density matrix is given by

$$i\hbar \frac{d}{dt}\rho_T(t) = [H, \rho_T(t)]. \tag{2.16}$$

Next, we switch to the interaction picture with the density matrix $\tilde{\rho}_T = U_0^\dagger \rho_T U_0$, where $U_0 = e^{-i(H_S+H_B)t/\hbar}$ which is described by

$$i\hbar \frac{d}{dt}\tilde{\rho}_T(t) = [H_{SB}(t), \tilde{\rho}_T(t)], \tag{2.17}$$

with $H_{SB}(t) = U_0^\dagger H_{SB} U_0$. The solution of Eq. (2.17) can be formally written as

$$\tilde{\rho}_T(t) = \tilde{\rho}_T(0) + \frac{1}{i\hbar}\int_0^t dt_1 [H_{SB}(t_1), \tilde{\rho}_T(t_1)]. \tag{2.18}$$

Inserting this result once more and continuing the iteration process n times,

$$\tilde{\rho}_T(t) = \tilde{\rho}_T(0) + \sum_{n\geqslant 1} \frac{1}{(i\hbar)^n}\int_0^t dt_1 ... \int_0^{t_{n-1}} dt_n [H_{SB}(t_1), ..., [H_{SB}(t_n), \tilde{\rho}_T(0)]]. \tag{2.19}$$

We assume that the system-bath interaction is weak, therefore we stop the iteration process at the second order in H_{SB}, which is also called the Born approximation. Then, we take the partial trace over the bath degrees of freedom,

$$\begin{aligned}\tilde{\rho}(t) = \tilde{\rho}(0) + \frac{1}{i\hbar}\int_0^t dt_1 \, \mathrm{Tr_B}\left\{[H_{SB}(t_1), \tilde{\rho}_T(0)]\right\} + \\ + \frac{1}{(i\hbar)^2}\int_0^t \int_0^{t_1} dt_1 dt_2 \, \mathrm{Tr_B}\left\{[H_{SB}(t_1), [H_{SB}(t_2), \tilde{\rho}_T(0)]]\right\},\end{aligned} \tag{2.20}$$

where $\tilde{\rho}(t) = \mathrm{Tr_B}\left\{\tilde{\rho}_T(t)\right\}$.

Next, we consider that the initial state between the system and the bath is uncorrelated $\rho_T(0) = \rho(0) \otimes \rho_B(0)$. The bath is very large, therefore we approximate its dynamics as very slow compared to the system dynamics $\rho_B(t) \approx \rho_B(0) \equiv \rho_B$. Therefore, the first order term in Eq. (2.20) is zero, since $\mathrm{Tr_B}\left\{[H_{SB}(t_1), \rho_B(0)]\right\} = 0$.

Using the theorem about the derivative of an integral with a variable upper limit and assuming that the system and the bath degrees of freedom can be factorized at all times, the master equation can be written as

$$\frac{d}{dt}\tilde{\rho}(t) = \frac{1}{(i\hbar)^2}\int_0^t dt' \, \mathrm{Tr_B}\left\{[H_{SB}(t), [H_{SB}(t'), \tilde{\rho}(t) \otimes \rho_B]]\right\} \tag{2.21}$$

The final approximation to be made is known as the Markov approximation, where the reservoir is assumed to have a short memory, such that the two-point correlation function is significant only when $t \approx t'$ and the integration upper limit can be extended to infinity without changing its result. The resulting Born-Markov master equation reads

$$\frac{d}{dt}\tilde{\rho}(t) = \frac{1}{(i\hbar)^2}\int_0^\infty dt' \, \mathrm{Tr_B}\left\{[H_{SB}(t), [H_{SB}(t'), \tilde{\rho}(t) \otimes \rho_B]]\right\} \tag{2.22}$$

Let us consider that the interaction Hamiltonian has the following form

$$H_{SB} = \hbar\big(SB^\dagger + S^\dagger B\big), \tag{2.23}$$

where S is an operator which acts only on the system, and B is an operator acting only on the bath. Let us insert the interaction Hamiltonian $H_{SB}(t) = \hbar\big(S(t)B^\dagger(t) + S^\dagger(t)B(t)\big)$ into Eq. (2.22). After we expand the commutators and rearrange the terms using the cyclic property of a trace one can write,

$$\begin{aligned}
&\mathrm{Tr_B}\left\{[H_{SB}(t), [H_{SB}(t'), \tilde{\rho}(t)\rho_B]]\right\} = \\
&\qquad \hbar^2\left[S(t)S^\dagger(t')\tilde{\rho}(t) - S^\dagger(t')\tilde{\rho}(t)S(t)\right]\mathrm{Tr_B}\left\{B^\dagger(t)B(t')\rho_B\right\} \\
&\qquad +\hbar^2\left[\tilde{\rho}(t)S^\dagger(t')S(t) - S(t)\tilde{\rho}(t)S^\dagger(t')\right]\mathrm{Tr_B}\left\{B(t')B^\dagger(t)\rho_B\right\} \\
&\qquad +\hbar^2\left[S^\dagger(t)S(t')\tilde{\rho}(t) - S(t')\tilde{\rho}(t)S^\dagger(t)\right]\mathrm{Tr_B}\left\{B(t)B^\dagger(t')\rho_B\right\} \\
&\qquad +\hbar^2\left[\tilde{\rho}(t)S(t')S^\dagger(t) - S^\dagger(t)\tilde{\rho}(t)S(t')\right]\mathrm{Tr_B}\left\{B^\dagger(t')B(t)\rho_B\right\}.
\end{aligned} \tag{2.24}$$

In order to derive the final expression for the master equation, which we will often make use of throughout this work let us consider the interaction of a two-level atom S with a bath consisting of many modes $B = \sum_k g_k b_k$, where g_k characterizes the strength of the coupling between the system and bath modes. Using the Baker-Campbell-Hausdorff formula

$$e^A B e^{-A} = \sum_0^\infty \frac{1}{m!}[A, B]_m, \tag{2.25}$$

where $[A,B]_0 = B$, $[A,B]_1 = [A,B]$, $[A,B]_m = [A,[A,[A...,B]]]$, one can calculate the expressions for the system and bath operators in the interaction picture,

$$\begin{aligned} S(t) &= e^{iH_S t/\hbar} S e^{-iH_S t/\hbar} = S e^{-i\omega_a t} \\ B(t) &= e^{iH_B t/\hbar} B e^{-iH_B t/\hbar} = \sum_k g_k b_k e^{-i\omega_k t}. \end{aligned} \tag{2.26}$$

After we insert this result into Eq. (2.24) and Eq. (2.22) one needs to calculate such terms as

$$\begin{aligned} &\int_0^\infty dt' \, \mathrm{Tr_B}\big\{B^\dagger(t)B(t')\rho_B\big\} e^{-i\omega_a(t-t')} = \\ &\qquad \sum_{j,k} g_k g_j \int_0^\infty dt' \, \mathrm{Tr_B}\left\{b_k^\dagger b_j \rho_B\right\} e^{i(\omega_k t - \omega_j t')} e^{-i\omega_a(t-t')}, \end{aligned} \tag{2.27}$$

where

$$\begin{aligned} \mathrm{Tr_B}\left\{b_k^\dagger b_j \rho_B\right\} &= \langle b_k^\dagger b_j\rangle = \delta_{jk} n_k \\ \mathrm{Tr_B}\left\{b_k b_j^\dagger \rho_B\right\} &= \langle b_k b_j^\dagger\rangle = \delta_{jk}(n_k+1), \\ \text{with } n_k &= \frac{1}{e^{\beta\hbar\omega_k}-1},\ \beta = \frac{1}{k_B T} \end{aligned} \tag{2.28}$$

for a thermal bath of bosons which obey the Bose-Einstein distribution. Next, we use the relation

$$\int_0^\infty dt' e^{\pm i\epsilon t'} = \pi\delta(\epsilon) \pm i\mathcal{P}\Big(\frac{1}{\epsilon}\Big) \tag{2.29}$$

where $\mathcal{P}$ denotes the Cauchy principal value of the integral, which corresponds to the Lamb frequency shift and is assumed to be very small compared to ω_a and can be neglected. Thus, the integral in Eq. (2.27) is equal to

$$\begin{aligned} \int_0^\infty dt' \, \mathrm{Tr_B}\left\{B^\dagger(t)B(t')\rho_B\right\} e^{-i\omega_a(t-t')} &= \frac{\gamma\bar{n}}{2} \\ \int_0^\infty dt' \, \mathrm{Tr_B}\left\{B(t')B^\dagger(t)\rho_B\right\} e^{-i\omega_a(t-t')} &= \frac{\gamma(\bar{n}+1)}{2}, \end{aligned} \tag{2.30}$$

where $\gamma = 2\pi\sum_k |g_k|^2\delta(\omega_k-\omega_a)$, and $\bar{n}$ is the particle density in the reservoir.

Finally, the master equation in the interaction picture reads

$$\begin{aligned} \frac{d}{dt}\tilde{\rho}(t) = \frac{\gamma(\bar{n}+1)}{2}&\big(2S\tilde{\rho}(t)S^\dagger - S^\dagger S\tilde{\rho}(t) - \tilde{\rho}(t)S^\dagger S\big) \\ +\frac{\gamma\bar{n}}{2}&\big(2S^\dagger\tilde{\rho}(t)S - SS^\dagger\tilde{\rho}(t) - \tilde{\rho}(t)SS^\dagger\big). \end{aligned} \tag{2.31}$$

Switching back into the the Schrödinger picture,

$$\begin{aligned}\frac{d\rho}{dt} = -\frac{i}{\hbar}[H_S, \rho] + \frac{\gamma(\bar{n}+1)}{2}\big(2S\rho S^\dagger - S^\dagger S\rho - \rho S^\dagger S\big) \\ + \frac{\gamma\bar{n}}{2}\big(2S^\dagger\rho S - SS^\dagger\rho - \rho SS^\dagger\big),\end{aligned} \tag{2.32}$$

which is known as the Lindblad equation or the master equation in the Lindblad form.

2.4.1 Lindblad master equation

Thus, the dynamics in open quantum systems is governed by the master equation for the system density matrix ρ, which can be written as

$$\frac{d\rho}{dt} = -\frac{i}{\hbar}[H_S, \rho] + \mathcal{L}[\rho], \tag{2.33}$$

where the first term describes the coherent dynamics of the system, whereas the second term represents the dissipative processes in the system given by the Liouvillian superoperator $\mathcal{L}[\rho]$. In this chapter, we have shown that within the Born-Markov approximation the dissipative dynamics can be described by the Liouvillian in the standard Lindblad form,

$$\mathcal{L}[\rho] = \sum_i \frac{\gamma_i}{2}\big(2S_i\rho S_i^\dagger - S_i^\dagger S_i\rho - \rho S_i^\dagger S_i\big), \tag{2.34}$$

where the sum runs over all given dissipative channels and γ_i is the rate of a given dissipative process associated with the jump operator S_i.

2.4.2 Decay processes

In the following, we will consider the individual spontaneous decay of atoms with the decay rate Γ into vacuum modes (particle density $\bar{n} = 0$), which can be written as

$$\mathcal{L}_\Gamma[\rho] = \frac{\Gamma}{2}\sum_i(2\sigma_i^-\rho\sigma_i^+ - \sigma_i^+\sigma_i^-\rho - \rho\sigma_i^+\sigma_i^-). \tag{2.35}$$

Similarly, the cavity decay with the loss rate κ can be derived, which reads

$$\mathcal{L}_\kappa[\rho] = \frac{\kappa}{2}(2a\rho a^\dagger - a^\dagger a\rho - \rho a^\dagger a). \tag{2.36}$$

2.4.3 Dephasing processes

Quantum systems interacting with the environment experience external perturbations which are inevitably imprinted on the system leading to effects such as dephasing. In the case of active atomic clocks, it is particularly important to model the influence of external electric and magnetic field fluctuations, as well as the fluctuations of the cavity mirrors. We can model these dephasing processes by the white noise frequency fluctuations, which two-time correlation function is given by the Dirac delta function

$$\langle \xi(t)\xi(t')\rangle = \gamma_d \delta(t-t'), \tag{2.37}$$

where γ_d is the characteristic frequency of the noise.

The fluctuations of the atomic transition frequency due to external perturbations can be described by the atomic dephasing via the Lindblad term $\mathcal{L}_\nu[\rho]$ [53], with the atomic dephasing rate ν and the jump operator $\sigma^+\sigma^-$. Similarly, one can show that thermal and mechanical fluctuations of the cavity length lead to the fluctuations of the cavity resonance frequency given by $\mathcal{L}_\xi[\rho]$ with the cavity dephasing rate ξ and the jump operator $a^\dagger a$ for a single mode cavity.

3 Collective superradiant emission of light

3.1 Superradiant emission in free space

Many interesting open problems in quantum science are a consequence of interacting particles, i.e. they change their collective behavior due to mutual interactions. For dipolar atomic ensembles in free space, the direct dipole-dipole mediated interactions between the atoms can significantly modify the radiative properties of the collective atomic ensemble, if the distances between atoms are less than λ_0, the wavelength of light that is resonant with the atomic transition. Superradiance [46] is a landmark example of cooperative behavior in quantum optics where closely spaced atoms coupled to the same radiation field modes can synchronize with each other and form a collective dipole, which can emit an intense burst of light. The peak intensity of the emitted light eventually becomes proportional to the square of the number of atoms N, as the distance between the atoms decreases. In Fig. 3.1 we show the total emission rate for N initially fully excited two-level atoms in the so-called Dicke limit [46], i.e. with inter-atomic separation $a = 0$, where $\Gamma_{ij} = \Gamma$. In this case, the total photon emission is evaluated as

$$I(t) = \sum_{i,j=1}^{N} \Gamma \langle \sigma_i^+ \sigma_j^- \rangle. \tag{3.1}$$

In this limit, the dynamics is given by $\dot{\rho} = \mathcal{L}_\Gamma[\rho]$ written in the rotating frame of the atomic frequency ω_a, and is governed by a Liouvillian of the form

$$\mathcal{L}_\Gamma[\rho] = \frac{\Gamma}{2} \sum_{i,j=1}^{N} (2\sigma_i^- \rho \sigma_j^+ - \sigma_i^+ \sigma_j^- \rho - \rho \sigma_i^+ \sigma_j^-), \tag{3.2}$$

with Γ being the spontaneous decay rate for a single atom. Due to the symmetry of the problem, this can be mapped to a system of N energy states, so-called Dicke states, instead of having to compute 2^N states. In this case we obtain N jump operators $S_m^- = |m-1\rangle\langle m|$ and associated state-dependent transition rates $\Gamma_m =$

$m(N-m+1)\Gamma$, where m denotes the excitation number. The emission rate now reads $I(t) = \sum_m \Gamma_m \langle S_m^+ S_m^- \rangle$. Thus, the evaluation of the superradiant decay dynamics of many emitters becomes possible and is shown in Fig. 3.1. Finally, we note that the largest decay rate occurs when the system is in the $N/2$-excitation state, $m = N/2$, with $\Gamma_{N/2} = N/2(N/2+1)\Gamma \propto N^2\Gamma$. This superradiant burst of photon emission occurs due to the synchronization of all dipole phases in the atomic ensemble. In the next section we shall see how this can be readily realized when the atoms are placed inside an optical cavity.

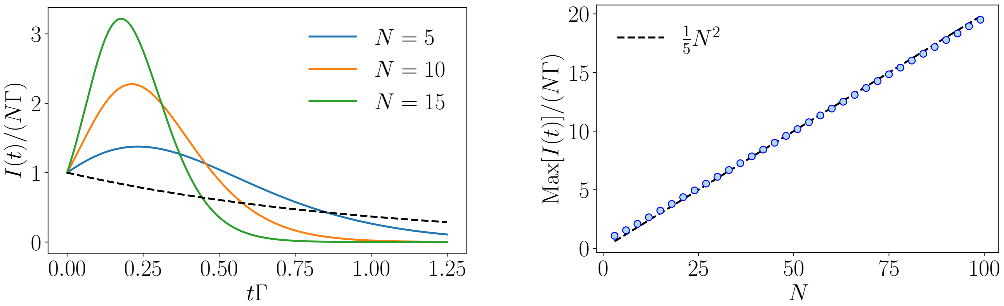

Figure 3.1: The photon emission (normalized by $N\Gamma$) as a function of time for a fully excited ensemble of N atoms in the Dicke limit. The black dashed line shows the photon emission of N non-interacting atoms decaying exponentially over time. We note, that the peak photon emission occurs at $t_{\max} \sim \log(N)/(N\Gamma)$. Right-hand side: The maximal photon emission rate as a function of the atom number shows the peak photon emission rate exhibits a quadratic scaling with N.

3.2 Superradiant laser

Similar to the synchronization process which emerges in free space superradiance, we will briefly discuss in this section superradiant lasing, as it occurs for a sufficiently large number of atoms coupled to the same cavity mode. We use a simple laser model here to illustrate the basic equations necessary to understand the methodology of this Thesis. It accounts for a single-mode cavity interacting with N identical two-level atoms, where the decay and pumping processes are described in terms of the Liouville operators. The master equation for the system density matrix reads

$$\frac{d\rho}{dt} = -\frac{i}{\hbar}[H,\rho] + \mathcal{L}_\kappa[\rho] + \mathcal{L}_\Gamma[\rho] + \mathcal{L}_R[\rho], \tag{3.3}$$

where $\mathcal{L}_\Gamma[\rho]$ and $\mathcal{L}_\kappa[\rho]$ are described in Eqs. (2.35) and (2.36) representing individual atomic decay and cavity losses, respectively. To observe a steady-state superradiance we introduce an incoherent pumping process in the system, which effect is described by the pumping rate R and the corresponding atomic raising operators σ_i^+ to create continuous population inversion among the atoms,

$$\mathcal{L}_R[\rho] = \frac{R}{2}\sum_i (2\sigma_i^+\rho\sigma_i^- - \sigma_i^-\sigma_i^+\rho - \rho\sigma_i^-\sigma_i^+). \tag{3.4}$$

The many-body Hamiltonian of the atomic ensemble interacting with a single-mode optical cavity is described by the Tavis-Cummings model

$$H = \hbar\omega_a \sum_{i=1}^{N} \sigma_i^+\sigma_i^- + \hbar\omega_c a^\dagger a + \hbar g \sum_{i=1}^{N} (\sigma_i^+ a + \sigma_i^- a^\dagger), \tag{3.5}$$

where we assume that all atoms are identical with the same atom-cavity coupling strength g. Note, that because of the symmetry of the problem, we can define collective operators $S^\pm = N^{-1}\sum_j \sigma_j^\pm$ and $S^z = N^{-1}\sum_j \sigma_j^z$, where $\sigma_j^z = \sigma_j^+\sigma_j^- - \sigma_j^-\sigma_j^+$ is the inversion operator for a single atom j. One can calculate the time evolution of the system by solving the master equation or using the cumulant expansion method described in the methods section below. Crucially, a nonzero collective atomic dipole $\langle S^z \rangle$ develops above the pumping threshold when a critical number of atoms is reached, a signature of atomic dipole phase locking in the collective strong coupling regime when $CN \gg 1$, where the single-atom cooperativity parameter $C = 4g^2/(\kappa\Gamma)$. The single-atom cooperativity is a dimensionless quantity that describes the ratio of the atomic photon emission rate into the cavity mode versus the cavity losses and the atomic photon emission rate into the free space. In the bad-cavity regime, the cavity decay rate κ is much bigger than g and Γ, thus the cooperativity parameter for a single atom is usually much smaller than one.

While photons spend very little time in the cavity, they play an important role mediating interatomic interactions between the atoms before leaving through one of the cavity mirrors. Thus, the phases of the atomic dipoles synchronize via the cavity mediated coupling, which leads to the buildup of a collective dipole among the atoms and coherent emission into the cavity. At low photon numbers, the coherence necessary for frequency stability is stored in the atoms rather than the cavity field. Consequently, the output frequency becomes robust to cavity fluctuations, which is the main limitation of conventional good-cavity lasers. This can be shown if we compare the spectral linewidth in the good- and the bad-cavity regimes. In the good-cavity regime, the cavity linewidth is much narrower than the bandwidth of the gain medium, namely $\kappa \ll \Gamma$. In this case, it can be found that the linewidth of the light exiting the cavity is given by $\Delta\nu \propto \kappa/|\langle a\rangle|^2$, which is the well-known Schawlow-Townes linewidth for lasers [54]. In the superradiant regime, it has been shown in Ref. [22, 55] that the minimum linewidth of the superradiant laser can reach $\Delta\nu \approx C\Gamma$, which has the potential to be much smaller than the natural linewidth of the atomic transition. For instance, in the case of ${}^1S_0 \rightarrow {}^3P_0$ clock transition in ^{87}Sr, theoretical predictions suggest that the ultimate linewidth can be way below 1 mHz [22].

3.3 Methods

3.3.1 Cumulant expansion method

Finding the exact solution of the master equation (2.33) analytically is almost never possible. Unfortunately, the exponential growth of the Hilbert space with the atom number also does not allow us to obtain the numerical solution of the density matrix evolution for many atoms. However, often we are only interested in finding the expectation values of some specific system operators. From the master equation (2.33) one can derive the time derivative for a system operator expectation value $\langle\mathcal{O}\rangle$ in the Heisenberg picture and after some manipulation using the cyclic permutation property of the trace

$$\frac{d}{dt}\langle\mathcal{O}\rangle = i\langle[H,\mathcal{O}]\rangle + \kappa\langle\mathcal{D}[a]\mathcal{O}\rangle + \Gamma\sum_i\langle\mathcal{D}[\sigma_i^-]\mathcal{O}\rangle + R\sum_i\langle\mathcal{D}[\sigma_i^+]\mathcal{O}\rangle, \tag{3.6}$$

where $\mathcal{D}[c]\mathcal{O} = \left(2c^\dagger\mathcal{O}c - c^\dagger c\mathcal{O} - \mathcal{O}c^\dagger c\right)/2$.

For instance, we can choose a set of operators $\{a, \sigma_i^-\}$ to obtain a system of Heisenberg equations of motion. However, the time derivatives of their expectation values will couple to expectation values involving more complex operators, namely $\langle a^\dagger a\rangle$, $\langle\sigma_i^+\sigma_j\rangle$ and $\langle a\sigma_i^+\rangle$. In order to obtain a closed set of equations, only correlations between operators up to a certain order should be considered, while all higher-order correlations are expanded in terms of lower orders. This approximation can be described in a systematic fashion, using the so-called cumulant expansion. More generally, the joint cumulant of an N-th order correlation $\langle O_1...O_N\rangle$ can be expressed as an alternating sum of products of their expectation values and is compactly written as [56]

$$C(O_1, ..., O_N) = \sum_{\pi} (|\pi| - 1)!(-1)^{|\pi|-1} \prod_{B\in\pi} \left\langle \prod_{i\in B} O_i \right\rangle \tag{3.7}$$

where π runs through the list of all partitions of $\{1, ..., N\}$, B runs through the list of all blocks of the partition π and $|\pi|$ is the number of parts in the partition. An approximation can be made by setting $C(O_1, ..., O_N) = 0$, which allows to express $\langle O_1 ... O_N\rangle$ with correlations of order $N - 1$ and lower. For instance, the expansion of expectation values involving three operators reads

$$\langle O_1 O_2 O_3\rangle \approx \langle O_1\rangle\langle O_2 O_3\rangle + \langle O_2\rangle\langle O_1 O_3\rangle + \langle O_3\rangle\langle O_1 O_2\rangle - 2\langle O_1\rangle\langle O_2\rangle\langle O_3\rangle. \tag{3.8}$$

This introduces an error since the third and higher-order correlations are neglected. However, as we present in Fig. 3.2, in a bad-cavity regime there is a good agreement between the full master equation and the cumulant expansion solution. We note that the cumulant expansion becomes exact when its order equals to the number of atoms in the system.

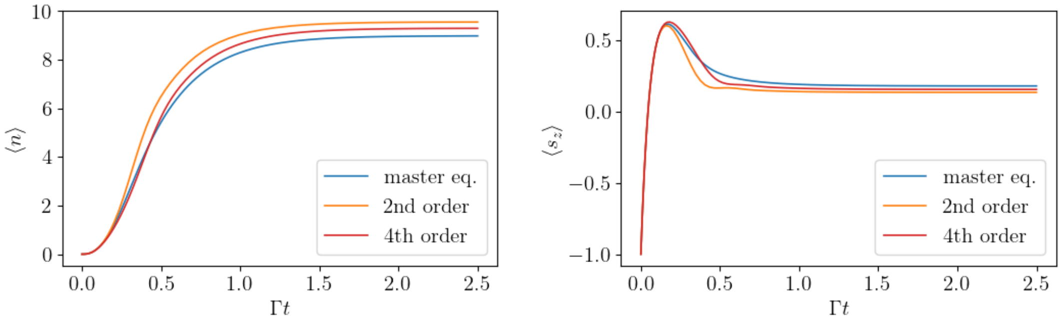

Figure 3.2: Comparison of the master equation solution (blue line) with the second-order (orange line) and fourth-order (red line) cumulant expansion dynamics for the mean intracavity photon number (left) and the population inversion (right) for $N = 6$ atoms. Parameters: $(\Delta, g, \kappa, R) = (0, 4\Gamma, 4\Gamma, 16\Gamma)$.

In Fig. 3.2 we calculate the dynamics of the mean intracavity photon number $\langle a^\dagger a\rangle$ and the population inversion on the lasing transition $\langle s_z\rangle$ as a function of time (in units of Γ) to show the comparison of the master equation solution (blue line) with the second order (orange line) and the fourth order (red line) cumulant expansion approach.

3.3.2 Spectrum of the cavity light field

To find the spectrum of the cavity output field we make use of the quantum regression theorem [57] and calculate the first-order correlation function $g^{(1)}(\tau) = \langle a^\dagger(t_0+\tau)a(t_0)\rangle$. If we choose $t_0 = t_{end}$, such that t_{end} is an arbitrary moment in time when the cavity photon dynamics has reached a stationary state, we can calculate $\partial_\tau g^{(1)}(\tau) = \langle \partial_\tau a^\dagger(\tau)a(0)\rangle$ via the master equation or using the cumulant expansion approach above, which in turn allows us to find $g^{(1)}(\tau)$. According to the Wiener-Khinchin theorem [58] the spectrum can be found as the Fourier transform of the first-order correlation function,

$$S(\omega) = 2\Re\left\{\int_0^\infty d\tau e^{-i\omega\tau} g^{(1)}(\tau)\right\}. \tag{3.9}$$

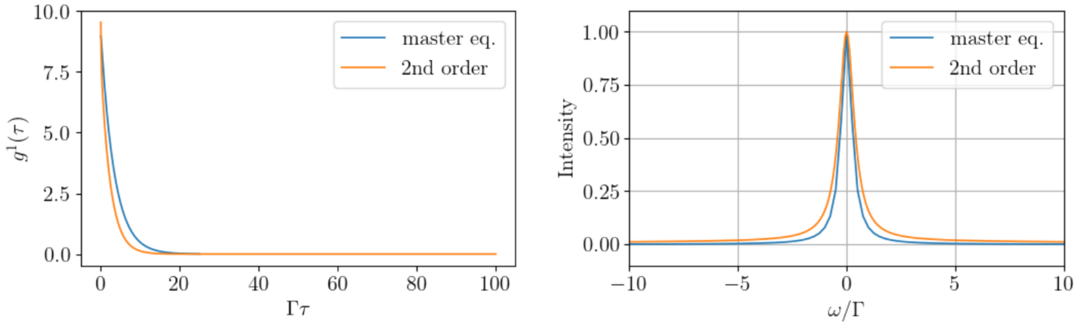

Figure 3.3: First-order correlation function dynamics (left) and cavity output spectrum (right) for $N = 6$ atoms obtained from the master equation solution (blue line) versus the second-order cumulant expansion (orange line). Parameters are the same as in Fig. 3.2.

4 Publication

The author of this thesis carried out the theoretical analysis as well as all analytical and numerical calculations presented in this work. C. H. provided helpful discussions and support in the physical interpretation of the data. D. P. co-supervised this work, and H. R. provided the idea and supervision of this publication.

Open Research Europe **1**(73) (2021)

Superradiant lasing in inhomogeneously broadened ensembles with spatially varying coupling

A. Bychek[1], C. Hotter[1], D. Plankensteiner[1] and H. Ritsch[1]

[1] *Institut für Theoretische Physik, Universität Innsbruck,*
Technikerstrasse 21, A-6020 Innsbruck, Austria

Background: Theoretical studies of superradiant lasing on optical clock transitions predict a superb frequency accuracy and precision closely tied to the bare atomic linewidth. Such a superradiant laser is also robust against cavity fluctuations when the spectral width of the lasing mode is much larger than that of the atomic medium. Recent predictions suggest that this unique feature persists even for a hot and thus strongly broadened ensemble, provided the effective atom number is large enough.
Methods: Here we use a second-order cumulant expansion approach to study the power, linewidth and lineshifts of such a superradiant laser as a function of the inhomogeneous width of the ensemble including variations of the spatial atom-field coupling within the resonator.
Results: We present conditions on the atom numbers, the pump and coupling strengths required to reach the buildup of collective atomic coherence as well as scaling and limitations for the achievable laser linewidth.

Conclusions: We show how sufficiently large numbers of atoms subject to strong optical pumping can induce synchronization of the atomic dipoles over a large bandwidth. This generates collective stimulated emission of light into the cavity mode leading to narrow-band laser emission at the average of the atomic frequency distribution. The linewidth is orders of magnitudes smaller than that of the cavity as well as the inhomogeneous gain broadening and exhibits reduced sensitivity to cavity frequency noise.

doi: 10.12688/openreseurope.13781.2

4.1 Introduction

Collective stimulated emission of coherent light by atoms inside an optical cavity is a fundamental phenomenon studied for decades in quantum optics [22, 46, 59–63]. Even very recently a large number of theoretical and experimental studies focused on continuous superradiance [22, 23, 63–70], aiming at the development of a superradiant laser [40, 41, 47, 48, 71–73]. Such a superradiant laser typically operates in a bad-cavity regime, where the cavity mode is much broader than the natural linewidth of the atoms providing the gain. In the limit of low photon number operation the coherence necessary for frequency stability is stored in the atoms rather than the cavity field. This makes the laser frequency insensitive to thermal and mechanical fluctuations of the cavity, which is the main limitation for conventional good-cavity lasers [38, 74]. In recent years pulsed superradiance has been experimentally demonstrated [40, 47, 48, 73] and a number of new theoretical ideas have been proposed [75–77]. However, the experimental realization of a continuous wave superradiant laser has not yet been achieved.

Effects such as frequency broadening in the gain medium are an inherent part of any experiment. Such processes are capable of disrupting the collective interaction between the atoms and the cavity field. In this work, we aim to offer a comprehensive study of these potentially detrimental effects. To this end, we study a model of a superradiant laser and focus on inhomogeneity among the atomic ensemble. The inhomogeneity is primarily associated with a distribution of the atomic resonance frequencies leading to stimulated emission into the cavity at a range of different frequencies. Similar differences in the atom-field coupling due to variation in the atomic positioning are also included in the system.

We numerically investigate the dynamics of an atomic medium with a wide range of resonance frequencies and show how the intensity of the pumping rate can lead to cooperative effects among the atoms such that superradiant lasing is achieved. Furthermore, we consider atoms to have different coupling strengths to the cavity. We also study the laser sensitivity to cavity noise.

4.2 Model

We consider an ensemble of N incoherently pumped two-level atoms inside a single mode optical cavity as shown in Figure 4.1. In a bad-cavity regime, where the cavity relaxation rate exceeds the natural linewidth of the atomic transition by many orders of magnitude ($\kappa \gg \Gamma$), the system constitutes a generic model of a superradiant laser. The i-th atom couples to the cavity field with the coupling strength g_i and has a resonance frequency ω_i which might be shifted from the unperturbed atomic transition frequency ω_a. Assuming that the cavity is on resonance with the unperturbed atomic transition frequency, we describe the coherent dynamics of the system by the Tavis-Cummings Hamiltonian in the rotating frame of the cavity,

$$H = -\sum_{i=1}^{N} \Delta_i \sigma_i^+ \sigma_i^- + \sum_{i=1}^{N} g_i (a\sigma_i^+ + a^\dagger \sigma_i^-). \tag{4.1}$$

Here, $\Delta_i = \omega_c - \omega_i$, $\sigma_i^+ = (\sigma_i^-)^\dagger = |e\rangle_i \langle g|_i$ denote the raising and lowering operators of the i-th atom, where $|g\rangle$ and $|e\rangle$ are the atomic ground and excited states, respectively, and $a^\dagger$ (a) is the photon creation (annihilation) operator of the cavity mode. The dissipative processes of this system are described by the Liouvillian terms

$$\begin{aligned}
\mathcal{L}_\kappa[\rho] &= \frac{\kappa}{2}(2a\rho a^\dagger - a^\dagger a\rho - \rho a^\dagger a) \\
\mathcal{L}_\Gamma[\rho] &= \frac{\Gamma}{2}\sum_i (2\sigma_i^- \rho \sigma_i^+ - \sigma_i^+ \sigma_i^- \rho - \rho \sigma_i^+ \sigma_i^-) \\
\mathcal{L}_R[\rho] &= \frac{R}{2}\sum_i (2\sigma_i^+ \rho \sigma_i^- - \sigma_i^- \sigma_i^+ \rho - \rho \sigma_i^- \sigma_i^+),
\end{aligned} \tag{4.2}$$

representing the loss of photons through the cavity at the rate κ, the spontaneous atomic decay with the single-atom spontaneous emission rate Γ, and the individual incoherent pumping with the pump strength R. Thus, the full dynamics of the system is determined by the master equation for the density matrix ρ in standard Lindblad

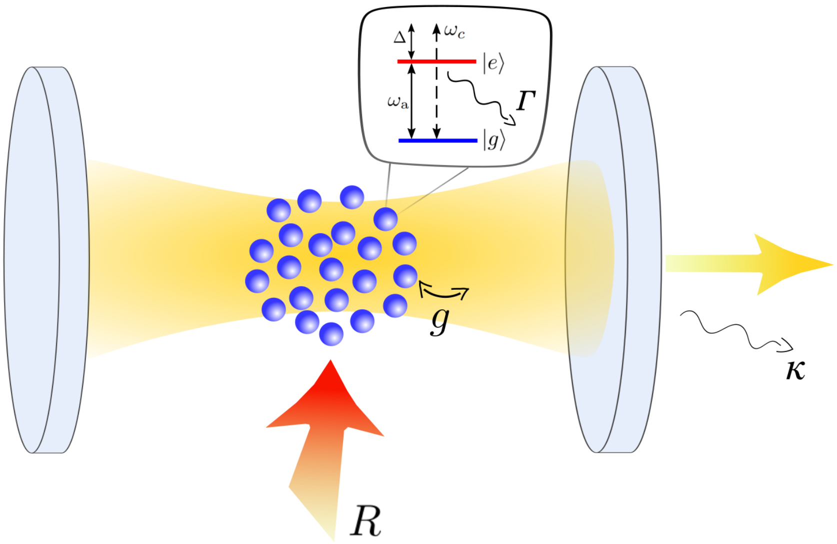

Figure 4.1: Schematic illustration of the system. The atomic medium is placed inside the optical resonator which has a resonance frequency ω_c. Each atom features a ground and an excited state separated by the transition energy ω_a. The transition couples to the cavity mode (g) as well as the environment (Γ). Additionally, the atoms are incoherently driven from the side (R) such that they can provide gain to the cavity mode.

form

$$\dot{\rho} = -i[H, \rho] + \mathcal{L}_\kappa[\rho] + \mathcal{L}_\Gamma[\rho] + \mathcal{L}_R[\rho]. \tag{4.3}$$

Since the exponential growth of the Hilbert space with the number of atoms renders the solution of the master equation (4.3) intractable for $N \gg 1$, we use a cumulant expansion method [22, 56]. First, we write down the equations for operator averages describing our system, which for a given operator $\mathcal{O}$ reads

$$\begin{aligned}\frac{d}{dt}\langle\mathcal{O}\rangle = i\langle[H, \mathcal{O}]\rangle + \kappa\langle\mathcal{D}[a]\mathcal{O}\rangle +& \\ \Gamma\sum_i\langle\mathcal{D}[\sigma_i^-]\mathcal{O}\rangle + R\sum_i\langle\mathcal{D}[\sigma_i^+]\mathcal{O}\rangle,&\end{aligned} \tag{4.4}$$

where $\mathcal{D}[c]\mathcal{O} = \left(2c^\dagger\mathcal{O}c - c^\dagger c\mathcal{O} - \mathcal{O}c^\dagger c\right)/2$. We note that in some cases (mentioned in the description of the results) we additionally include cavity dephasing and atomic dephasing described by the terms $\xi\langle\mathcal{D}[a^\dagger a]\mathcal{O}\rangle$ and $\nu\sum_i\langle\mathcal{D}[\sigma_i^+\sigma_i^-]\mathcal{O}\rangle$, respectively. The cavity dephasing accounts for the effective noise imposed on the system by thermal fluctuations of the cavity mirrors, whereas the atomic dephasing models perturbations on the lasing transition.

To obtain a closed set of differential equations we use the cumulant expansion method [56] up to second order:

$$
\begin{aligned}
&\frac{d}{dt}\langle a^\dagger a\rangle = -\kappa\langle a^\dagger a\rangle + i\sum_{m=1}^{N} g_m\langle a\sigma_m^+\rangle - i\sum_{m=1}^{N} g_m\langle a^\dagger\sigma_m^-\rangle \\
&\frac{d}{dt}\langle a\sigma_m^+\rangle = -\big((\kappa+\Gamma+R+\xi+\nu)/2 + i\Delta_m\big)\langle a\sigma_m^+\rangle + ig_m\langle a^\dagger a\rangle - ig_m\langle\sigma_m^+\sigma_m^-\rangle \\
&\quad - 2ig_m\langle a^\dagger a\rangle\langle\sigma_m^+\sigma_m^-\rangle - i\sum_{j;m\neq j}^{N} g_j\langle\sigma_m^+\sigma_j^-\rangle \\
&\frac{d}{dt}\langle\sigma_m^+\sigma_m^-\rangle = ig_m\langle a^\dagger\sigma_m^-\rangle - ig_m\langle a\sigma_m^+\rangle - (\Gamma+R)\langle\sigma_m^+\sigma_m^-\rangle + R \\
&\frac{d}{dt}\langle\sigma_m^+\sigma_j^-\rangle = ig_m\langle a^\dagger\sigma_j^-\rangle - ig_j\langle a\sigma_m^+\rangle - 2ig_m\langle a^\dagger\sigma_j^-\rangle\langle\sigma_m^+\sigma_m^-\rangle + 2ig_j\langle a\sigma_m^+\rangle\langle\sigma_j^+\sigma_j^-\rangle \\
&\quad - (\Gamma+R+\nu)\langle\sigma_m^+\sigma_j^-\rangle.
\end{aligned}
\tag{4.5}
$$

In order to calculate the spectrum of the cavity light field we make use of the Wiener-Khinchin theorem [58], which states that the spectrum can be computed as the Fourier transform of the first-order correlation function $g^{(1)}(\tau) = \big\langle a^\dagger(\tau)a(0)\big\rangle$,

$$
S(\omega) = 2\Re\left\{\int_0^\infty d\tau e^{-i\omega\tau} g^{(1)}(\tau)\right\}. \tag{4.6}
$$

We use the quantum regression theorem [57] to write down the set of differential equations for the two-time correlation function, which in matrix form reads,

$$
\frac{d}{d\tau}\begin{pmatrix} \langle a^\dagger(\tau)a(0)\rangle \\ \langle\sigma_1^+(\tau)a(0)\rangle \\ \vdots \\ \langle\sigma_N^+(\tau)a(0)\rangle \end{pmatrix} = \mathbf{A}\begin{pmatrix} \langle a^\dagger(\tau)a(0)\rangle \\ \langle\sigma_1^+(\tau)a(0)\rangle \\ \vdots \\ \langle\sigma_N^+(\tau)a(0)\rangle \end{pmatrix}, \tag{4.7}
$$

where

$$
\mathbf{A} = -\begin{pmatrix} \frac{\kappa+\xi}{2} & -ig_1 & \dots & -ig_N \\ ig_1\langle\sigma_1^z\rangle^{st} & \frac{\Gamma+R+\nu}{2} + i\Delta_1 & \dots & 0 \\ \vdots & \vdots & \ddots & \vdots \\ ig_N\langle\sigma_N^z\rangle & 0 & \dots & \frac{\Gamma+R+\nu}{2} + i\Delta_N \end{pmatrix}. \tag{4.8}
$$

We obtain the laser emission spectrum by taking the Laplace transform of Eq. 4.7, where the initial conditions are the steady-state solutions of Eqs. 4.5, for example $\langle a^\dagger(\tau=0)a(0)\rangle = \langle a^\dagger a\rangle^{st}$.

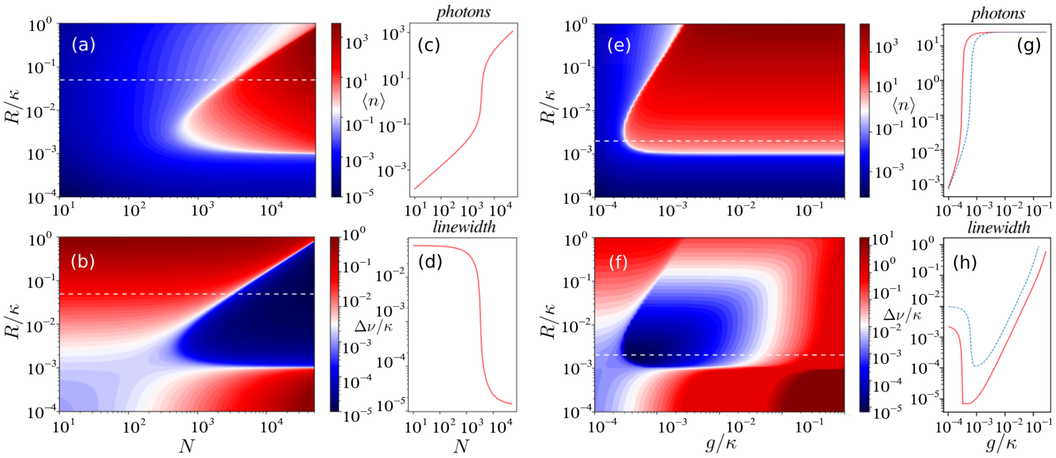

Figure 4.2: (a) The mean photon number and (b) the linewidth (in units of κ) as functions of the number of atoms N and pumping rate R for the parameter set $(\Delta, g, \Gamma, \xi, \nu) = (0, 0.002\kappa, 0.001\kappa, 0, 0)$. (c-d) The cut through the white dashed line in (a-b) for $R = 0.05\kappa$. (e-f) The mean photon number and the linewidth as functions of the atom-cavity coupling strength g and pumping rate R. Additional cavity dephasing occurs at the rate $\xi = \kappa$. Parameters: $\Delta = 0, \Gamma = 0.001\kappa, N = 5 \times 10^4$. (g-h) The cut through the white dashed line in (e-f): the ultra-narrow linewidth is robust to cavity dephasing $\xi = \kappa$ (red solid line) in the regime where the photon number is low. For the blue dashed line atomic dephasing was added to the system with the rate $\nu = 10\Gamma$.

In this section, we suppose that all atoms in the ensemble are identical with the same detunings $\{\Delta_i\} = \Delta$ and couplings $\{g_i\} = g$ to the cavity mode. This reduces the problem to a set of four differential equations in Eqs. 4.5. The mean intracavity photon number and the laser linewidth $\Delta\nu$ (the FWHM of the spectrum) are depicted in Figure 4.2 as functions of the number of atoms, pumping rate, and atom-cavity coupling strength. Superradiance is expected in the parameter regime where the single-atom cooperativity parameter $C = 4g^2/(\kappa\Gamma) < 1$, but the system is in the collective strong coupling regime [22], where $CN \gg 1$. Figures 4.2(a-d) show the emergence of the superradiant regime as the number of atoms increases. Above the lasing threshold the collective emission of light with an ultra-narrow linewidth is observed. In this collective regime the phases of the atomic dipoles are synchronized via photon exchange through the cavity which leads to the buildup of a collective dipole among the atoms.

A key feature of such a laser is its insensitivity to thermal and mechanical fluctuations

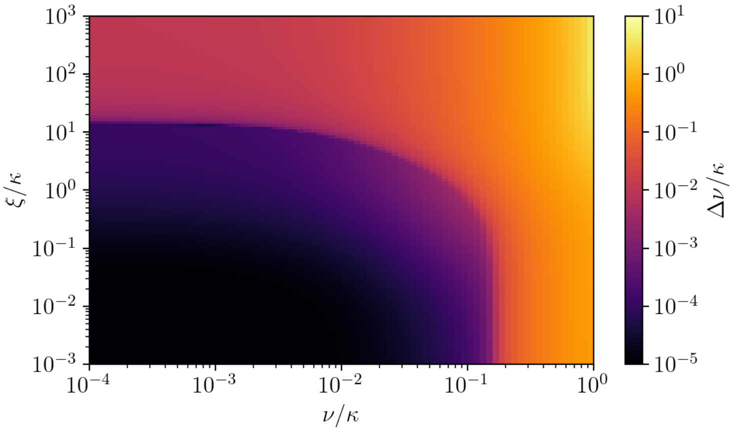

Figure 4.3: The linewidth of the emission spectrum of $N = 5 \times 10^4$ atoms as a scan over cavity dephasing (ξ) and atomic dephasing (ν). The optimal parameters are taken from Fig. 4.2(f), where the system is in the superradiant regime for $(\Delta, g, \Gamma, R) = (0, 0.001\kappa, 0.001\kappa, 0.01\kappa)$.

of the cavity length, since the coherence is primarily stored in the atoms rather than in the cavity field. To show the robustness against cavity noise we include cavity dephasing with the rate ξ in the equations. In Figure 4.2(f) we scan the linewidth over the coupling strength g and pumping rate R for an ensemble of $N = 5 \times 10^4$ atoms. In the superradiant regime, the laser linewidth is less than the natural linewidth of the atomic transition and approaches the value $\Delta\nu \sim C\Gamma$, which can be well below 1 mHz for the ${}^1S_0 \to {}^3P_0$ transition in ^{87}Sr, as has been pointed out in Ref. [22]. Furthermore, we study the influence of noise on the laser linewidth in more detail. In Figure 4.3 we scan the linewidth over both cavity and atomic dephasing, where the other parameters of the system correspond to the superradiant regime. One can see that the linewidth of the superradiant laser can be extremely robust to noise sources within a wide range.

So far the results are based on the idea of absolutely identical atoms. In the next sections, we focus on inhomogeneity within the atomic medium. In particular, we will consider the atoms to be subject to distinct frequency shifts and different couplings to the resonator mode.

4.3 Atomic ensembles with inhomogeneous broadening

While the individual atoms in free space are identical and have the same transition frequencies in principle, in practice they are often subject to individual perturbations introducing local lineshifts, e.g. from trapping within the cavity, motion, or optical pumping. Specifically, it can be an inhomogeneous trapping lattice or pump lasers with a Gaussian profile. Doppler shifts would have similar broadening effects in ring cavities, whereas in a standing-wave cavity they would generate a time-dependent atom-field coupling which we do not consider here. In this section we study the overall effects of inhomogeneous broadening of the gain medium on the laser properties.

In contrast to the case of identical atoms, where the atom number in Eqs. 4.5 and 4.7 only enters as a constant factor, the inhomogeneity among atomic frequencies requires keeping track of the time evolution of each atom separately. For the solution of the collective dynamics one then needs to solve $\mathcal{O}(N^2)$ equations. This is only possible for a limited atom number and we thus have to resort to further approximation methods in order to treat larger ensembles. As a possible approach to approximate a large ensemble with a continuous frequency distribution we combine several atoms in subgroups representing their average atomic frequencies, which we call clusters, see also Refs. [69, 70, 78]. Each atom in a cluster is assumed to be completely identical to all other atoms in the same frequency cluster. This preserves the central physics of the inhomogeneous broadening, but at the same time substantially reduces the number of equations.

First, we simulate $N = 5$ atoms in five clusters centered at $\Delta_m = \omega_c - \omega_m$, where $\Delta_m \in [-\kappa : \kappa]$. Note that this is equivalent to $M = 5$ frequency clusters each containing a single atom. At low excitation the resulting cavity output spectrum then consists of precisely five spectral lines at the frequency of each cluster. Basically, these are five independent lasers using the same cavity mode simultaneously. If we increase N and set the number of atoms per cluster according to a Gaussian normal distribution with the standard deviation $\sigma = \kappa$, the structure of the spectrum in Figure 4.4(a) will remain unchanged, with each peak becoming more pronounced. In particular, in Figure 4.4(b) we observe growing collective emission among atoms of the same cluster so that the linewidth of each peak becomes smaller as the atom number in the corresponding cluster increases. In Figure 4.4(c) we show how more and more lines appear as we increase the number of clusters up to $M = 201$ until the output merges into a single broad emission line. Note that an increase of the collective

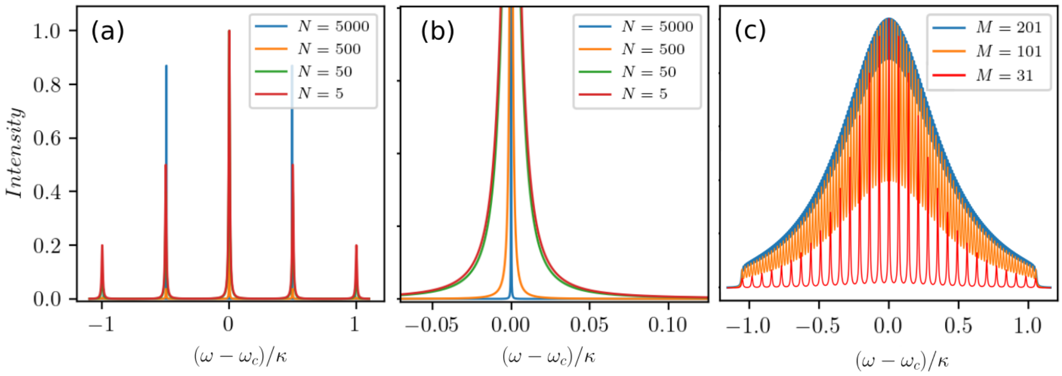

Figure 4.4: Cavity output spectra for weakly driven atomic ensembles composed of several discrete clusters with varying atomic frequencies. (a) $M = 5$ clusters of atoms with the detunings $\Delta_m = [-\kappa; -\kappa/2; 0; \kappa/2; \kappa]$ for different total numbers of atoms $N = 5, ..., 5000$. (b) A zoom-in showing the narrowing of the central peak in the spectrum from (a) around the resonance frequency. (c) Transition of the spectral distribution from discrete to quasi-continuous for an increasing number of clusters. Parameters: $(g, \Gamma, R) = (0.002\kappa, 0.001\kappa, 0.01\kappa)$.

coupling to $g\sqrt{N} \sim \kappa$ or a randomization of the individual cluster detunings do not lead to any substantial difference in the spectral profile of the laser. Hence, one can expect a single broadened peak in the emission spectrum in the more realistic case of a large ensemble of atoms with a continuous frequency distribution.

So far we limited investigations to weak incoherent pumping in order to avoid significant additional broadening of the atomic linewidth due to pumping. However, this broadening effect can actually aid the buildup of coherences between the clusters. When the pumping is strong enough such that the distinct spectral lines overlap, the discrete spectral lines of the clusters merge into a single central peak (see Figure 4.5). In other words, more intracavity photons and broader individual atomic gain lines ultimately lead to a dramatic narrowing of the laser line. We attribute this effect to a dynamical phase transition from the unsynchronized phase of the dipoles to the synchronized one. Note that an analogous phenomenon has previously been studied in Ref. [79] for two mesoscopic ensembles of atoms collectively coupled to a cavity with opposite detunings. Furthermore, we show how an atom number imbalance at a particular frequency in Figure 4.5(b) and overall atom number fluctuations modeled by slight random deviations from a Gaussian distribution in Figure 4.5(c) lead to a shift of the spectral lines. However, in the synchronized regime the lineshift of the

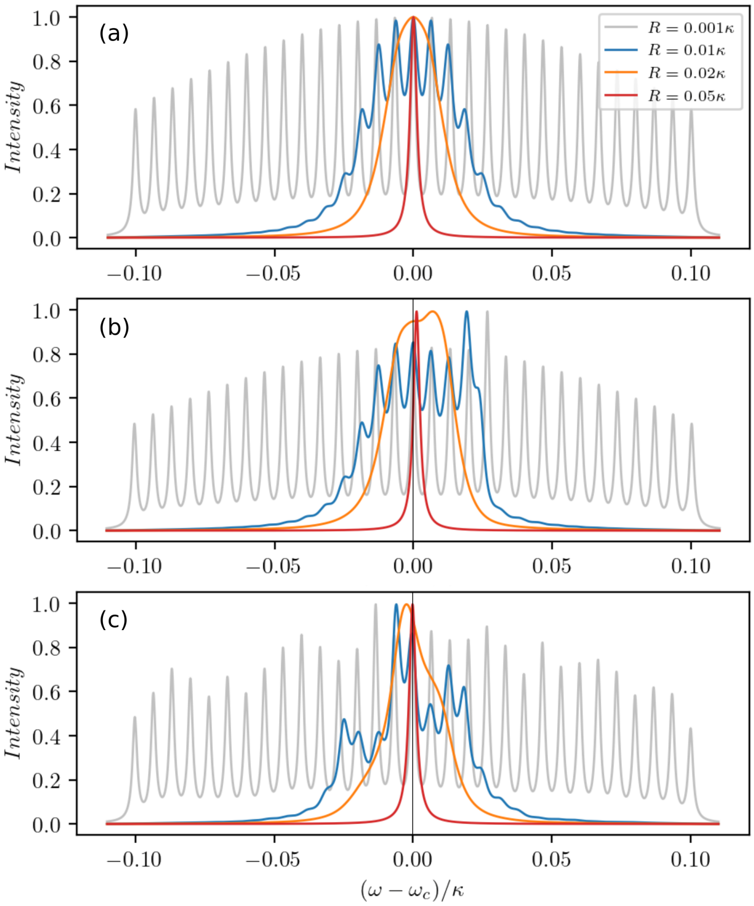

Figure 4.5: Cavity output spectra of a large inhomogeneously broadened ensemble of $N = 10^4$ atoms for different pumping rates $R = 0.001\kappa$ (grey), 0.01κ (blue), 0.02κ (orange), 0.05κ (red). The ensemble is represented by $M = 31$ clusters with the number of atoms per cluster chosen according to a Gaussian normal distribution (a) with the standard deviation $\sigma = 0.1\kappa$, (b) when adding particle imbalance at $\Delta = 0.027\kappa$, (c) with overall atom number fluctuations. The emission intensity is normalized and the other parameters are chosen as $\Delta \in [-\sigma : \sigma]$, $g = 0.002\kappa$, $\Gamma = 0.001\kappa$.

central peak is much smaller than its linewidth.

The collapse of the emission spectrum into a single central line occurs at a critical pump strength R_c. This critical value strongly depends on the overall width of the frequency distribution, but shows almost no dependence on the number of subensembles M and the total number of atoms N. The critical transition pump strength is shown for different standard deviations σ of the atomic frequency distribution in Figure 4.6.

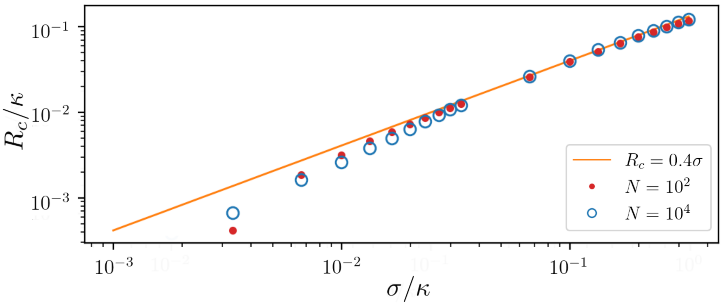

Figure 4.6: Critical value of pumping above which the collective superradiant regime is established depending on the standard deviation σ of the atomic frequency distribution. The data points show the numerical results for an ensemble of $N = 10^2$ (red dots) and $N = 10^4$ (blue circles) atoms sampled by $M = 31$ clusters. For comparison we plot the linear (solid line) function $R_c = 0.4\sigma$ as a linear approximation to the data points. Parameters: $\Delta \in [-3\sigma : 3\sigma], g = 0.001\kappa, \Gamma = 0.001\kappa$.

The data points show the numerical results for an ensemble of $N = 10^2$ (red dots) and $N = 10^4$ (blue circles) atoms sampled by $M = 31$ clusters. For comparison, we also plot the linear (solid line) function $R_c = 0.4\sigma$. We calculate the critical pumping by computing the spectrum for different R. We then determine the critical value of the pump strength as the value at which the spectrum has only a single local maximum, i.e. all separate peaks have merged into a single spectral line. We find a linear dependence for large inhomogeneously broadened ensembles while for narrow ensembles a significantly lower pump strength is required.

Once the laser is operating at a single distinct emission frequency, we can characterize the properties of the output light by the linewidth and the average photon number. The results for different distributions of atomic frequencies are shown in Figure 4.7, where $\Delta \in [-3\sigma : 3\sigma]$ and $\Gamma \leq 3\sigma \leq \kappa$. Figure 4.7(a) illustrates how a narrow linewidth appears for different σ as the number of atoms increases. Note that we chose a pumping strength well above the critical value for a wide atomic frequency distribution (red line). The sharp decrease of the linewidth is accompanied by an increase in the average photon number as can be seen in Figure 4.7(b). This is indicative of a lasing threshold being crossed at a certain number of atoms.

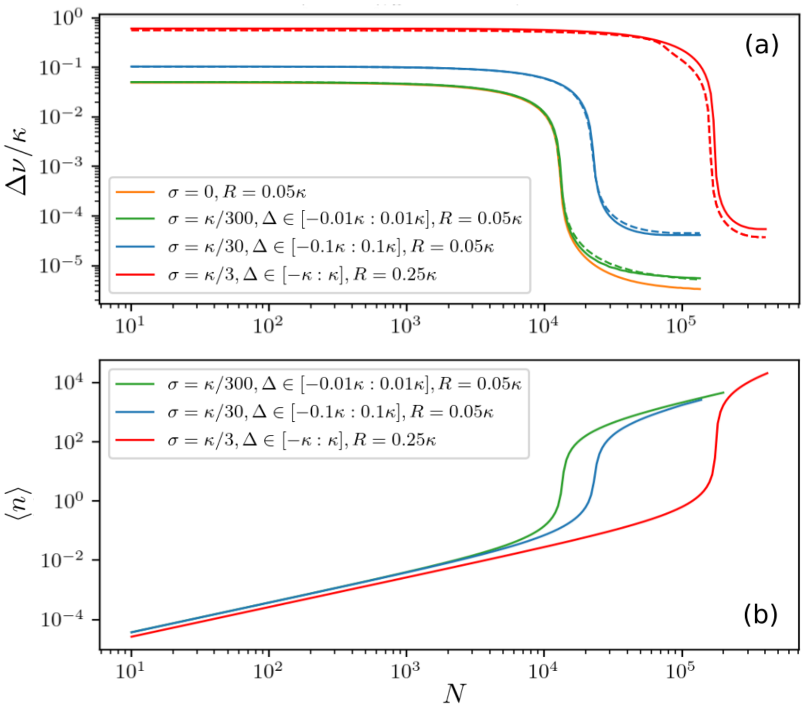

Figure 4.7: (a) Laser spectral linewidth and (b) mean photon number for inhomogeneously broadened ensembles with different standard deviations σ and spectral widths of atomic frequencies $\Delta \in [-3\sigma : 3\sigma]$, where $\sigma = \kappa/300$ (green line), $\sigma = \kappa/30$ (blue line), $\sigma = \kappa/3$ (red line) as a function of the total number of atoms. The number of clusters is $M = 31$ with the number of atoms per cluster chosen according to a Gaussian normal distribution. The dashed lines represent the results including an additional spatial variation of the atom-field coupling $g(x) = g_0 \cos(kx)$. The ensemble is comprised of $M = 11$ frequency clusters and $K = 5$ clusters of different couplings. The couplings are chosen such that the effective coupling strength $g_{\text{eff}} = \sqrt{(\sum_m g_m^2)/K} \equiv g$. Parameters: $g = 0.001\kappa$, $g_0 = 0.0013\kappa$, $\Gamma = 0.001\kappa$.

4.4 Inhomogeneously broadened ensembles with variable coupling strength

Up to now we have assumed that the atoms are perfectly positioned inside the cavity such that they couple equally to the cavity mode. Let us now include spatial variations of the atom-field coupling within the resonator. We consider the ensemble of atoms with the position-dependent coupling strength $g(x) = g_0 \cos(kx)$, where g_0 is the coupling constant, $k = 2\pi/\lambda$ is the cavity mode wave number and x represents the position of an atom. In order to describe the atom-field dynamics we use a similar cluster approach as before. We assume equidistant positions for different clusters $x_m \in [0, ..., \lambda/4)$ and corresponding couplings $g_m(x) = g_0 \cos(kx_m) = \{g_1, g_2, ..., g_K\}$, where K is the total number of clusters. Note, that the sign of the coupling is irrelevant in our system, therefore we only consider couplings with $g_m > 0$.

The dashed lines in Figure 4.7 show the results for $M = 11$ frequency clusters and $K = 5$ clusters of different couplings. As can be seen in Figure 4.7(a), for atoms with different couplings to the cavity mode the dependence of the linewidth on the number of atoms remains roughly the same as for atoms equally coupled to the cavity. This holds as long as the effective overall coupling strength $g_{\text{eff}} = \sqrt{(\sum g_m^2)/K}$ is constant. Thus, the linewidth is essentially unaffected by atoms having different couplings to the cavity.

Finally, let us include cavity dephasing in order to describe lasing in a large inhomogeneously broadened ensemble in the presence of cavity noise. The spectral linewidth and mean photon number under strong cavity dephasing at the rate $\xi = \kappa$ are depicted in Figure 4.8 (blue dashed line). Note that establishing coherence in such a largely broadened ensemble requires sufficiently strong pumping. This subsequently leads to a large number of photons in the cavity mode making the setup sensitive to cavity fluctuations, see Figure 4.2(f). However, additional atomic dephasing can actually relax the constraint on the pumping, since both incoherent pumping and atomic dephasing are closely tied to the same physical effect of broadening the atomic emission line. Thus individual atomic dephasing induce additional atom-atom coupling by enlarging the overlap of distinct spectral lines, which finally leads to better synchronization. Adding atomic dephasing to the system at the rate $\nu = 0.01\kappa$ allows for maintaining collective interactions in the ensemble and at the same time enables a reduction of the pump strength by one order of magnitude to $R = 0.005\kappa$. In the low photon number regime, a linewidth on the order of the natural atomic linewidth Γ can be achieved in the presence of strong atomic and cavity dephasing (dash-dotted grey line).

The presented results can be reproduced by using the source code *N_atoms_M_clusters_Delta.jl* (see *Software availability*) [80]. The file contains an example of the cluster approach written in Julia version 1.5.0 using the parameters in Figure 4.5. Numerical simulations were performed with the open-source framework Differentialequations.jl [81]. The toolbox QuantumCumulants.jl [82] has been used to check the equations and verify the second-order cumulant expansion. The graphs

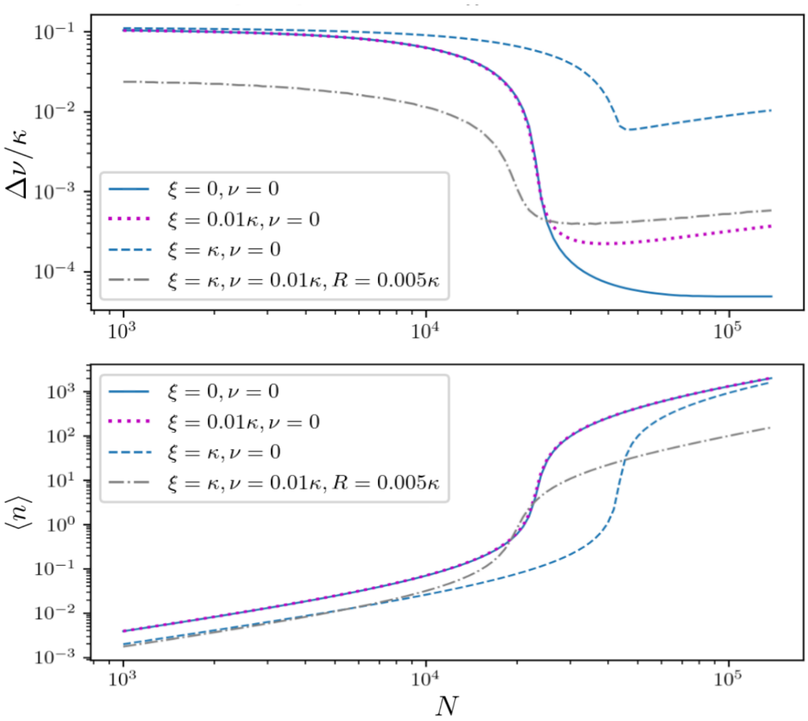

Figure 4.8: Laser linewidth (upper panel) and mean photon number (lower panel) for an inhomogeneously broadened ensemble with spatially varying coupling for $\sigma = \kappa/30$, $\Delta \in [-0.1\kappa : 0.1\kappa]$ and $R = 0.05\kappa$ (solid line). Adding various cavity dephasing at the rate $\xi = \kappa$ (dashed blue line) and $\xi = 0.01\kappa$ (dotted magenta line) we can identify an optimal atom number, above which the cavity noise overwhelms the linewidth narrowing due to large photon numbers. The dash-dotted grey line shows the results when adding additional atomic dephasing at the rate $\nu = 0.01\kappa$. This additional broadening allows synchronization of the individual clusters in the weak pumping regime $R = 0.005\kappa$ ultimately leading to a smaller linewidth.

were produced using the Matplotlib library [83].

4.5 Conclusions

We studied superradiant lasing when the gain medium is subject to substantial inhomogeneous frequency broadening and variable coupling. In extensive numerical simulations based on a second-order cumulant expansion we were able to confirm previous predictions that sufficiently large numbers of atoms subject to strong optical pumping can induce synchronization of the atomic dipoles over a large bandwidth. This generates collective stimulated emission of light into the cavity mode leading to narrow-band laser emission at the average of the atomic frequency distribution. The linewidth is orders of magnitudes smaller than that of the cavity as well as the inhomogeneous gain broadening and exhibits reduced sensitivity to cavity frequency noise. We determine the operational conditions and, in particular, the best pump rate to choose for achieving the smallest linewidth for a given atom number and cavity. The minimum occurs not at very low photon numbers but at intracavity photon numbers reaching a significant fraction of the atom number.

Typically, full synchronization requires fairly strong pumping, which increases the effective atomic linewidth. We determined the minimum pump strength to achieve collective phase-locked oscillation of all atomic dipoles. Interestingly, some individual line-broadening effects such as atomic dephasing can actually induce synchronization at significantly lower pump rates. Furthermore, our simulations also show that variations in the atom-field coupling strength induced by the cavity mode structure play only a minor role for the laser stability and noise. In fact, they can be compensated by an increase of the effective overall coupling using a larger atom number or stronger pump.

In the present work, we did not take into account collisions or dipole-dipole interactions between atoms. The effect of dipole-dipole interactions have been studied in a small-scale full quantum model in Ref. [23] and do not appear too detrimental. Moreover, collisions could even have a positive effect on synchronization [84] but a quantitative prediction is complicated. So far our model is still based on a very simplistic effective pump description via an individual, independent and equal pump rate for each atom. More detailed studies of optical pumping schemes including the shifts induced by the pump light will be at the center of future studies.

Acknowledgments

We acknowledge funding from the European Union's Horizon 2020 research and innovation program under the Marie Sklodowska-Curie Grant Agreement No. 860579 MoSaiQC (A. B.) and Grant Agreement No. 820404 iqClock (C. H., D. P., H. R.).

4.6 Supplemental material

4.6.1 Cross-correlations between atoms in different clusters.

As we refer to in the main text, we model a continuous atomic frequency distribution with the standard deviation σ by choosing equidistant cluster detunings Δ_m with the number of atoms per cluster N_m given by a Gaussian distribution with the standard deviation σ. The Heisenberg equations for an ensemble of N atoms sampled by M clusters can be written as

$$\begin{aligned}
&\frac{d}{dt}\langle a^\dagger a\rangle = -\kappa\langle a^\dagger a\rangle + \sum_{m=1}^{M} ig_m N_m \langle a\sigma_m^+\rangle - \sum_{m=1}^{M} ig_m N_m \langle a^\dagger \sigma_m^-\rangle \\
&\frac{d}{dt}\langle a\sigma_m^+\rangle = -\big((\kappa+\Gamma+R)/2 + i\Delta_m\big)\langle a\sigma_m^+\rangle + ig_m\langle a^\dagger a\rangle - 2ig_m\langle a^\dagger a\rangle\langle\sigma_{am}^+\sigma_{am}^-\rangle \\
&\quad - ig_m\langle\sigma_{am}^+\sigma_{am}^-\rangle - ig_m(N_m-1)\langle\sigma_{am}^+\sigma_{bm}^-\rangle - \sum_{j;m\neq j}^{M} ig_j N_j\langle\sigma_m^+\sigma_j^-\rangle \\
&\frac{d}{dt}\langle\sigma_{am}^+\sigma_{am}^-\rangle = ig_m\langle a^\dagger\sigma_m^-\rangle - ig_m\langle a\sigma_m^+\rangle - (\Gamma+R)\langle\sigma_{am}^+\sigma_{am}^-\rangle + R \qquad\qquad \text{(A1)} \\
&\frac{d}{dt}\langle\sigma_{am}^+\sigma_{bm}^-\rangle|_{a\neq b} = ig_m\langle a^\dagger\sigma_m^-\rangle(1-2\langle\sigma_{am}^+\sigma_{am}^-\rangle) - ig_m\langle a\sigma_m^+\rangle(1-2\langle\sigma_{am}^+\sigma_{am}^-\rangle) \\
&\quad - (\Gamma+R)\langle\sigma_{am}^+\sigma_{bm}^-\rangle \\
&\frac{d}{dt}\langle\sigma_m^+\sigma_j^-\rangle|_{m\neq j} = -i(\Delta_m-\Delta_j)\langle\sigma_m^+\sigma_j^-\rangle + ig_m\langle a^\dagger\sigma_j^-\rangle(1-2\langle\sigma_{am}^+\sigma_{am}^-\rangle) \\
&\quad - ig_j\langle a\sigma_m^+\rangle(1-2\langle\sigma_{aj}^+\sigma_{aj}^-\rangle) - (\Gamma+R)\langle\sigma_m^+\sigma_j^-\rangle,
\end{aligned}$$

where indices a, b refer to an atom, and m, j are cluster indices. The last equation describes the cross-correlations between atoms in different clusters. Next, we study the phase and the amplitude of these correlations as the system reaches the steady-state. In the weak pumping regime, the correlations are zero and therefore there is no coherence between the distinct spectral lines of the output spectra in Figure 4.4. However, in the synchronized regime shown in Figure 4.5(a) for $R = 0.05\kappa$, the existing cross-correlations of the m-th cluster with the other clusters $j = m..M$ are presented in Figure 4.9(a).

Let us follow these correlations as the system goes from the unsynchronized phase to the synchronized one. We study the magnitude of cross-correlations between the first (outer) cluster and the central cluster in Figure 4.5(a) as a function of the pumping strength. The correlations are zero in the weak pumping regime and grow with the

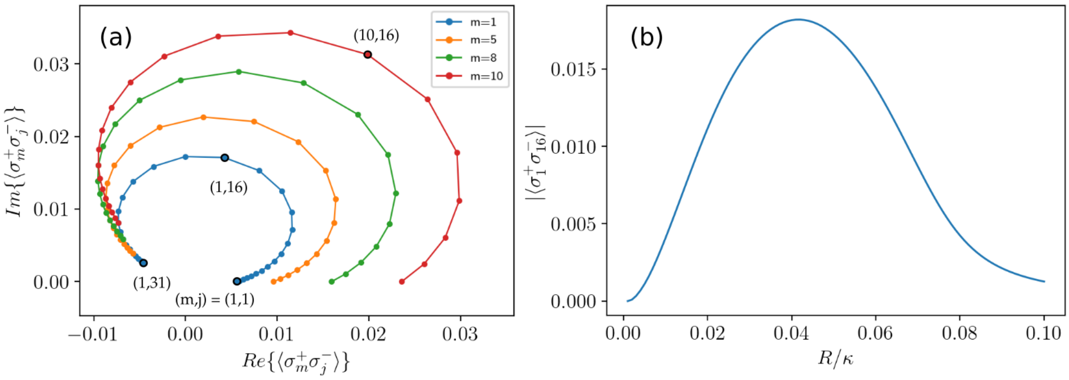

Figure 4.9: Cross-correlations between the 31 clusters presented in Figure 4.5(a). (a) Real and imaginary part of $\langle\sigma_m^+\sigma_j^-\rangle$ correlations between atoms in the m-th and j-th clusters on the complex plane for $R = 0.05\kappa$. (b) The magnitude of the cross-correlations between atoms in the first and the central clusters as a function of the pumping strength.

pumping strength as shown in Figure 4.9(b). The function reaches its maximal value when the ensemble is fully synchronized. However, as pumping continues to grow the correlations decrease due-to growing dephasing imposed by pumping.

4.6.2 Data availability

- Figshare: Superradiant_laser_Figures. https://doi.org/10.6084/m9.figshare.15321819 [85]
- This project contains the following underlying data: Data used in Figures 2-8. All data have .jld2 file extension using JLD2.jl data package in Julia
- Data are available under the terms of the Creative Commons Zero "No rights reserved" data waiver (CC0 1.0 Public domain dedication)

4.6.3 Software availability

- Source code available from: https://github.com/by-anna/Clusters
- Archived source code at time of publication: https://doi.org/10.5281/zenodo.4916393 [80]
- License: MIT License

5 Publication

The author of this thesis provided the results for the frequency stability and spectral linewidth of active optical atomic clocks with inhomogeneous atomic ensembles presented in Sec. 5.3. G. K. carried out the theoretical analysis, numerical calculations and interpretation of the data. S. D. provided support in the numerical development of the code. U. S., M. B., and M. Z. provided helpful discussions and support in the physical interpretation of the data. All authors participated in the discussion and interpretation of the results and contributed to the manuscript preparation.

PHYSICAL REVIEW A **106**(5), 053114 (2022)

Ultimate stability of active optical frequency standards

G. A. Kazakov[1], S. Dubey[1], A. Bychek[2], U. Sterr[3], M. Bober[4], M. Zawada[4]

[1]*Atominstitut, TU Wien, Stadionallee 2, 1020 Vienna, Austria*
[2]*Institut für Theoretische Physik, Universität Innsbruck,*
Technikerstrasse 21, A-6020 Innsbruck, Austria
[3]*Physikalisch-Technische Bundesanstalt (PTB),*
Bundesallee 100, 38116 Braunschweig, Germany
[4]*Institute of Physics, Faculty of Physics, Astronomy and Informatics, Nicolaus*
Copernicus University, Grudziądzka 5, PL-87-100 Toruń, Poland

Active optical frequency standards provide interesting alternatives to their passive counterparts. Particularly, such a clock alone continuously generates highly-stable narrow-line laser radiation. Thus a local oscillator is not required to keep the optical phase during a dead time between interrogations as in passive clocks, but only to boost the active clock's low output power to practically usable levels with the current state of technology. Here we investigate the spectral properties and the stability of active clocks, including homogeneous and inhomogeneous broadening effects. We find that for short averaging times the stability is limited by photon shot noise from the limited emitted laser power and at long averaging times by phase diffusion of the laser output. Operational parameters for best long-term stability were identified. Using realistic numbers for an active clock with ^{87}Sr we find that an optimized stability of $\sigma_y(\tau) \approx 4 \times 10^{-18}/\sqrt{\tau[\mathrm{s}]}$ is achievable.

doi: 10.1103/PhysRevA.106.053114

5.1 Introduction

Modern-day optical clocks are passive frequency standards [86], where the frequency of a laser pre-stabilized to an ultra-stable optical cavity is periodically compared with the frequency of a narrow and robust *clock transition* in a sample of trapped atoms (or ions). The measurement sequence includes an interrogation time, during which the phase of the laser is imprinted to the atomic sample, and a *dead time*, when the laser pre-stabilised to an ultra-stable macroscopic cavity keeps the frequency, playing the role of a flywheel. Such a clock has demonstrated an excellent stability at the level of 6.6×10^{-19} after 1 hour of averaging [37], however, on shorter timescale this stability is limited by thermal and mechanical fluctuations of the length of this ultra-stable cavity. This problem may be overcome with the help of an *active optical frequency standard* based on a laser operating deep in the bad-cavity regime [22, 87], where the linewidth of the cavity is much broader than the linewidth of the gain. The gain of such a laser can be formed by forbidden transitions in alkaline-earth atoms, the same as used for passive optical lattice clocks. Similar to a hydrogen maser, the frequency of such a laser is determined by the frequency of lasing transition and is robust to fluctuations of the cavity length, which improves the stability on shorter timescales.

In the present paper we study the stability that can be attained with such a laser and compare it with the one of a passive optical clock based on an atomic ensemble with similar characteristics. For the sake of definiteness, we consider the model of two-level laser with continuous incoherent repumping [22]. Bad-cavity lasers based on other schemes, such as atomic beam lasers [87], optical conveyor lasers [88], and lasers with sequential coupling of atomic ensembles [89] should have similar characteristics, up to some numerical factors. In Section 5.2 we present general expressions for the short-term stability of a secondary laser phase locked to a low-power narrow-line continuous-wave bad-cavity laser. In Section 5.3 we calculate the linewidth of the bad-cavity laser's Lorentzian spectrum and discuss how this linewidth depends on the natural linewidth of the lasing transition in the employed gain atoms, on inhomogeneous broadening and dephasing of the atomic transition, on the number of atoms providing the gain, and on parameters of the cavity. We optimize the cooperativity as well as the rate of incoherent pumping to attain a minimum linewidth at a given atomic number and cavity finesse. We express these optimized parameters as well as the linewidth and the respective number of intracavity photons via characteristic properties of the atomic ensemble. In Section 5.4 we estimate the achievable performance for ensembles of atoms trapped in an optical lattice potential and compare the respective frequency stabilities that can be obtained with the help of active and passive frequency standards based on such ensembles.

5.2 Active optical frequency standard and its stability

The spectral characteristics of a bad cavity laser's output field E can be described by its power spectral density $S_E(f)$. It can be obtained from the two-time correlation function $\mathcal{R}(\tau)$ with the help of the well-known Wiener-Khinchin theorem, see equation (5.21) in Section 5.3.3 and [66]. In first approximation $\mathcal{R}(\tau)$ may be described by an exponentially decaying function that corresponds to a Lorentzian lineshape of $S_E(f)$ centered at an ordinary frequency $f_0 = \omega_0/(2\pi)$ with half-width $\Delta f = \Delta\omega/(2\pi)$. Such a signal has white frequency noise with a single sided spectral power density $S_y(f)$ of fractional frequency fluctuations $y = \Delta\omega/\omega_0$ equal to

$$S_y(f) = \frac{\Delta f}{\pi f_0^2} = \frac{2\Delta\omega}{\omega_0^2}, \tag{5.1}$$

corresponding to a spectral power density $S_\phi(f)$ of phase fluctuations

$$S_\phi(f) = \frac{\Delta f}{\pi f^2} = 2\Delta\omega f^2, \tag{5.2}$$

and Allan deviation

$$\sigma_y'(\tau) = \sqrt{\frac{\Delta\omega}{\omega_0^2\tau}}. \tag{5.3}$$

In addition, due to the finite rate of emitted photons, the field of power P shows quantum fluctuations, leading to a limited signal-to-noise ratio expressed as the ratio of signal power to power of the noise per unit bandwidth $\mathrm{SNR} = P/(\hbar\omega_0)$ [90]. Theses fluctuations appear as white amplitude and phase noise of the signal. When the active-laser output is heterodyned with an ideal powerful and perfectly stable cw laser, the amplitude noise is usually of no importance to the frequency stability, and the power spectral density of white phase noise S_ϕ amounts to

$$S_\phi(f) = \mathrm{SNR}^{-1} = \frac{\hbar\omega_0}{P}, \tag{5.4}$$

with the corresponding Allan deviation [91, 92]

$$\sigma''_y(\tau) = \frac{1}{\tau}\sqrt{\frac{3\hbar f_h}{\omega_0 P}}. \tag{5.5}$$

As the Allan deviation would diverge for white phase noise with unlimited bandwidth, the noise is set to zero for frequencies above a cut-off frequency f_h (in ordinary frequency units) to obtain a finite value. In practice this low-pass behavior can appear from the bandwidth of a phase locked loop using the heterodyne signal.

To avoid the dependence on the arbitrary cut-off frequency, in this case the modified Allan deviation is often used:

$$\operatorname{mod}\sigma''_y(\tau) = \frac{1}{\tau^{3/2}}\sqrt{\frac{3\hbar}{2\omega_0 P}}. \tag{5.6}$$

Adding the random walk noise of the phase associated with damping of two-time correlation of the cavity field and the white phase noise associated with shot noise in the number of emitted photons results in the overall Allan deviation

$$\sigma_y(\tau) = \sqrt{(\sigma'_y(\tau))^2 + (\sigma''_y(\tau))^2} = \sqrt{\frac{\Delta\omega}{\omega_0^2\tau} + \frac{3\hbar f_h}{\omega_0 P\tau^2}}. \tag{5.7}$$

and the overall modified Allan deviation

$$\operatorname{mod}\sigma_y(\tau) = \sqrt{\operatorname{mod}\sigma'_y(\tau)^2 + \operatorname{mod}\sigma''_y(\tau)^2} = \sqrt{\frac{\Delta\omega}{2\omega_0^2\tau} + \frac{3\hbar}{2\omega_0 P\tau^3}}. \tag{5.8}$$

At short averaging times τ it is determined by the bad-cavity laser's output power P and at long times by its linewidth $\Delta\omega$.

The contribution $\sigma''_y(\tau)$ (5.5) to the total instability $\sigma_y(\tau)$ is associated with the photon shot noise. Its influence depends on the bandwidth of the feedback loop to phase lock a secondary laser with good short-term stability to the bad cavity laser (see discussion in Section 5.4). The contribution $\sigma'_y(\tau)$ (5.3) is more fundamental in that sense that it does not depend on the properties of the secondary laser and it limits the stability on longer timescale.

In the next section we consider a generic model of a two-level bad cavity laser with incoherent pumping and find general expressions for the minimum linewidth $\Delta\omega$ and the necessary set of optimized parameters.

5.3 Linewidth of a bad cavity laser

In this section we overview the dependence of the linewidth on the characteristics of the bad-cavity laser with continuous incoherent repumping and estimate the minimum linewidth which can be achieved in such type of laser. First we consider a two-level model of a bad-cavity laser with incoherent pumping, as studied in [22]. Such a laser has two lasing thresholds $R_{\min}$ and $R_{\max}$; below the lower threshold $R_{\min}$ the pumping is not enough to create the necessary inversion for the lasing and above the upper threshold $R_{\max}$ the pumping destroys the coherence, thus also preventing the coherent emission. In the homogeneous case (i.e., when all atoms contributing to the gain have exactly the same parameters, such as coupling strength with the cavity field, transition frequency, dephasing rate, etc.), and when the laser operates far from the lower and the upper lasing thresholds, the linewidth $\Delta\omega_{\min}$ of such a laser can be estimated [22] as

$$\Delta\omega_{\min} \approx C\gamma_s = 4g^2/\kappa. \tag{5.9}$$

Here κ is the decay rate of the energy of the cavity field, g is the coupling strength between the laser field and the atomic transition (the Hamiltonian is presented in expression 5.11), γ_s is the spontaneous rate of the lasing transition, and $C = 4g^2/(\kappa\gamma_s)$ is the *cooperativity parameter*. It may seem that one should just take the cooperativity C as small as possible to minimize the linewidth. However, expression (5.9) is valid only if the pumping rate R is much bigger than the lower and much smaller than the upper lasing thresholds $R_{\min}$ and $R_{\max}$ respectively. Accurate expressions for these thresholds in the homogeneous case will be derived in section 5.3.2. One may see from expressions (5.32) and (5.33) that both lasing thresholds approache each other when the cooperativity C decreases at a given number N of atoms. Therefore, a minimum linewidth is attained in such a range of parameters where the condition $R_{\text{min}} \ll R \ll R_{\text{max}}$ is not fulfilled anymore and where the estimate (5.9) is not valid. Thus we need to find a more accurate estimate for $\Delta\omega_{\text{min}}$.

The spectral properties of a continuous-wave laser can be derived from the two-time correlation function of its output field $\mathcal{R}(\tau) = \langle \hat{a}^\dagger(t_0+\tau)\hat{a}(t_0)\rangle$, which in the bad-cavity regime is directly proportional to the correlation of the atomic coherence [22]. In the present paper we limit our consideration to a model where the laser gain is formed by N two-level atoms subjected to incoherent pumping and coupled to the cavity field. Such a two-level model can correctly represent the dynamic of a real multilevel superradiant laser with continuous repumping and single lasing transition, if the lifetimes of the intermediate levels are much shorter than any other timescale in the system except, may be, the decay rate of the cavity field [93]. Because the Hilbert space describing such a system grows exponentially with atom number N, one has to use some approximation to reduce the problem size. We restrict our consideration to a second-order cumulant approximation, following [22] and [94], which allows calculating both output power and spectrum of the superradiant laser. In subsection 5.3.1 we briefly overview the model and explain the most important details of the calculation. In subsection 5.3.2 we consider the particular case of a homogeneous system, where all the atoms are equally coupled to the cavity field and share the same transition frequency and all other parameters. We obtain analytical expressions for the output power and the linewidth in this simplest case and perform a qualitative analysis of their dependencies. In subsection 5.3.3 we study the linewidth quantitatively, both for the simple homogeneous model and for a more realistic model with inhomogeneous coupling of the atoms to the cavity field and inhomogeneous broadening of the lasing transition.

5.3.1 Inhomogeneous system: description of the model and equations

We consider an ensemble of N two-level atoms confined in space (for example, with the help of an optical lattice potential) and interacting with a single cavity mode, see Figure 5.1. We neglect dipole-dipole interactions between different atoms as well as collective coupling of the atoms to the bath. The averaged value of an operator $\hat{O}$

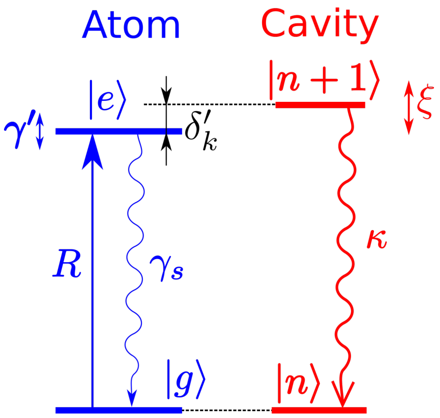

Figure 5.1: Level diagram of a 2-level atom coupled to the cavity field. Here δ'_k is the shift between the cavity and the atomic transition frequency, R is the incoherent pumping rate, γ_s is the spontaneous decay rate, γ' is the dephasing rate of the atom, κ is the energy decay rate of the cavity field, and ξ is the cavity dephasing rate.

describing such a system can be written as

$$\frac{\langle d\hat{O}\rangle}{dt} = \frac{i}{\hbar}\langle[\hat{\mathcal{H}}, \hat{O}]\rangle + \langle\hat{\hat{\mathcal{L}}}[\hat{O}]\rangle. \tag{5.10}$$

The Hamiltonian $\hat{\mathcal{H}}$ in the rotating frame can be written as

$$\hat{\mathcal{H}} = \hbar\left[\delta_c \hat{a}^\dagger\hat{a} + \sum_{j=1}^{N} g_j(\hat{\sigma}^j_{eg}\hat{a} + \hat{a}^\dagger\hat{\sigma}^j_{ge}) + \sum_j \Delta_j \hat{\sigma}^j_{ee}\right], \tag{5.11}$$

were $\hat{a}^\dagger$ and $\hat{a}$ are field creation and annihilation operators, index j runs over the atoms, $\hat{\sigma}^j_{\alpha\beta} = |\alpha^j\rangle\langle\beta^j| \bigotimes_{k\neq j} \hat{\mathbb{1}}^k$ are single-atom transition operators, $|\alpha^j\rangle$ and $|\beta^j\rangle$ run over ground $|g^j\rangle$ and excited $|e^j\rangle$ states of jth atom, g_j is a coupling coefficient between jth atom and the field, Δ_j is the shift of the transition in jth atom caused by some non-homogeneous effects, and δ_c is the shift of the cavity resonance frequency from the frequency of our rotating frame.

The Liouvillian term describing the dissipative process is equal to

$$\hat{\hat{\mathcal{L}}}[\hat{O}] = \kappa\hat{\hat{\mathcal{D}}}[\hat{a}]\hat{O} + \xi\hat{\hat{\mathcal{D}}}[\hat{a}^\dagger\hat{a}]\hat{O} + \sum_{j=1}^{N}\left[\gamma_s\hat{\hat{\mathcal{D}}}[\hat{\sigma}^j_{ge}]\hat{O} + R_j\hat{\hat{\mathcal{D}}}[\hat{\sigma}^j_{eg}]\hat{O} + \gamma'_j\hat{\hat{\mathcal{D}}}[\hat{\sigma}^j_{ee}]\hat{O}\right], \tag{5.12}$$

where $\hat{\hat{\mathcal{D}}}[\hat{p}]\hat{O} = \hat{p}^\dagger\hat{O}\hat{p} - \frac{1}{2}(\hat{p}^\dagger\hat{p}\hat{O} + \hat{O}\hat{p}^\dagger\hat{p})$ is a Lindbladian superoperator. Here κ is the decay rate of the energy of the cavity mode, γ_s is the spontaneous decay rate of the upper lasing state, ξ is the dephasing rate of the cavity field, R_j and γ'_j are the rates of incoherent pumping and dephasing of jth atom.

The closed set of differential equations for the stochastic means of system operators can be written with the help of a cumulant expansion up to the second order and the phase invariance as in [94]

$$\frac{d}{dt}\langle \hat{a}^\dagger \hat{a}\rangle = -\kappa\langle \hat{a}^\dagger \hat{a}\rangle + i\sum_{j=1}^{N} g_j(\langle \hat{\sigma}^j_{eg}\hat{a}\rangle - \langle \hat{a}^\dagger \hat{\sigma}^j_{ge}\rangle), \tag{5.13}$$

$$\frac{d}{dt}\langle \hat{\sigma}^k_{eg}\hat{a}\rangle = -\left[\frac{\kappa'_k}{2} + i\delta'_k\right]\hat{\sigma}^k_{eg} + ig_k\left[\langle \hat{a}^\dagger \hat{a}\rangle(1 - 2\langle \hat{\sigma}^k_{ee}\rangle) - \langle \hat{\sigma}^k_{ee}\rangle\right] - i\sum_{j\neq k} g_j\langle \hat{\sigma}^k_{eg}\hat{\sigma}^j_{ge}\rangle, \tag{5.14}$$

$$\frac{d}{dt}\langle \hat{\sigma}^k_{ee}\rangle = ig_k\left[\langle \hat{a}^\dagger \hat{\sigma}^k_{ge}\rangle - \langle \hat{\sigma}^k_{eg}\hat{a}\rangle\right] - (\gamma_s + R_k)\langle \hat{\sigma}^k_{ee}\rangle + R_k, \tag{5.15}$$

$$\frac{d}{dt}\langle \hat{\sigma}^k_{eg}\hat{\sigma}^l_{ge}\rangle = -\left[\Gamma'_{kl} + i\Delta_{lk}\right]\langle \hat{\sigma}^k_{eg}\hat{\sigma}^l_{ge}\rangle - ig_k\langle \hat{a}^\dagger \hat{\sigma}^l_{ge}\rangle(2\langle \hat{\sigma}^k_{ee}\rangle - 1) + ig_l\langle \hat{\sigma}^k_{eg}\hat{a}\rangle(2\langle \hat{\sigma}^l_{ee}\rangle - 1), \tag{5.16}$$

where $\kappa'_k = \kappa + \xi + R_k + \gamma'_k + \gamma_s$, $\delta'_k = \delta_c - \Delta_k$, $\Gamma'_{kl} = \gamma_s + (R_k + R_l + \gamma'_k + \gamma'_l)/2$ and $\Delta_{lk} = \Delta_l - \Delta_k$. These equations can, in principle, be solved numerically. However, the number of equations scales quadratically with the number of the atoms. For practical simulations of ensembles with tens of thousands of atoms, one needs to group the atoms into M clusters, where all N_j atoms of jth cluster are considered as identical. Also, if the rate κ is much larger than all the evolution rates of atomic polarizabilities, it is convenient to perform an adiabatic elimination of the fast variables $\langle \hat{a}^\dagger \hat{a}\rangle$, $\langle \hat{a}^\dagger \hat{\sigma}_{ge}\rangle$, $\langle \hat{\sigma}_{eg}\hat{a}\rangle$. Then one may express

$$\langle \hat{a}^\dagger \hat{a}\rangle = \left[\kappa - \sum_k \frac{4N_k g_k^2 \kappa'_k}{\kappa'^2_k + 4\delta'^2_k}[2\langle \hat{\sigma}^k_{ee}\rangle - 1]\right]^{-1}$$
$$\times \sum_k \frac{4g_k N_k}{\kappa'^2_k + 4\delta'^2_k}\left[\kappa'_k\left(g_k\langle \hat{\sigma}^k_{ee}\rangle + \sum_j N'_{j,k} g_j \Re(\langle \hat{\sigma}^k_{eg}\hat{\sigma}^j_{ge}\rangle)\right) + 2\delta'_k\left(\sum_j N'_{j,k} g_j \Im(\langle \hat{\sigma}^k_{eg}\hat{\sigma}^j_{ge}\rangle)\right)\right] \tag{5.17}$$

and

$$\langle\hat{\sigma}_{eg}^{k}\hat{a}\rangle = \frac{2}{\kappa_k' + 2i\delta_k'}\left\{ig_k\left[\langle\hat{a}^\dagger\hat{a}\rangle(1-2\langle\hat{\sigma}_{ee}^{k}\rangle) - \langle\hat{\sigma}_{ee}^{k}\rangle\right] - i\sum_j N_{j,k}' g_j\langle\hat{\sigma}_{eg}^{k}\hat{\sigma}_{ge}^{j}\rangle\right\}. \tag{5.18}$$

Here the sums are taken over clusters instead of atoms, N_k is the number of atoms in the cluster, and

$$N_{j,k}' = \begin{cases} N_j, & j \neq k \\ \max(0, N_k - 1), & j = k \end{cases} \tag{5.19}$$

Substituting expressions (5.17) and (5.18) into equations (5.15) and (5.16), and solving them numerically, one can find the steady-state values of $\langle\hat{\sigma}_{eg}^{j}\hat{a}\rangle$ and $\langle\hat{\sigma}_{ee}^{j}\rangle$, if only the atomic dipoles get synchronized. Then one may express the steady-state values of $\langle\hat{a}^\dagger\hat{a}\rangle$, $\langle\hat{\sigma}_{eg}^{j}\hat{a}\rangle$ and $\langle\hat{a}^\dagger\hat{\sigma}_{ge}^{j}\rangle$ with the help of equations (5.17) and (5.18). The output power P of the laser is equal to

$$P = \eta\hbar\omega_0\kappa\langle\hat{a}^\dagger\hat{a}\rangle, \tag{5.20}$$

where η is the relative transmission of the outcoupling mirror, and ω_0 is the angular frequency of the laser radiation.

Finally, let us discuss how to calculate the spectrum of the superradiant laser. According to the Wiener-Khinchin theorem, the spectral density $S_E(f)$ of the signal can be obtained as a real part of Fourier transform of the 2-time correlation function $\mathcal{R}(\tau) = \langle\hat{a}^\dagger(t_0+\tau)\hat{a}(t_0)\rangle$:

$$S_E(f) \propto \mathrm{Re}\int_0^\infty \mathcal{R}(\tau)e^{-2\pi i f\tau}d\tau. \tag{5.21}$$

In an established steady-state regime $\langle\hat{a}^\dagger(t_0+\tau)\hat{a}(t_0)\rangle = \langle\hat{a}^\dagger(\tau)\hat{a}(0)\rangle \equiv \langle\hat{a}^\dagger\hat{a}_0\rangle$, where $\hat{a}^\dagger = \hat{a}^\dagger(t)$, and $\hat{a}_0 = \hat{a}(0)$. To find this function, one needs to solve the set of equations obtained with the help of the quantum regression theorem

$$\frac{d}{dt}\langle\hat{a}^\dagger\hat{a}_0\rangle = -\left[\frac{\kappa+\xi}{2} - i\delta_c\right]\langle\hat{a}^\dagger\hat{a}_0\rangle + i\sum_k N_k g_k\left\langle\hat{\sigma}_{eg}^{k}\hat{a}_0\right\rangle, \tag{5.22}$$

$$\frac{d}{dt}\langle\hat{\sigma}_{eg}^{k}\hat{a}_0\rangle = -\left[\frac{\gamma_s + R_k + \gamma_k'}{2} - i\Delta_k\right]\langle\hat{\sigma}_{eg}^{k}\hat{a}_0\rangle - ig_k\left\langle\hat{\sigma}_z^{k}\right\rangle\langle\hat{a}^\dagger\hat{a}_0\rangle. \tag{5.23}$$

where $\left\langle\hat{\sigma}_z^{k}\right\rangle = \left\langle\hat{\sigma}_{ee}^{k}\right\rangle - \left\langle\hat{\sigma}_{gg}^{k}\right\rangle$. Substituting here the established time-independent values of $\langle \hat{\sigma}_z^k \rangle$ into (5.22) and (5.23) and performing the Laplace transform, one obtains a set of linear equations of the form $(\mathbb{A} + \mathbb{I}\, s) \cdot \mathbb{X} = \mathbb{B}$, where $\mathbb{I}$ is identity matrix,

$$\mathbb{A} = \begin{bmatrix} \frac{\kappa+\xi}{2} - i\delta_c & -iN_1 g_1 & \cdots\ \cdots & -iN_M g_M \\ ig_1 \left\langle \sigma_z^1 \right\rangle & \frac{\gamma+R_1+\gamma_1'}{2} - i\Delta_1 & \cdots 0 \cdots & 0 \\ \vdots & \vdots & \ddots & \vdots \\ ig_M \left\langle \sigma_z^M \right\rangle & 0 & \cdots 0 \cdots & \frac{\gamma+R_M+\gamma_M'}{2} - i\Delta_M \end{bmatrix}, \tag{5.24}$$

$$\mathbb{B} = \begin{bmatrix} \langle \hat{a}^\dagger \hat{a} \rangle_s \\ \langle \hat{\sigma}_{eg}^1 \hat{a} \rangle_s \\ \vdots \\ \langle \hat{\sigma}_{eg}^M \hat{a} \rangle_s \end{bmatrix}, \quad \mathbb{X} = \begin{bmatrix} \mathfrak{L}\{\langle \hat{a}^\dagger \hat{a}_0 \rangle\}(s) \\ \mathfrak{L}\{\langle \hat{\sigma}_{eg}^1 \hat{a}_0 \rangle\}(s) \\ \vdots \\ \mathfrak{L}\{\langle \hat{\sigma}_{eg}^M \hat{a}_0 \rangle\}(s) \end{bmatrix},$$

$\mathfrak{L}\{f\}(s) = \int_0^\infty f(t) e^{-st} dt$ is the Laplace transform, and the subscript s denotes "steady-state". Using the connection between Laplace and Fourier transforms, one can calculate the power spectral density of the bad-cavity laser output

$$S_E(f) \propto \mathrm{Re}\left[\mathfrak{L}\{\langle \hat{a}^\dagger \hat{a}_0 \rangle\}(2\pi i f)\right]. \tag{5.25}$$

From the power spectral density obtained with the help of (5.24) and (5.25), one obtains the lasers's full linewidth at half maximum $\Delta f = \Delta\omega/(2\pi)$.

5.3.2 Homogeneous case: analytic expressions and qualitative considerations

In this section we consider the simplest case of a bad-cavity laser with homogeneous gain, i.e., the situation when all the atoms have the same transition frequency ω_a, pumping and dephasing rate R and γ' and coupling strength g to the cavity field. The steady-state solution and the linewidth for such a simple system in second-order cumulant approximation can be found analytically or semi-analytically. This analysis has been partially performed, for example, in [22], and here we overview the main results and derive a few new useful relations. The correspondence between our notation and notation used there is the following: $R = w$, $\gamma_s = \gamma$, $\gamma' = 2/T_2$, and $g = \Omega/2$.

First, from equations (5.13) – (5.15) one may easily express that in the homogeneous case

$$\langle \hat{a}^\dagger \hat{a} \rangle_s = \frac{N(\gamma_s + R)}{2\kappa} \left(\frac{R - \gamma_s}{R + \gamma_s} - \langle \hat{\sigma}_z \rangle_s \right) \tag{5.26}$$

$$\langle \hat{\sigma}^1_{eg} \hat{\sigma}^2_{ge} \rangle_s = \frac{\langle \hat{\sigma}_z \rangle_s (\gamma_s + R)}{2\Gamma'} \left(\frac{R - \gamma_s}{R + \gamma_s} - \langle \hat{\sigma}_z \rangle_s \right), \tag{5.27}$$

where $\Gamma' = \gamma_s + R + \gamma'$, $\kappa' = \kappa + \xi + \Gamma'$. Substituting these expressions into equation (5.17), one may obtain, after some algebra, the following quadratic equation for $\langle \hat{\sigma}_z \rangle_s$:

$$\begin{aligned} \langle \hat{\sigma}_z \rangle_s^2 \left(\frac{N(\gamma_s + R)}{2\kappa} + \frac{(N-1)(\gamma_s + R)}{2\Gamma'} \right) + \frac{(R - \gamma_s)(\kappa'^2 + 4(\delta_c - \Delta)^2)}{8g^2\kappa'} - \frac{1}{2} \\ - \langle \hat{\sigma}_z \rangle_s \left[\frac{(R + \gamma_s)(\kappa'^2 + 4(\delta_c - \Delta)^2)}{8g^2\kappa'} + \frac{1}{2} + \frac{(R - \gamma_s)}{2} \left(\frac{N}{\kappa} + \frac{N-1}{\Gamma'} \right) \right] = 0. \end{aligned} \tag{5.28}$$

Solving this equation, we obtain the steady-state values $\langle \hat{\sigma}_z \rangle_s$, as well as $\langle \hat{a}^\dagger \hat{a} \rangle_s$ and $\langle \hat{\sigma}^1_{eg} \hat{\sigma}^2_{ge} \rangle_s$ with the help of (5.26) and (5.27).

Further in this Section we suppose, for the sake of simplicity, that all the atoms are in resonance with the cavity ($\delta_c = \Delta = 0$), and that the cavity dephasing rate ξ is negligible ($\xi = 0$). Then the equation (5.28) simplifies to

$$\begin{aligned} \langle \hat{\sigma}_z \rangle_s^2 \left(\frac{N(\gamma_s + R)}{2\kappa} + \frac{(N-1)(\gamma_s + R)}{2\Gamma'} \right) + \frac{(R - \gamma_s)\kappa'}{8g^2} - \frac{1}{2} \\ - \langle \hat{\sigma}_z \rangle_s \left[\frac{(R + \gamma_s)\kappa'}{8g^2} + \frac{1}{2} + \frac{(R - \gamma_s)}{2} \left(\frac{N}{\kappa} + \frac{N-1}{\Gamma'} \right) \right] = 0. \end{aligned} \tag{5.29}$$

Consider the equation (5.29). First, taking $N \approx N - 1$ and neglecting γ_s, R and g in comparison with κ, one may express its approximate solutions as

$$\langle \hat{\sigma}_z \rangle_{s,1} \approx \frac{\kappa\Gamma'}{4g^2N}, \quad \langle \hat{\sigma}_z \rangle_{s,2} \approx \frac{R - \gamma_s}{R + \gamma_s}, \tag{5.30}$$

and only the first solution gives $\langle \hat{a}^\dagger \hat{a} \rangle_s \neq 0$. This solution allows us to estimate the lasing thresholds. Substituting (5.30) into (5.26), one may find that lasing is possible, i.e., $\langle \hat{a}^\dagger \hat{a} \rangle_s > 0$, only if

$$\frac{R - \gamma_s}{R + \gamma_s} > \frac{\kappa(\gamma_s + R + \gamma')}{4g^2N} = \frac{\gamma_s + R + \gamma'}{NC\gamma_s}, \tag{5.31}$$

where we have introduced the cooperativity parameter $C = 4g^2/(\kappa\gamma_s)$, in order to find limits of the pumping rate R:

$$\begin{aligned} R_{\min} &= \frac{NC\gamma_s - \gamma' - \sqrt{(NC\gamma_s - \gamma')^2 - 8\gamma_s^2 NC}}{2} - \gamma_s, \\ R_{\max} &= \frac{NC\gamma_s - \gamma' + \sqrt{(NC\gamma_s - \gamma')^2 - 8\gamma_s^2 NC}}{2} - \gamma_s. \end{aligned} \tag{5.32}$$

With $\gamma_s, \gamma' \ll NC\gamma_s$ it gives

$$\begin{aligned} R_{\min} &\approx \gamma_s \frac{NC\gamma_s + \gamma'}{NC\gamma_s - \gamma'}, \\ R_{\max} &\approx NC\gamma_s - \gamma', \end{aligned} \tag{5.33}$$

in correspondence with [95].

The spectrum for the homogeneous case can be found from the set of linear equations (5.22) and (5.23) where, instead of performing the Laplace transform of the solution, we can just calculate $\Delta\omega$ as $\Delta\omega = 2|\lambda|$. Here λ is the eigenvalue with smallest absolute value of the matrix of this system (which can be easily proven by Fourier transform of exponentially decaying term in $\langle \hat{a}^\dagger \hat{a}_0 \rangle$). Taking $\kappa \gg |\lambda|$, one may express

$$\Delta\omega = \Gamma' - \frac{4g^2 N \langle \hat{\sigma}_z \rangle_s}{\kappa}. \tag{5.34}$$

One may see that to calculate the linewidth one has to go beyond the semiclassical approximation: indeed, an attempt to substitute $\langle \hat{\sigma}_z \rangle_{s,1}$ from (5.30) into (5.34) gives $\Delta\omega = 0$. The straightforward way to calculate $\Delta\omega$ is to solve the quadratic equation (5.29) exactly, however, the result occurs to be too bulky for simple qualitative analysis. Instead, we calculate a correction to the approximate solution (5.30), expanding the coefficients of equation (5.29) into Fourier series. After some algebra we get

$$\Delta\omega \approx \frac{\Gamma'(\Gamma' + NC\gamma_s)}{2\langle \hat{a}^\dagger \hat{a} \rangle_s \kappa} - \frac{\Gamma'}{N}. \tag{5.35}$$

In the limit $\gamma_s, \gamma' \ll R \ll NC\gamma_s$ it gives $\Delta\omega \approx C\gamma_s$. This result has been reported in [22] as a minimum attainable linewidth at given cooperativity C. We can not, however, take C arbitrary small, otherwise we get into situation where $R_{\min} > R_{\max}$, and lasing becomes impossible. The minimum value of C, above which the lasing is still possible, can be found from equalizing R_{min} and R_{max} in (5.32), which gives

$$(NC_{\text{min}}\gamma_s - \gamma')^2 = 8NC_{\text{min}}\gamma_s^2. \tag{5.36}$$

At $\gamma' = 0$ this minimum value is $C_{\text{min}} = 8/N$. Moreover, at very small C the condition $\gamma_s, \gamma' \ll R \ll NC\gamma_s$ also can not be fulfilled, and the optimal value of C, where the minimum linewidth is attained, is larger than (but proportional to) C_{min}.

We can conclude that the minimum attainable linewidth $\Delta\omega_{\text{min}}$ is proportional to γ_s/N. Therefore, it is convenient to express $\Delta\omega$ in units of γ_s/N as a function of CN. Also, from expressions (5.26) and (5.30) we note that the dimensionless value $\langle\hat{a}^\dagger\hat{a}\rangle\kappa/(N\gamma_s)$ does not depends on κ and N at given values of CN, R/γ_s and γ'/γ_s.

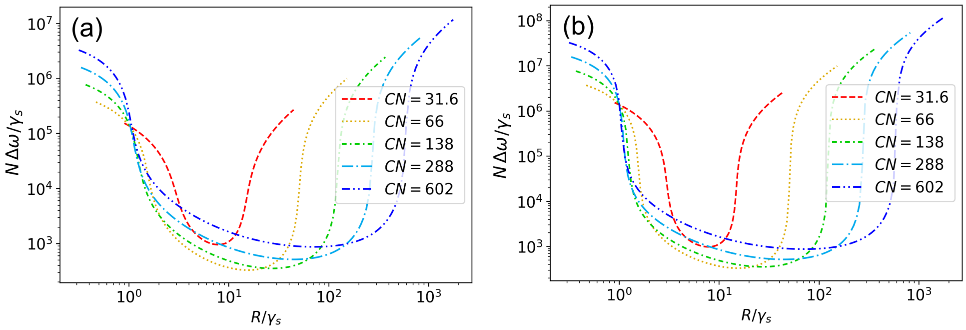

Figure 5.2: Dependency of linewidth $\Delta\omega$ on repumping rate R for a homogeneous system at different values of CN for different values of number N of atoms and finesse $\mathcal{F}$ of the cavity. (a): $N = 10^4$, $\mathcal{F} = 10^4$. (b): $N = 10^5$, $\mathcal{F} = 10^5$. In both cases the atomic dephasing rate is $\gamma' = 0.1\ \text{s}^{-1}$ and the cavity length is $l_{\text{cav}} = 10$ cm, which corresponds to $\kappa = \pi c/(\mathcal{F} l_{\text{cav}}) \approx 9.4 \times 10^5\ \text{s}^{-1}$ and $\kappa \approx 9.4 \times 10^4\ \text{s}^{-1}$ respectively.

5.3.3 Minimized linewidth

In this subsection we investigate in more details the dependence of the optimized spectral linewidth $\Delta\omega$ on various parameters of the superradiance laser. First, we consider the homogeneous case. In Figure 5.2 we present the linewidth $\Delta\omega$ for different values of CN as function of incoherent repumping rate R, calculated according to the method described in subsection 5.3.2. One may see that, being expressed in units of γ_s/N, all the linewidths show a quite similar behavior, except near the lower and the upper lasing thresholds.

For any of the curves, similar to the ones presented in Figure 5.3, we can find

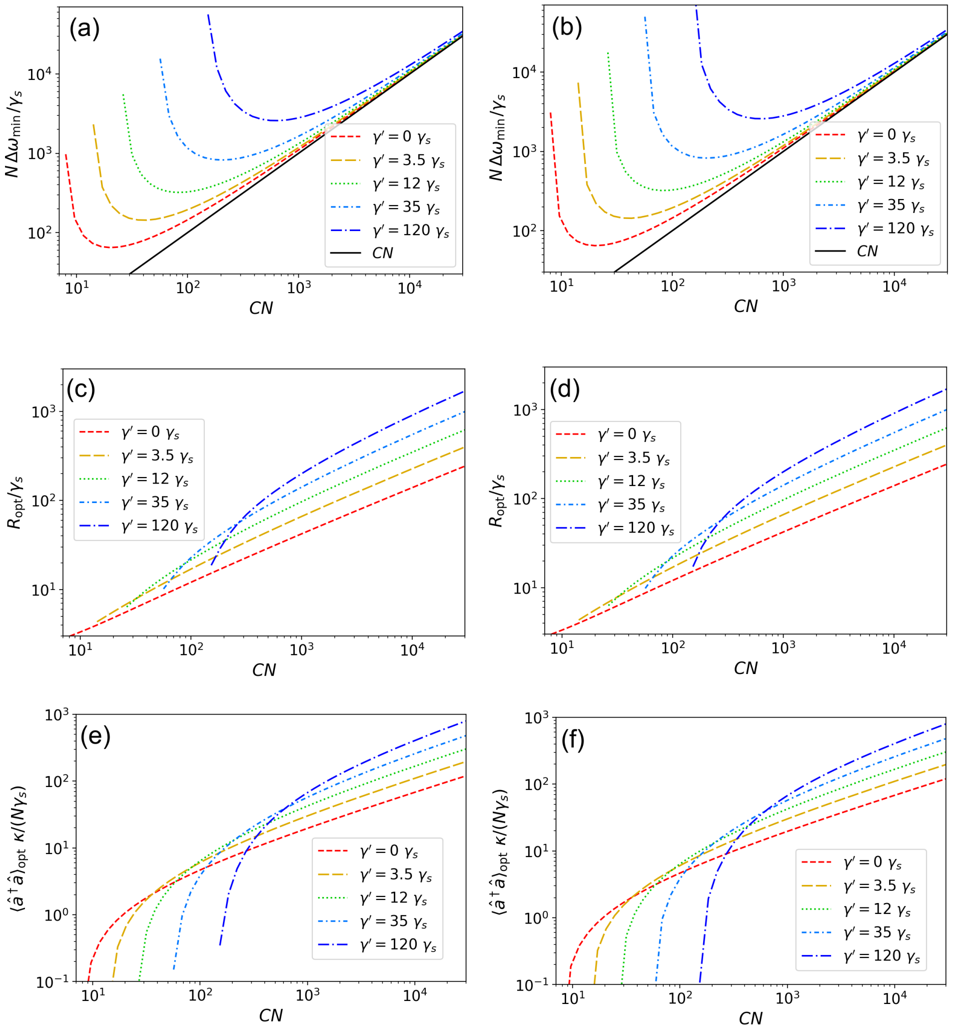

Figure 5.3: Dependency of minimum attainable linewidth $\Delta\omega_{\min}$, the optimal repumping rate R_{opt} in units of γ_s ((c),(d)), and the respective intracavity photon number $\langle \hat{a}^\dagger \hat{a} \rangle_{\text{opt}}$ multiplied by $\kappa/(N\gamma_s)$ ((e),(f)) on the parameter CN for different values of atomic dephasing γ'. The graphs are for different values of number N of atoms and finesse $\mathcal{F}$ of the cavity: (a, c, e): $N = 10^4$, $\mathcal{F} = 10^4$. (b, d, f): $N = 10^5$, $\mathcal{F} = 10^5$. In (a) and (b) the asymptotic CN behavior is indicated by a black line.

the minimum linewidth $\Delta\omega_{\min}$, obtained at some optimal repumping rate R_{opt}. In Figure 5.3 we present the dependency of these minimized linewidths on CN for different values of the atomic dephasing rate γ', number N of the atoms and the cavity finesse $\mathcal{F}$. Note that the value $\Delta\omega_{\min}$ expressed in units γ_s/N as well as the optimal repumping rate R_{opt} does not depend on N (i.e. the optimized linewidth $\Delta\omega_{\min}$ is inversely proportional to N at a given value of CN). Similarly, the ratio of $\langle \hat{a}^\dagger \hat{a} \rangle \cdot \kappa$ to $N\gamma_s$ corresponding to the minimized linewidth as well as the optimal repumping rate R_{opt} depend on the atomic dephasing rate γ' but not on $\mathcal{F}$ or N. In this example the cavity length l_{cav} has been taken as $l_{\text{cav}} = 10$ cm, although the results are not sensitive to variations of the cavity length as long as the laser operates in the bad-cavity regime, as discussed in section 5.4.

We should also note that the value $\langle \hat{a}^\dagger \hat{a} \rangle \cdot \kappa/(N\gamma_s)$ has a simple physical interpretation: it is the ratio of number of photons emitted from the cavity mode (in case of perfect outcoupling mirror $\eta = 1$) to the single-atom spontaneous emission rate γ_s multiplied by the number of atoms. Near the maximum of the output power this ratio is proportional to N, however, near the minimum of the linewidth it is independent on N. In the absence of atomic dephasing, the minimum attainable linewidth (optimized by both the repumping rate R and the cooperativity C) is about $\Delta\omega_{opt} \approx 64\gamma_s/N$.

Up to now we calculated the linewidths in the frame of a fully homogeneous model. However, in real systems different atoms may expect different level shifts, they may expect different dephasings due to interaction with environment, and different pumping rates. Last but not least, different atoms can be coupled differently with the superradiance cavity field. This happens particularly when the atoms trapped within the magic optical lattice created inside the superradiance cavity are coupled to the standing-wave mode of the same cavity, because of the mismatch of the magic wavelength trapping the atoms and the wavelength of the superradiance mode, see expression 5.43 in section 5.4. The spectral linewidth of the superradiance radiation can be calculated using the method described in subsection 5.3.1.

In Figure 5.4 we present the dependencies of the minimum attainable linewidth $\Delta\omega_{\text{min}}$ and the intracavity photon number $\langle \hat{a}^\dagger \hat{a} \rangle$ on cooperativity CN, calculated for repumping rates R_{opt} which minimise the linewidth. We grouped the atoms into $M = 21$ cluster containing equal numbers of atoms. Coupling coefficients g_j for jth cluster were taken proportional to $\cos(\frac{\pi(j-0.5)}{2M})$; all the other parameters are the same for all the clusters, also $\Delta_j = \delta_c = \xi = 0$. The cooperativity C is defined according to

$$CN = \sum_j \frac{4g_j^2}{\kappa\gamma_s}. \tag{5.37}$$

For comparison, we present the dependencies of $\Delta\omega_{\text{min}}$ and $\langle \hat{a}^\dagger \hat{a} \rangle_{\text{opt}}$ calculated according to the homogeneous model. One can see that the homogeneous model slightly

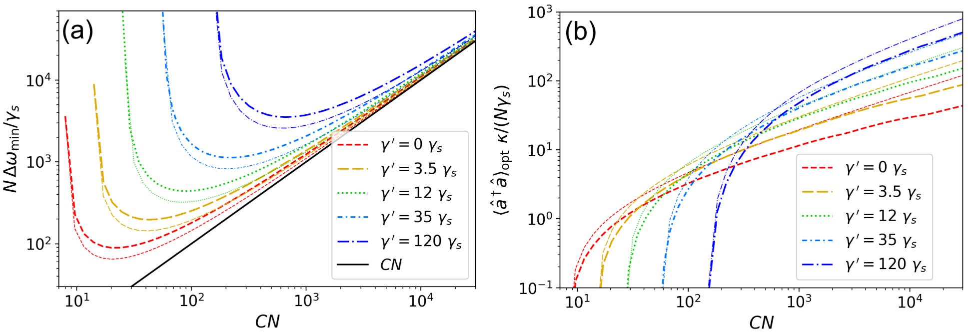

Figure 5.4: Dependency of minimum attainable linewidth $\Delta\omega_{\min}$ in units of γ_s/N (a), and the respective intracavity photon number $\langle\hat{a}^\dagger\hat{a}\rangle_{\rm opt}$ multiplied by $\kappa/(N\gamma_s)$ (b) on the parameter CN for a system with inhomogeneous cosine-modulated coupling (thick curves) system for different values of atomic dephasing rate γ' at $N = 10^5$, $\mathcal{F} = 10^5$. The cavity length is $l_{\rm cav} = 10$ cm. Thin curves represent the linewidths and the intracavity photon numbers calculated according to the homogeneous model, the same color and style corresponds to the same value of γ'.

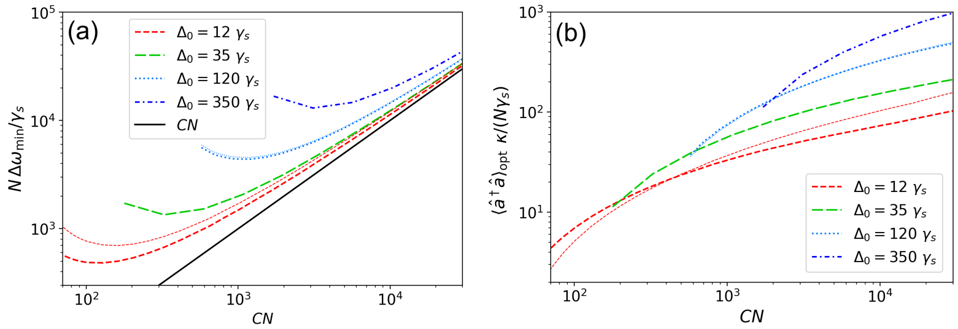

Figure 5.5: Dependency of minimum attainable linewidth $\Delta\omega_{\min}$ in units of γ_s/N (a), and the respective intracavity photon number $\langle\hat{a}^\dagger\hat{a}\rangle_{\rm opt}$ multiplied by $\kappa/(N\gamma_s)$ (b) on the parameter CN for a system with inhomogeneous cosine-modulated coupling for different values of broadening Δ_0 at $N = 10^5$, $\mathcal{F} = 10^5$. The atomic dephasing rate is $\gamma' = 0$ (thick curves), and $\gamma' = 12\gamma_s$ (thin curves; only for $\Delta_0 = 12\gamma_s$ and $\Delta_0 = 120\gamma_s$, the same color-style encoding corresponds to the same values of Δ_0). The cavity length is $l_{\rm cav} = 10$ cm.

underestimates the attainable linewidth and overestimates the intracavity photon number, both by a factor of about 1.4 near the optimally chosen CN. Particularly, at $\gamma' = 12\gamma_s$ the minimum linewidth s $\Delta\omega \approx 4.3\times10^2\ \gamma_s/N$ for inhomogeneous coupling, and $\Delta\omega \approx 3.1\times10^2\ \gamma_s/N$ for homogeneous coupling.

Figure 5.5 shows the minimised linewidth $\Delta\omega_{\mathrm{min}}$ for a system where not only the coupling of the atoms to the cavity mode is inhomogeneous, but also the lasing transitions in different atoms have different shifts Δ_j. Such shifts can be caused by variations of environmental parameters over the atomic ensemble. Here we considered the simplest case where the atomic detunings Δ_j are evenly distributed over 11 clusters between $\pm\Delta_0$, and the couplings are also distributed over 7 clusters; therefore we have 77 clusters in total. At $\gamma' = \Delta_0 = 12\gamma_s$ the minimum attainable linewidth $\Delta\omega_{\mathrm{min}} \approx 7 \times 10^2\ \gamma_s/N$, whereas increasing Δ_0 to 120 γ_s would increase the linewidth to about $\Delta\omega_{\mathrm{min}} \approx 4.65 \times 10^3\ \gamma_s/N$.

Finally, it is useful to consider the dependence of the linewidth $\Delta\omega_{\mathrm{opt}}$ - doubly minimized both in R and CN - on the dephasing rate γ' and on the inhomogeneous broadening Δ_0. By fitting the result of the simulations we obtain the estimated linewidth in the form

$$\Delta\omega_{\mathrm{opt}} \approx (90\gamma_s + 30\gamma' + 35\Delta_0)/N. \tag{5.38}$$

Expressing the linewidth via the more useful dispersion of the shifts $\Delta_0' = \Delta_0/\sqrt{3}$ for the flat distribution assumed in the simulations, gives approximately

$$\Delta\omega_{\mathrm{opt}} \approx (90\gamma_s + 30\gamma' + 60\Delta_0')/N \tag{5.39}$$

Similarly one can find approximate expressions for the optimal pumping rate R_{opt}, for the collective cooperativity CN_{opt}, and for the intracavity photon number, where the smallest linewidth $\Delta\omega_{\mathrm{opt}}$ is achieved:

$$R_{\mathrm{opt}} \approx 5\gamma_s + 1.13\gamma' + 1.5\Delta_0' \tag{5.40}$$

$$CN_{\mathrm{opt}} \approx 25 + 5.5\frac{\gamma'}{\gamma_s} + 20\frac{\Delta_0'}{\gamma_s} \tag{5.41}$$

$$\langle \hat{a}^\dagger \hat{a} \rangle_{\mathrm{opt}} \approx \frac{N}{\kappa}\left(0.9\gamma_s + 0.25\gamma' + 1.45\Delta_0'\right) \tag{5.42}$$

5.4 Estimation of attainable stability

To perform quantitative estimations, we need to consider realistic parameters of the atomic ensemble. The double forbidden ${}^1S_0 \leftrightarrow {}^3P_0$ transition (clock transition) in fermionic isotopes of alkaline-earth-like atoms (Be, Mg, Ca, Sr, Zn, Cd, Hg and Yb) seems to be a good choice for optical clocks with neutral atoms. This transition is totally forbidden in bosonic isotopes and becomes slightly allowed in fermionic isotopes by hyperfine mixing. These atoms can be trapped in a the magic-wavelength optical lattice potential and pumped into the upper $^3P_0$ lasing state. In an active optical clock the clock transition should be coupled to a high-finesse cavity in the strong cooperative coupling regime, which is problematic for wavelengths of about 458 nm (corresponding to clock transition in Mg) and shorter. Therefore, Ca, Sr and Yb with wavelengths of the clock transition λ equal to 660, 698 and 578 nm, respectively, are the most feasible candidates for the role of gain atoms in active optical clocks. In the present paper we will primarily perform our estimations for the ^{87}Sr isotope, because, first, this element is the most used one in modern optical clocks with neutral atoms and its relevant characteristics are the most studied among all the alkaline-earth-like atoms. Second, the natural linewidth of the clock transition in ^{87}Sr ($\gamma_\mathrm{s} = 8.48 \times 10^{-3}$ s^{-1} [96]) lies between the linewidths of ^{43}Ca (2.2×10^{-3} s^{-1}) and Yb (43.5×10^{-3} s^{-1} and 38.5×10^{-3} s^{-1} for ^{171}Yb and ^{173}Yb respectively) [97].

The finesse $\mathcal{F}$ of the best cavities at a wavelength of 698 nm can reach values of up to 10^6, however, it is quite difficult to build such a cavity. More feasible finesse values would range from tens to hundreds of thousands. For the sake of definiteness, we take $\mathcal{F} = 10^5$ as a typical parameter.

The coupling strengths g_j between the lasing transition in the jth atom and the cavity field can be estimated as

$$g_j \approx \frac{1}{w_c}\sqrt{\frac{6c^3\gamma_s}{l_\mathrm{cav}\omega_0^2}}\cos(k_0 z_j), \tag{5.43}$$

where $k_0 = \omega_0/c$ is the wave number of the cavity mode, w_c is the cavity waist radius, and z_j is the z-coordinate of the jth atom along the cavity axis [98]. For the sake of simplicity, here we neglect the dependency of the coupling strength g on the distance from the atom to the cavity axis proportional to $\exp(-(x_j^2 + y_j^2)/w_c^2)$ (which can be relevant for atoms trapped in 2D or 3D optical lattices as well as for relatively hot atomic ensembles in shallow 1D optical lattice). Note that the cooperativity $C = 4\sum_j g_j^2/(N\kappa\gamma_s)$ does not depend on the length of the cavity l_cav but only on the cavity finesse $\mathcal{F}$ and the cavity mode waist w_c, because both g_j^2 and κ are inversely proportional to l_cav. Therefore, the cavity length l_cav is not a very important parameter, as long as the energy decay rate $\kappa = \pi c/(l_\mathrm{cav}\mathcal{F})$ of the cavity mode is much larger than the linewidth of the laser gain. For the calculations performed in section 5.3 we take $l_{\text{cav}} = 10$ cm, which corresponds to a decay rate $\kappa = 9.42 \times 10^4\ \text{s}^{-1} \approx 2\pi \times 15$ Hz at $\mathcal{F} = 10^5$.

Let us first compare the ultimate stability of an incoherently pumped active optical frequency standard with the stability of a quantum projection noise (QPN) limited passive frequency standard, assuming the same number of trapped atoms in both standards and no inhomogeneous broadening or decoherence. The fundamental limit of the superradiant laser linewidth is then $\Delta\omega \approx 90\ \gamma_s/N$, as follows from expression (5.39). This corresponds to a short-term stability

$$\sigma_{y,\text{lim}}(\tau) \approx \frac{1}{\omega}\sqrt{\frac{90\gamma_s}{N\tau}} \approx \frac{9.5}{\omega}\sqrt{\frac{\gamma_s}{N\tau}}. \tag{5.44}$$

For passive optical clocks the quantum projection noise limited stability $\sigma_{y,\text{QPN,Rams}}$ and $\sigma_{y,\text{QPN,Rabi}}$ for Ramsey and Rabi interrogation schemes respectively can be estimated as [37, 86]

$$\sigma_{y,\text{QPN,Rams}}(\tau) = \frac{1}{\omega\sqrt{NT_p\tau}}, \tag{5.45}$$

$$\sigma_{y,\text{QPN,Rabi}}(\tau) \approx \frac{1.69}{\omega\sqrt{NT_p\tau}}, \tag{5.46}$$

if the total Rabi or Ramsey interrogation time T_p is much longer than all the other durations required for state preparation and measurement, and if it is much shorter than the excited state lifetime $1/\gamma_s$. Comparing equations (5.44) with (5.45) and (5.46) one may see that at the same atom number the ultimate stability (5.44) attainable with an active optical clock with incoherent pumping can be matched by the QPN limited stability of a passive clock, at interrogation times of $T_p = 1/(90\,\gamma_s) \approx 0.011/\gamma_s$ for Ramsey, and at $T_p = 1.69^2/(90\,\gamma_s) \approx 0.032/\gamma_s$ for Rabi interrogation. For clocks using ^{87}Sr these times are $T_p = 1.31$ s for Ramsey, and $T_p = 3.74$ s for Rabi interrogation. For the $^1S_0 \leftrightarrow {}^3P_0$ transition in ^{173}Yb the corresponding times are 0.25 s and 0.72 s respectively, and for ^{43}Ca 5.05 s and 14.4 s .

A more realistic comparison between the achievable stability of the active and passive optical frequency standards must include additionally dephasing of the atomic transition, as well as imperfections of the local oscillator in a passive clock . The transverse dephasing rate $\gamma' = 2/T_2$ of the atomic transition is limited by Raman scattering of photons from the optical lattice potential [99], and by site-to-site tunneling of the atoms [100]. In a shallow cubic 3D optical lattice with ^{87}Sr [101] an optimized coherence time $T_2 \approx 10$ s was achieved, which corresponds to $\gamma' \approx 0.2$ s^{-1}. This decoherence time may be even further reduced with the help of technically more challenging setups , such as using of optical lattices with increased lattice constants formed, for example, by interfering laser beams at different angles or by optical tweezer arrays [101] . Moreover, collisions with residual background gas also destroy the coherence and reduce the trap lifetime. From this point of view, $\gamma' = 0.2$ s^{-1} seems to be a good estimate for the minimum atomic decoherence rate that can be achieved without extraordinary efforts. Assuming an inhomogeneous broadening Δ_0 of the atomic ensemble of $\Delta_0 \approx 2\pi \times 15$ mHz ≈ 0.09 s^{-1}, one may estimate the optimized linewidth $\Delta\omega_{\text{opt}}$ of the superradiance laser as $\Delta\omega_{\text{opt}} \approx 10/N$ s^{-1}, corresponding to a stability of a ^{87}Sr active clock

$$\sigma'_y(\tau) = \frac{1}{\omega}\sqrt{\frac{\Delta\omega}{\tau}} \approx \frac{1.17 \times 10^{-15}}{\sqrt{N\,\tau}}. \tag{5.47}$$

For $N = 10^4$ it results in an instability of 10^{-17} at 1 s of averaging, and of 10^{-18} after 100 seconds, whereas a bad-cavity laser with $N = 10^5$ atoms would provide an instability of $\sigma'_y(\tau) \approx 3.7 \times 10^{-18}/\sqrt{\tau[\text{s}]}$.

Let us now compare this stability with the one that can be attained in a passive clock with the same number of atoms. An ideal quantum projection noise-limited, zero dead time, passive ^{87}Sr optical clock can attain such a stability at interrogation times of $T_p = 0.1$ s for Ramsey, and $T_p = 0.29$ s for Rabi interrogation, as follows from equations (5.45) and (5.46). These interrogation times are short compared to the inverse inhomogeneous broadening and to the decoherence time of the atomic ensemble as estimated above, thus, these effects would not yet limit the passive clock. However, in a passive optical clock based on the sequential discontinuous interrogation of the clock transition in single atomic ensembles, the frequency fluctuations of the local oscillator contribute substantially to the instability due to the Dick effect [102].

For example, in ref. [37] the contribution to instability $\sigma_{y,\text{Dick}}$ from this Dick effect was on the level of $\sigma_{y,\text{Dick}} \approx 3.8 \times 10^{-17}/\sqrt{\tau[\text{s}]}$ (see Fig. 5.7). Such a level of stability has been obtained with a local oscillator laser pre-stabilized to an elaborate 21 cm cryogenic silicon resonator at 124 K. The bad cavity laser can provide similar stability at a linewidth $\Delta\omega \approx 0.01$ s^{-1}, that can be attained with $N = 10^4$ atoms and a dephasing rate $\gamma' \approx 1.5$ s^{-1}, or with $N = 10^5$, $\gamma' \approx 5$ s^{-1} ($T_2 = 2/\gamma' = 0.4$ s), if the inhomogeneous broadening Δ'_0 is much less than the dephasing rate. Therefore,

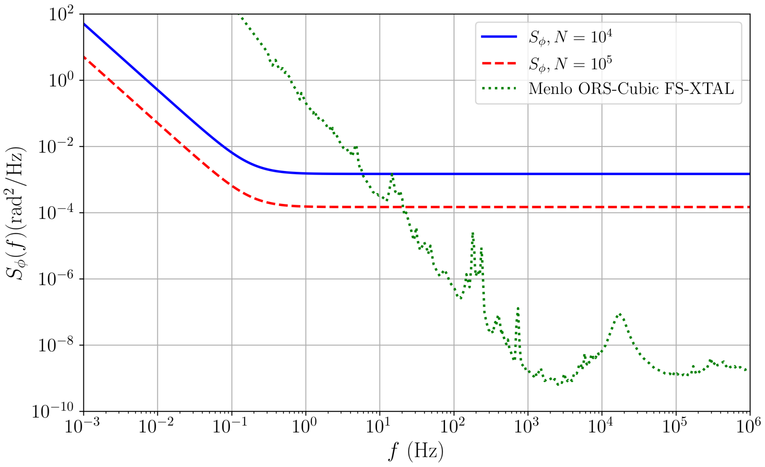

Figure 5.6: Spectral power density of phase fluctuations S_ϕ for an active clock with 10^4 atoms (blue line), 10^5 atoms (dashed red line) and for a commercial cavity stabilized laser (green dash-dotted line)

the short-term stability of an active optical frequency standard may match and even significantly exceed the stability of passive clocks limited to the noise of local oscillator via the Dick effect. On the other hand, the quantum projection noise-limited stability of a passive clock based on a similar atomic ensemble can be still better than the one of the passive standard.

We should note, that the Dick effect in passive optical clocks can be avoided (or at least significantly suppressed down to contributions of finite-length $\pi/2$ pulses) by an interleaved, zero dead time operation of two clocks [103]. When comparing two clocks using the same atomic transition, the Dick effect can also be eliminated and the interrogation time extended to beyond the coherence time of the laser by using synchronous interrogation [37, 103, 104] of the two atomic ensembles. In the extreme case, comparing different parts of the same cloud, a fractional instability of $\sigma_y \approx 4 \times 10^{-18}/\sqrt{\tau[\mathrm{s}]}$ could been achieved [105]. Similarly, comparing clocks on operating on different atomic transitions, differential spectroscopy [106] or dynamical decoupling methods [107] can be employed.

At the optimum stability the output power P of the bad cavity laser amounts to a photon flux of $P/\hbar\omega_0 = \eta\kappa\langle\hat{a}^\dagger\hat{a}\rangle \approx \eta N(0.9\gamma_s + 0.25\gamma' + 1.45\Delta_0')$, see expressions (5.20) and (5.42). Taking $\eta = 0.5$ and parameters of the atomic ensemble listed above ($\gamma_s = 8.48 \times 10^{-3}$ s$^{=1}$, $\gamma' = 0.2$ s$^{=1}$ and $\Delta_0' = \Delta_0/\sqrt{3} \approx 0.054$ s^{-1}), the photon flux at

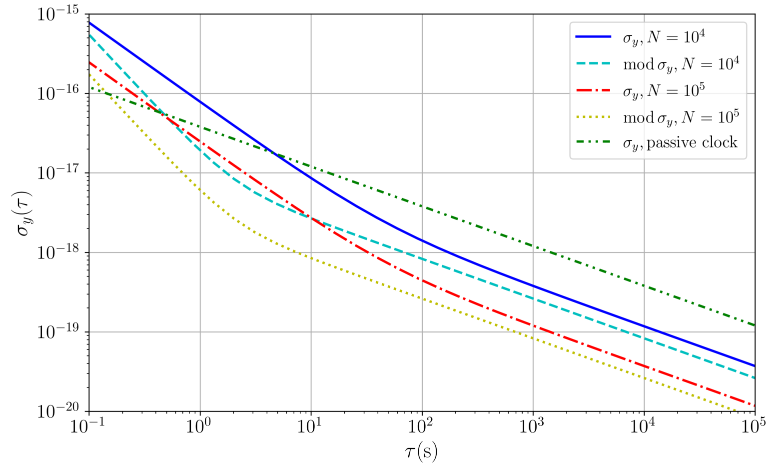

Figure 5.7: Stability of the ^{87}Sr active clock output expressed as Allan deviation σ_y with $f_h = 10$ Hz for $N = 10^4$ (blue solid line) and $N = 10^5$ (red dash-dotteded line). The corresponding modified Allan deviation mod σ_y is shown by the cyan dotted line and the yellow dotted line. The different slopes are due to contributions from photon shot noise and atomic phase diffusion. For comparison, the stability of a Dick effect limited passive clock as discussed in the text is shown as green dash-dot-dot line.

the optimized cooperativity and pumping rate will be about 680 s^{-1} for $N = 10^4$ and 6800 s^{-1} for $N = 10^5$.

This output power of the active clock is usually too small for practical application, thus a suitable secondary laser needs to be phase locked to the weak output to boost the available power. The bandwidth of this phase-lock depends on the stability of the (shot noise limited) active clock and the stability of the free running secondary laser. In Fig. 5.6 the phase noise of the superradiant laser output for 10^4 and 10^5 atoms is shown in comparison to the phase noise of a commercial laser system, based on a 5 cm long cubic cavity (Menlo Systems OFR-cubic FS-XTAL [108]) with fractional frequency instability $\text{mod}\,\sigma \approx 10^{-15}$. For best overall performance, the bandwidth should extend up to the crossing between the phase noise curves of the secondary laser and of the superradiant laser. In the example shown here this crossing is around 10 Hz in agreement with our previous choice of a 10 Hz cut-off frequency f_h for the white phase noise contribution to the Allan deviation.

The Allan deviations for the superradiant laser output are shown in Fig. 5.7. Including the phase locked laser would only cap the strong increase of the stability towards short averaging times and limit the instability to values of 10^{-15} below 0.1 s.

Besides the fundamental limit to the stability from the superradiant laser's linewidth, also the stability of the active clock may degrade due to a drift or fluctuations of the environmental parameters, such as the bias magnetic field. For example, the Zeeman shift of the π-transition $|^3P_0, m\rangle \rightarrow |^1S_0, m\rangle$ in ^{87}Sr amounts to about $\Delta\omega/B = 2\pi \cdot 1.10$ Hz/μT $\cdot\, m_F$ [109], that results in a shift of about $2\pi \times 4.95$ Hz/μT for transition between the two stretched states $|^3P_0, m = 9/2\rangle$ and $|^1S_0, m = 9/2\rangle$. For example, to attain a 10^{-18} level of relative uncertainty of the clock transition frequency, one has to decrease the uncertainty of the bias magnetic field to below 87 pT. In passive clocks the linear Zeeman effect is usually canceled by taking the average between Zeeman transitions with opposite shifts alternating from one interrogation cycle to the other. This method eliminates drifts and slow fluctuations of the bias magnetic field but can not cancel fluctuations on timescale below a single interrogation cycle duration. In contrast, active clocks may operate on two Zeeman transitions simultaneously, generating two-frequency laser radiation from both π-transitions between pairs of stretched states $|^3P_0, m = 9/2\rangle \rightarrow |^1S_0, m = 9/2\rangle$ and $|^3P_0, m = -9/2\rangle \rightarrow |^1S_0, m = -9/2\rangle$. The arithmetic mean of both these frequencies will be robust to fluctuations of the first-order Zeeman shift, as well as of a vector Stark shift from the lattice field. Both transitions can contribute independently to lasing, if they both interact with the same mode of the cavity and if they are detuned from each over far enough to neither get synchronized nor significantly affect each other. This condition can be easily attained under realistic conditions: for example, a bias magnetic field $B = 1$ G $= 0.1$ mT splits these two transitions by about $2\pi \times 1$ kHz. This splitting is less than the linewidth κ of the cavity (estimated above as $\kappa \approx 2\pi \times 15$ kHz at $l_{\text{cav}} = 10$ cm and $\mathcal{F} = 10^5$), but it is much larger than the optimized pumping rate $R_{\text{opt}} \approx 0.35$ s^{-1} [95, 110], as estimated from equation (5.40).

5.5 Conclusion

In this paper we studied the ultimate frequency stability that can be obtained with active optical frequency standards. We investigated the dependence of the linewidth of a bad-cavity laser with incoherent pumping on its parameters and obtained an estimated minimum linewidth (Eq. 5.38) under optimized conditions. We showed that the instability $\sigma_{y,\text{Dick}} \approx 3.8 \times 10^{-17}/\sqrt{\tau[\text{s}]}$ of a passive optical frequency standard associated with the Dick effect for one of the best local oscillators pre-stabilized to a cryogenic Si cavity [37] can be matched by a bad-cavity laser with $N = 10^5$ ^{87}Sr atoms with coherence time $T_2 \approx 0.4$ s. As active optical frequency standards are not degraded by the Dick effect associated with dead time and noises of the local oscillator, they can outperform "traditional" passive optical frequency standards in stability. Also, active optical frequency standard may play a role as local oscillators in future passive optical clocks. Even if their short-term stability is poorer by small factor than the quantum projection noise limited stability of a passive optical clock with a similar number of clock atoms, the stability can still be significantly better than that of a good-cavity laser pre-stabilized to an ultra-stable cavity, as used in modern passive optical clocks.

Acknowledgment

We acknowledge support by Project 17FUN03 USOQS, which has received funding from the EMPIR programme cofinanced by the Participating States and from the European Unionâs Horizon 2020 Research and Innovation Programme, by the European Union Horizon 2020 research and innovation programme Quantum Flagship projects No 820404 "iqClock", No 860579 "MoSaiQC", Narodowe Centrum Nauki (Quantera Q-Clocks 2017/25/Z/ST2/03021) and SFB 1227 DQ-mat, Project-ID 274200144, within Project B02.

Numerical simulations were performed with the open source frameworks DifferentialEquations.jl [81]. The graphs were produced using the open source plotting library Matplotlib [83]. Programs to simulate physical models are available at Zenodo repository, `https://zenodo.org/record/6500087` [111].

6 Publication

The author of this thesis carried out the theoretical analysis and interpretation of the data as well as all analytical and numerical calculations presented in this work. H. R. provided the concept, physical interpretation of the data and supervision of this work.

New Journal of Physics **25**(11), 113010 (2023)

A superradiant two-level laser with intrinsic light force generated gain

A. Bychek[1] and H. Ritsch[1]

[1] *Institut für Theoretische Physik, Universität Innsbruck,*
Technikerstrasse 21, A-6020 Innsbruck, Austria

The implementation of a superradiant laser as an active frequency standard is predicted to provide better short-term stability and robustness to thermal and mechanical fluctuations when compared to standard passive optical clocks. However, despite significant recent progress, the experimental realization of continuous wave superradiant lasing still remains an open challenge as it requires continuous loading, cooling, and pumping of active atoms within an optical resonator. Here we propose a new scenario for creating continuous gain by using optical forces acting on the states of a two-level atom via bichromatic coherent pumping of a cold atomic gas trapped inside a single-mode cavity. Analogous to atomic maser setups, tailored state-dependent forces are used to gather and concentrate excited-state atoms in regions of strong atom-cavity coupling while ground-state atoms are repelled. To facilitate numerical simulations of a sufficiently large atomic ensemble, we rely on a second-order cumulant expansion and describe the atomic motion in a semi-classical point-particle approximation subject to position-dependent light shifts which induce optical gradient forces along the cavity axis. We study minimal conditions on pump laser intensities and detunings required for collective superradiant emission. Balancing Doppler cooling and gain-induced heating we identify a parameter regime of a continuous narrow-band laser operation close to the bare atomic frequency.

doi: 10.1088/1367-2630/ad0750

6.1 Introduction

In view of establishing a new outstanding and robust optical time and frequency standard the quest to build a continuous superradiant laser operating on a very narrow atomic transition has been the subject of intense theoretical and experimental research in the past decade [22, 23, 40, 55, 66, 70, 75, 94, 112, 113]. These studies are also fueled by the remarkable operating characteristics and relative simplicity of its microwave analogue, the hydrogen maser [114, 115]. Recently pulsed superradiance has been experimentally observed using laser-cooled atomic ensembles [47, 71, 116]. Some proof of principle setups based on magneto-optical trapping demonstrated quasi-continuous operation on kHz transitions [41, 43]. The major remaining challenge is to achieve sufficient gain via continuous inversion on the relevant clock transition without significantly perturbing the atomic levels.

One straightforward approach which is currently pursued is based on a continuous ultracold beam of excited atoms passing through an optical resonator [40, 42, 44, 45, 72, 75, 117–120]. In the past years, considerable progress has been made in this direction, yet the main challenge is to create a sufficient inverted atomic flux needed for collective superradiant emission. As an alternative, some calculations suggest optimized multilevel pumping schemes, where a careful choice of laser powers and detunings minimizes the transition level shifts at reasonable pumping rates [93]. Still this needs many lasers, which have to be combined to pump and cool the atomic ensemble simultaneously in order to keep the density of the active gas constant.

As in a standard micromaser, where population inversion is created by coherent pumping of atoms followed by magneto-mechanical separation of ground- and excited-state atoms in the mode volume, one could look for an analogous scheme for an optical setup. As the length scales are several orders of magnitude smaller at optical frequencies, the magnetic gradients for a sufficient state separation are very difficult to achieve and also potentially shift the clock transition in a detrimental way. However, one could make use of state-dependent optical forces, and thus excitation and separation could be done by suitably designed laser fields. At the same time, it has already been shown in previous experiments on BEC formation in Strontium that dressing lasers can create large enough optical level shifts in a dimple configuration to manipulate only a chosen sub-ensemble of the atoms with an extra laser without affecting the majority of the unperturbed atoms outside the dimple [42].

Here, we suggest a new scenario for creating an intrinsic light force generated inversion mechanism. The idea is to combine the internal degrees of freedom of atoms with the motional ones to create the necessary inversion. We will study configurations, where pumping and gain occur in different spatial regions of the cavity by taking into account atomic motion and state-dependent forces resulting from a spatially dependent periodic drive of the transition. After all, an inverted ensemble of only very weakly perturbed atoms can be created in regions of strong atom-cavity coupling. For sufficiently many atoms we show that this should lead to collective narrow-band lasing close to the bare atomic transition frequency.

A detailed quantum description including the necessary number of atoms to achieve sufficient gain at low excitation powers goes beyond the available computational power to numerically simulate the coupled atom-field dynamics. Therefore, we have to resort to approximations and only limited atom numbers from which we are able to extract predictions for scaling towards larger ensembles. Hence we treat the atomic motion semi-classically and use a quantum description only for the internal atomic dynamics and the cavity field. As it has been observed for instance in Ref. [121], a semi-classical description of motion shows a good agreement with the full quantum description, where the external degrees of freedom are quantized. Still, we have to make use of a cumulant expansion approach [56] for studying larger atom numbers.

The paper is organized as follows. First, in Sec. 6.2.1 we introduce the spatial light shifts and optical forces present in the system. In Sec. 6.2.2, we present the system overview and calculate the coupled atom-field dynamics under the coherent laser drive. It is then shown in Sec. 6.2.3, that a bichromatic coherent drive can lead to a continuous narrow-band laser operation. We extend the model for an ensemble of atoms with light force induced inversion in Sec. 6.3. We start with the full quantum approach in Sec. 6.3.1 and proceed with the second-order cumulant expansion in Sec. 6.3.2 in order to describe the collective atomic dynamics and spectrum of the light field in the cavity.

6.2 Model definition

6.2.1 Light shifts and forces

A two-level atom coherently driven by a laser detuned from the atomic resonance frequency experiences energy light shifts [122]. Under this drive the ground and excited states of the atom are no longer eigenstates of the system. The Hamiltonian of the atom (ω_a) under the coherent laser drive (ω_Ω) in a rotating frame of the laser field can be written as ($\hbar = 1$)

$$H_a = -\Delta_a \sigma^+ \sigma^- + \Omega(\sigma^+ + \sigma^-) = -\frac{\Delta_a}{2}\mathbb{1} - \frac{\Delta_a}{2}\sigma^z + \Omega\sigma^x, \tag{6.1}$$

where $\Delta_a = \omega_\Omega - \omega_a$, Ω is the transition Rabi frequency, and $\sigma^x = \sigma^+ + \sigma^-$, $\sigma^z = \sigma^+\sigma^- - \sigma^-\sigma^+$ are the Pauli matrices. It is known that any 2x2 Hermitian matrix can be expressed in a unique way as a linear combination of the Pauli matrices

$$H_{2\times 2} = h_0\mathbb{1} + \vec{h}\vec{\sigma}, \tag{6.2}$$

with all coefficients being real numbers $h_0 = const$, $h_1 = h\sin\Theta\cos\phi$, $h_2 = h\sin\Theta\sin\phi$, $h_3 = h\cos\Theta$, where $h = |\vec{h}| = \sqrt{h_1^2 + h_2^2 + h_3^2}$. It is easy to show that the eigenvalues of this matrix are

$$E_\pm = h_0 \pm h, \tag{6.3}$$

and the corresponding eigenvectors can be expressed as an effective rotation of the uncoupled states,

$$\begin{aligned} |+\rangle &= \sin\frac{\Theta}{2}\exp(\frac{i\phi}{2})|g\rangle + \cos\frac{\Theta}{2}\exp(-\frac{i\phi}{2})|e\rangle \\ |-\rangle &= \cos\frac{\Theta}{2}\exp(\frac{i\phi}{2})|g\rangle - \sin\frac{\Theta}{2}\exp(-\frac{i\phi}{2})|e\rangle. \end{aligned} \tag{6.4}$$

Therefore, the eigenvalues of the Hamiltonian (6.1) can be written as

$$E_\pm = -\frac{\Delta_a}{2} \pm \sqrt{\Omega^2 + \Delta_a^2/4}, \tag{6.5}$$

with the corresponding eigenstates known as the dressed states,

$$|+\rangle = \sin\frac{\Theta}{2}|g\rangle + \cos\frac{\Theta}{2}|e\rangle, \quad |-\rangle = \cos\frac{\Theta}{2}|g\rangle - \sin\frac{\Theta}{2}|e\rangle, \tag{6.6}$$

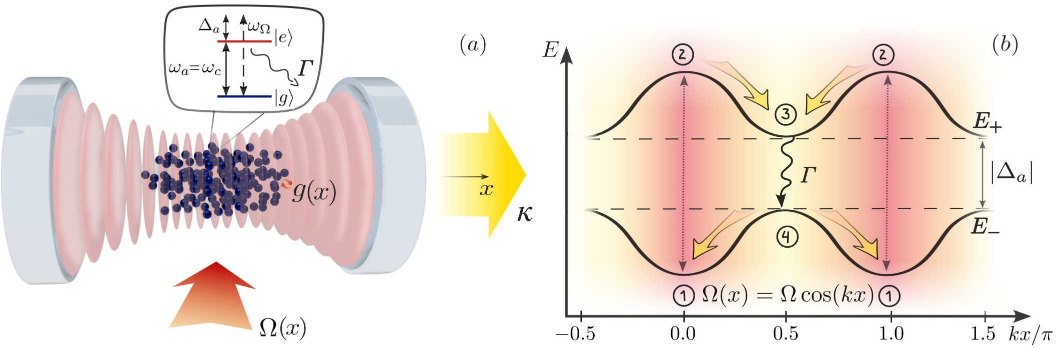

Figure 6.1: Schematics of the system. (a) Two-level atoms (ω_a) inside a single-mode cavity (ω_c) are coherently driven by a laser (ω_Ω) with the Rabi frequency $\Omega(x)$, where Γ is the single-atom spontaneous emission rate, $g(x)$ is the atom-cavity coupling, and κ is the cavity loss rate. (b) Eigenvalues of the Hamiltonian given in Eq. (6.1) under a spatially dependent coherent laser drive $\Omega(x) = \Omega\cos(kx)$ with the negative detuning $\Delta_a = \omega_\Omega - \omega_a$, where yellow arrows show a dipole force acting on the states of the two-level atom as described in the main text.

where $tg\,\Theta = -\frac{2\Omega}{\Delta_a}$.

Let us now consider a two-level atom moving in one dimension along the axis of a linear cavity, as schematically presented in figure 6.1(a). When the atom is illuminated by a laser whose Rabi frequency has a spatial periodic distribution $\Omega(x) = \Omega\cos(kx)$ formed by a standing wave with the wavelength $\lambda = 2\pi/k$ the energy shifts can be plotted as shown in figure 6.1(b). This creates a mean dipole force $\langle F\rangle = -\langle\nabla H\rangle$ acting on the atom, which has the opposite sign for $|+\rangle$ and $|-\rangle$ states. In this regard one could think of a population inversion scheme shown in figure 6.1(b). An atom located at position (1) with some non-zero initial velocity is pumped by the laser into state (2) and experiences the dipole force as it continues to move. This force pushes the atom to position (3) where there is no force acting on the atom. If this process occurs at a faster rate than the lifetime $\tau \sim \Gamma^{-1}$ of the excited state, then the atom emits a photon with the frequency close to the bare atomic transition frequency and undergoes the transition into state (4) where it is dragged by the light force left or right to position (1) and the process repeats itself.

Thus, such a scheme could be used to spatially separate the region of pumping from the lasing in the system. In other words, we create the population inversion in the specific regions of the cavity, those regions where we would like to have a maximal coupling to the cavity.

6.2.2 Semi-classical master equation for the coupled atom-field dynamics

A stable laser operation requires a continuous inversion mechanism to keep the population inversion on a lasing transition. In the previous section, we introduced the scenario for creating effective inversion on a lasing transition using light forces. While in principle many possible geometries to achieve this purpose can be investigated, we will restrict ourselves here to a simple generic case, where the underlying mechanisms can be studied in detail. Hence we consider a 1D motion in a single-mode Fabry-Perot cavity with a sine wave laser mode and apply a standing cosine wave pump field. Ground-state atoms will be trapped and cooled close to the antinodes of the cosine mode. Atoms excited to the upper level at these points are pushed towards the nodes of the cosine mode, where they maximally couple to the cavity sine mode. Let us identify a parameter regime, which leads to the desired local inversion and gain. In other words, one needs to find a regime of stable narrow-band lasing at the bare atomic frequency, with a linewidth that is much smaller than the cavity linewidth and that is well distinguished from the other light sources present in the cavity. This requires several conditions to be ensured:

- $\kappa > \Gamma$ - the system is in the bad-cavity regime, which provides the low intracavity photon number operation and thus reduced sensitivity to cavity noise;

- $\Delta_a < 0$, and $|\Delta_a| > \Omega$ - the driving laser is far red-detuned from the atomic transition frequency to minimize the amount of coherently scattered photons from the drive into the cavity;

- $2\sqrt{\Omega^2 + \Delta_a^2/4} > \kappa$ - the maximal light shift in equation (6.5) is larger than the cavity linewidth to spatially separate the region of pumping (1-2) from the lasing (3-4) in figure 6.1(b).

The Hamiltonian of the two-level atom subjected to a coherent drive inside a single-mode optical cavity can be described by the Jaynes-Cummings model in the rotating frame of the drive

$$H = -\Delta_a \sigma^+ \sigma^- - \Delta_c a^\dagger a + g(x)(a^\dagger \sigma^- + a\sigma^+) + \Omega(x)(\sigma^+ + \sigma^-), \tag{6.7}$$

where $\Delta_c = \omega_\Omega - \omega_c$ is the laser detuning from the cavity mode, $g(x) = g\sin(kx)$

and $\Omega(x) = \Omega\cos(kx)$ are the atom-cavity interaction strength and Rabi frequency, respectively, which are functions of the atomic position along the cavity mode with the wave number k. The quantum dynamics of the open atom-cavity system can be described by the master equation for the system density matrix ρ in the Lindblad form

$$\dot{\rho} = -i[H,\rho] + \mathcal{L}_\kappa[\rho] + \mathcal{L}_\Gamma[\rho], \tag{6.8}$$

where the loss of photons through the cavity mirrors and individual atomic decay are given by

$$\begin{aligned} \mathcal{L}_\kappa[\rho] &= \frac{\kappa}{2}(2a\rho a^\dagger - a^\dagger a\rho - \rho a^\dagger a) \\ \mathcal{L}_\Gamma[\rho] &= \frac{\Gamma}{2}(2\sigma^-\rho\sigma^+ - \sigma^+\sigma^-\rho - \rho\sigma^+\sigma^-), \end{aligned} \tag{6.9}$$

with the cavity loss rate κ and single-atom spontaneous emission rate Γ, respectively. In order to approximate the atomic motion and light forces acting on the atom, we include the semi-classical equations of motion in the system description,

$$\begin{aligned} \dot{\langle x\rangle} &= \langle p\rangle/m = 2\omega_r\langle p\rangle/k_a^2 \\ \dot{\langle p\rangle} &= -\langle\nabla H\rangle, \end{aligned} \tag{6.10}$$

where $\omega_r = k_a^2/(2m)$ is the atomic recoil frequency given by the atomic mass and wave number of the atomic transition. Here we neglect the effects of momentum diffusion arising from spontaneous emission. One could account for these effects by going beyond the mean-field approach in calculating the position and momentum, which would substantially increase the amount of equations in our simulations. At the same time, in the ultimate case of a superradiant laser, the emission rate Γ is usually very small compared to other parameters, such that spontaneous emission recoil should only lead to minor corrections in the atomic dynamics.

First of all, we would like to calculate the coupled atom-photon dynamics in the cavity. For a non-moving atom under a coherent drive the solution is known as the damped Rabi oscillations eventually leading to population of the excited state by no more than fifty percent [123], i.e. no inversion. However, due to atomic motion and forces acting differently on the states of the atom, the local population inversion can become positive in certain positions.

For the remainder of this work, we set the cavity mode to be on resonance with the bare atomic transition frequency and select a recoil frequency value that facilitates rapid cooling for an adequate representation of the results. We consider a linear cavity

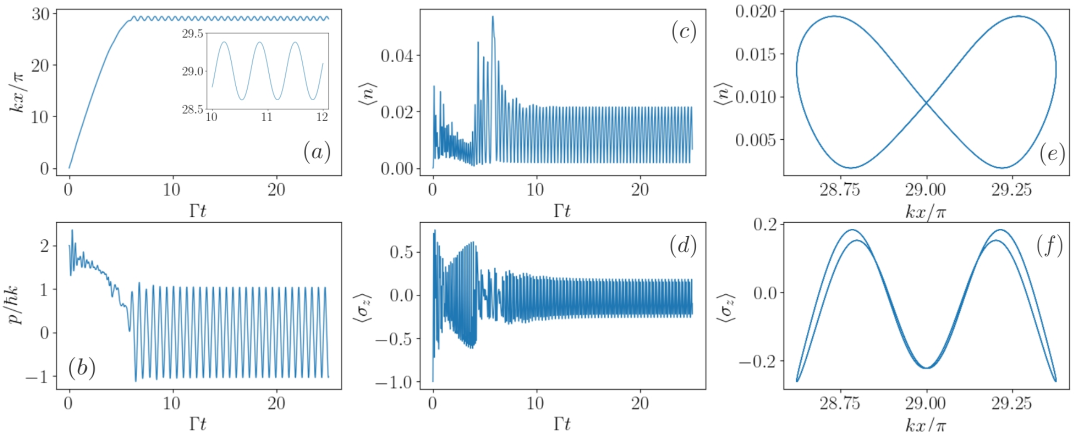

Figure 6.2: Atomic dynamics and lasing under the coherent drive with $|\Delta_a| < \Omega$. Parameters: $\kappa = 20\Gamma$, $g = 4\Gamma$, $\Omega = 30\Gamma$, $\Delta_a = -10\Gamma$, $\omega_r = 6\Gamma$.

with a cosine wave pump $\Omega(x) = \Omega\cos(kx)$ and a sine wave cavity mode with the coupling strength $g(x) = g\sin(kx)$, where $k = k_a$ is the cavity mode wave number. Since we are in the parameter regime where $\kappa > \Gamma$ and $g < \kappa$, the Hilbert space of the photon field can be truncated at low photon numbers. Figures 6.2-6.3 show the atomic dynamics and lasing under the coherent drive for two different cases of $|\Delta_a| < \Omega$ and $|\Delta_a| > \Omega$. The position and momentum of the atom are given in units of π/k and $\hbar k$, respectively, in figures 6.2(a)-(b). The mean photon number in the cavity and atomic inversion are shown as a function of time in figures 6.2(c)-(d) and a function

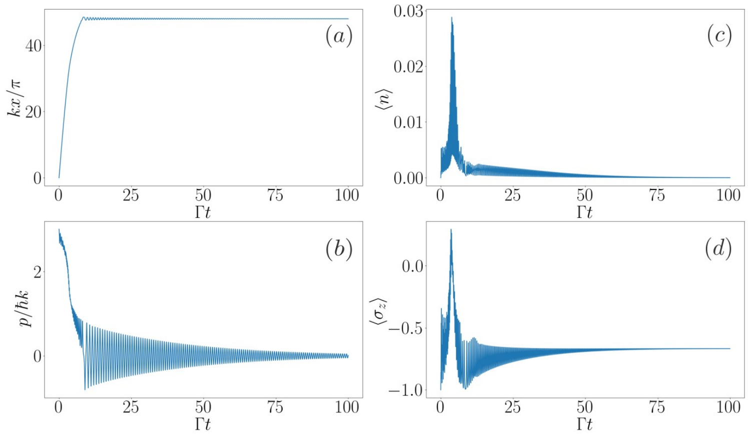

Figure 6.3: Cooling and trapping of an atom in the cavity under the coherent drive with $|\Delta_a| > \Omega$. Parameters: $\kappa = 20\Gamma$, $g = 4\Gamma$, $\Omega = 10\Gamma$, $\Delta_a = -20\Gamma$, $\omega_r = 6\Gamma$.

of position in figures 6.2(e)-(f).

In the case of $|\Delta_a| < \Omega$, we have found the parameter regime, where atomic cooling is balanced by heating from the driving laser, see figures 6.2(a)-(b). Starting from a given initial momentum, the atom experiences laser cooling until it reaches a quasi-stationary state. As seen in figure 6.2(a), the atom oscillates between a particular node and the neighboring antinodes of the driving field while the atomic inversion $\langle\sigma_z\rangle = \langle\sigma^+\sigma^-\rangle - \langle\sigma^-\sigma^+\rangle$ in figure 6.2(f) becomes positive towards the points of the maximal coupling strength. Followed by photon emission and a maximum in average photon number in figure 6.2(e) this dynamics is close to the ideal scenario depicted in figure 6.1(b). The results demonstrate that in principle the above scenario may take place, unfortunately this can not be used as a good pumping scheme due to the fact that mostly scattered photons from the drive will dominate the cavity output spectrum.

On the other side, after studying the case of $|\Delta_a| > \Omega$, we have observed that the drive from a single laser is never sufficient enough to create the desired population inversion. As presented in figure 6.3, in this case the applied far-detuned drive results in strong cooling for the atom and there is no inversion on the lasing transition at any point. Therefore, one may think of the idea of adding an extra laser drive to populate the excited state, with the parameters particularly chosen and optimized to ensure the above conditions in the cavity.

6.2.3 Two-level dynamics with a bichromatic coherent drive

In the previous section, we have indicated the parameter regime of our interests in the context of the superradiant laser. We observed that the driving from a single laser is not sufficient to create the desired population inversion on the lasing transition. In this section, the idea is to use this laser exclusively to create the spatial light shifts, as depicted in figure 6.4(a). In order to populate the excited state we introduce the second laser drive $\eta(x) = \eta\cos(kx)$ into the system. The frequency of the second laser drive is now tuned to the resonance with the dressed states given by equations (6.5)-(6.6), however not at their maximal light shifts, but at the points where the dipole force acting on the atom is close to its maxima, see figure 6.4(b). This allows the excited atom to reach the lasing position more efficiently since there is strong acceleration from the force. We expect that a combination of these laser drives acting together can lead to collective narrow-band emission, provided that optimal driving intensities and

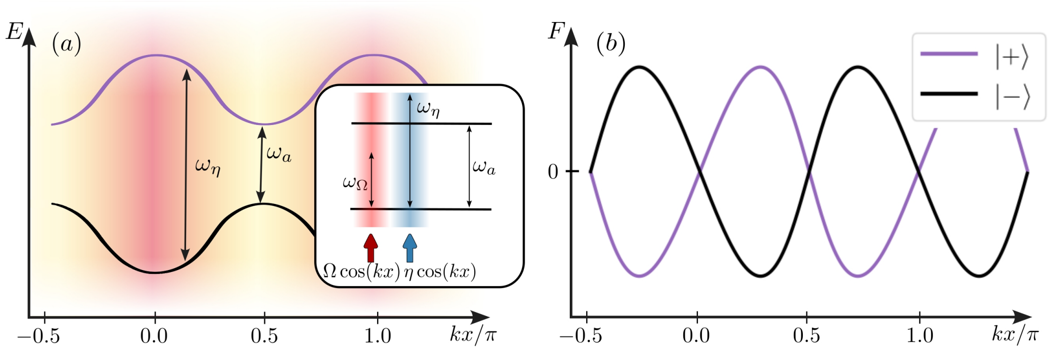

Figure 6.4: (a) The schematics of an atom under the bichromatic coherent drive. (b) Dipole force acting on the dressed states of the atom.

detunings are found. However, the master equation becomes significantly more difficult to solve as the second laser drive does not allow to eliminate the time dependence in the Hamiltonian. Thus the Hamiltonian of the system in the rotating frame of the first laser can be written as

$$H_2 = H + \eta\cos(kx)(\sigma^+ e^{i\Delta_\eta t} + \sigma^- e^{-i\Delta_\eta t}), \tag{6.11}$$

where $\Delta_\eta = \omega_\Omega - \omega_\eta$. Note, that if the laser drive is not strong enough it will not be able to create population inversion. On the other hand, a strong laser drive will produce both a lot of coherently scattered photons and strong heating in the system. In order to find the dynamics of the system we solve the master equation (6.8) with the Hamiltonian (6.11). It is then the Rabi frequency and detuning of the second laser which have to be scanned and mutually adjusted.

Figure 6.5 shows the atomic dynamics and lasing under the bichromatic coherent drive in the regime, where the light from the second drive pushes the atom to move along the cavity axis such that the atomic momentum reaches its quasi-stationary state, see figures 6.5(a)-(b). This results in a linear motion of the atom, where it is being pumped at the maximal driving intensity and continues to undergo the inversion scheme depicted in figure 6.1(b). As the atom moves, the atomic inversion becomes positive in the vicinity of the unperturbed bare atomic transition frequency, which is followed by the photon emission, as can be seen in figures 6.5(d)-(f). Figure 6.5(c) shows the mean photon number in the cavity (blue), which can be split into the laser part (orange) and coherently scattered part (green). The coherently scattered field amplitude is phase dependent as it comes from the coherent laser drive and its

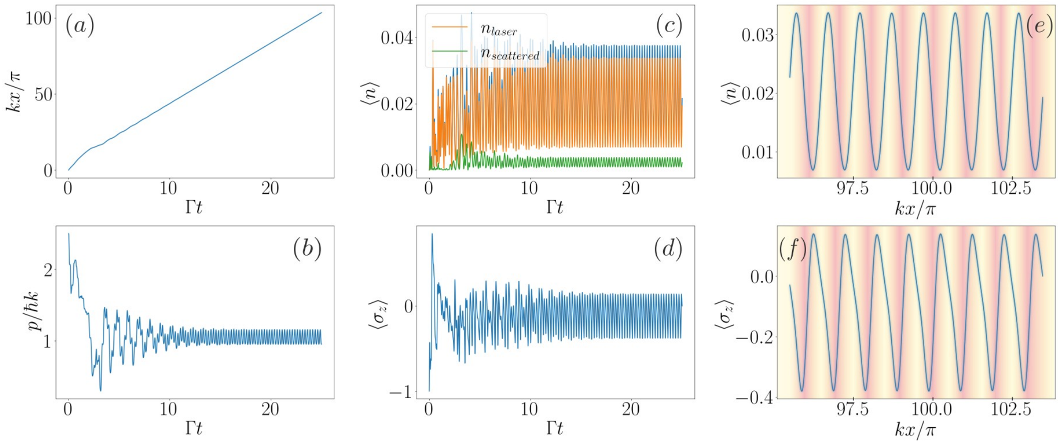

Figure 6.5: Atomic dynamics and lasing under the bichromatic coherent drive. Parameters: $\kappa = 20\Gamma$, $g = 4\Gamma$, $\Omega = 10\Gamma$, $\Delta_a = -20\Gamma$, $\eta = 8\Gamma$, $\Delta_\eta = -25\Gamma$, $\omega_r = 6\Gamma$.

intensity can be calculated as $|\langle a\rangle|^2$, while the incoherently scattered field from inverted atoms is phase independent. To obtain the laser part we subtract the coherently scattered part from the total photon number. Furthermore, one can see a stable laser operation with the oscillations of the photon number around the mean value. This example demonstrates how the specially tuned bichromatic coherent drive can lead to continuous lasing with intrinsic light force induced inversion.

6.3 Collective dynamics with light force induced inversion

6.3.1 Full quantum approach

An extension of the full quantum model to an ensemble of atoms remains feasible only for a small atom number due to the exponential growth of the Hilbert space. Here we present the results for the case of $N = 8$, where we truncate the Hilbert space of the field in the cavity at low photon numbers. We choose the initial atomic momenta to be randomly distributed around a selected velocity as $|p_m^0| \in \{p_0 - \epsilon, ..., p_0 + \epsilon\}$, which is of the order of several $\hbar k$ and $x_m^0 = m\pi/k$ for $m = 1..N$, see figure 6.6. In addition, even when initial atomic momenta are one or even two orders of magnitude larger than $\hbar k$ one can observe the laser cooling process. As such atoms do not contribute to the desired lasing until they get cold enough, it substantially reduces the efficiency of the scheme. On the other hand, atoms with the initial velocity close

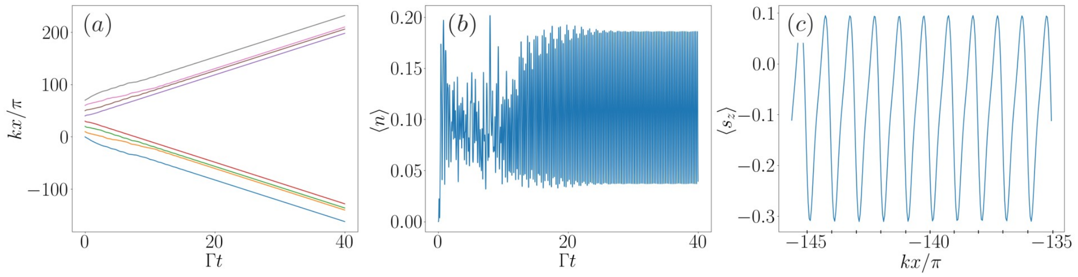

Figure 6.6: (a) Dynamics of $N = 8$ atoms under the bichromatic coherent drive. (b) Mean photon number in the cavity depending on time (in units of Γ). (c) The position dependence of the atomic inversion during the stable final stage of the time evolution. The initial distribution of momenta $|p_m^0| \in \{2, ..., 2.5\}\hbar k$ and positions $x_m^0 = m\pi/k$ for $m = 1..N$. The parameters are the same as in figure 6.5.

to zero immediately become trapped in the potential minima and do not contribute to the dynamics as well. Therefore, the ideal initial conditions would be to primarily reduce the temperature of atoms and perform a velocity selection. As the atoms move one can see the stabilization of photon emission and increase in the mean photon number. Figure 6.6(c) shows how the atomic inversion changes with the position similar to the case of a single atom in figure 6.5.

6.3.2 Second-order cumulant expansion

Next, we would like to extend our model to an ensemble of $N \gg 1$ atoms subjected to the bichromatic coherent drive, as described in the previous section. As each atom in the ensemble behaves differently depending on its initial position and momentum,

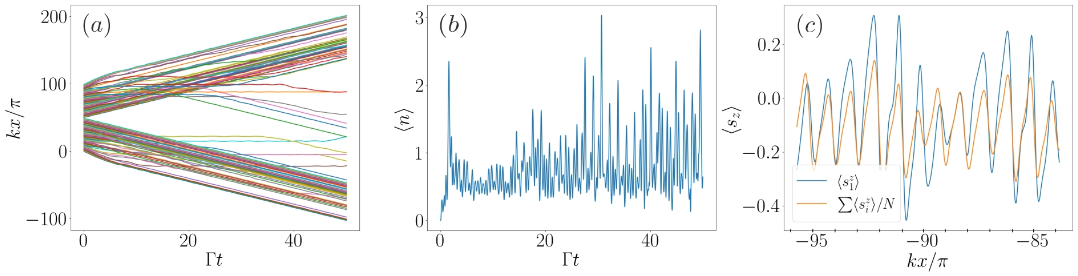

Figure 6.7: Atomic dynamics and lasing in the ensemble of $N = 100$ atoms under the bichromatic coherent drive. The parameters are the same as in figure 6.5.

the numerical solution of the master equation (6.8) with the Hamiltonian given in Eq. (6.11) becomes challenging. In order to describe a large ensemble of atoms we make use of the second-order cumulant expansion [56] to write down the closed set of the Heisenberg equations for the system operators [94]:

$$
\begin{aligned}
&\frac{d}{dt}\langle a\rangle = -(\kappa/2 - i\Delta_c)\langle a\rangle - ig\sum_j N_j \sin(x_j)\langle\sigma_j^-\rangle \\
&\frac{d}{dt}\langle\sigma_m^-\rangle = -(\Gamma/2 - i\Delta_{am})\langle\sigma_m^-\rangle + ig\sin(x_m)\langle a\rangle(2\langle\sigma_m^+\sigma_m^-\rangle - 1) \\
&\quad + i(\Omega + \eta e^{i\Delta_\eta t})\cos(x_m)(2\langle\sigma_m^+\sigma_m^-\rangle - 1) \\
&\frac{d}{dt}\langle a^\dagger a\rangle = -\kappa\langle a^\dagger a\rangle + ig\sum_j N_j\sin(x_j)(\langle a\sigma_j^+\rangle - \langle a^\dagger\sigma_j^-\rangle) \\
&\frac{d}{dt}\langle a\sigma_m^+\rangle = -(\frac{\kappa+\Gamma}{2} + i\Delta_{am} - i\Delta_c)\langle a\sigma_m^+\rangle + ig\sin(x_m)(\langle a^\dagger a\rangle - 2\langle a^\dagger a\rangle\langle\sigma_m^+\sigma_m^-\rangle - \langle\sigma_m^+\sigma_m^-\rangle) \\
&\quad - ig\sum_{j;m\neq j}\sin(x_j)\langle\sigma_m^+\sigma_j^-\rangle - i(\Omega + \eta e^{-i\Delta_\eta t})\cos(x_m)\langle a\rangle(2\langle\sigma_m^+\sigma_m^-\rangle - 1) \\
&\frac{d}{dt}\langle\sigma_m^+\sigma_m^-\rangle = -\Gamma\langle\sigma_m^+\sigma_m^-\rangle - ig\sin(x_m)(\langle a\sigma_m^+\rangle - \langle a^\dagger\sigma_m^-\rangle) \\
&\quad - i(\Omega + \eta e^{i\Delta_\eta t}))\cos(x_m)\langle\sigma_m^+\rangle + i(\Omega + \eta e^{-i\Delta_\eta t}))\cos(x_m)\langle\sigma_m^-\rangle \\
&\frac{d}{dt}\langle\sigma_m^+\sigma_j^-\rangle = -\Gamma\langle\sigma_m^+\sigma_j^-\rangle - ig_m\sin(x_m)\langle a^\dagger\sigma_j^-\rangle(2\langle\sigma_m^+\sigma_m^-\rangle - 1) \\
&\quad + ig_j\sin(x_j)\langle a\sigma_m^+\rangle(2\langle\sigma_j^+\sigma_j^-\rangle - 1) + i(\Omega + \eta e^{i\Delta_\eta t}))\cos(x_j)\langle\sigma_m^+\rangle(2\langle\sigma_j^+\sigma_j^-\rangle - 1) \\
&\quad - i(\Omega + \eta e^{-i\Delta_\eta t}))\cos(x_m)\langle\sigma_j^-\rangle(2\langle\sigma_m^+\sigma_m^-\rangle - 1) \\
&\frac{d}{dt}\langle x_m\rangle = 2\omega_r\langle p_m\rangle/k^2 \\
&\frac{d}{dt}\langle p_m\rangle = -2g\cos(x_m)\Re\{\langle a\sigma_m^+\rangle\} + 2\Omega\sin(x_m)\Re\{\langle\sigma_m^+\rangle\} \\
&\quad + \eta\sin(x_m)(\langle\sigma_m^+\rangle e^{i\Delta_\eta t} + \langle\sigma_m^-\rangle e^{-i\Delta_\eta t}),
\end{aligned}
\tag{6.12}
$$

where $m = 1..N$ and $\Re$ is used to denote the real part of an expectation value of an operator. Figure 6.7 shows the solution of equations (6.12) for $N = 100$ atoms with the same distribution of initial positions and momenta as used in the full model considered in the previous section. The resulting dynamics becomes much more complicated to describe, but one can see a similar behavior with the case of a single atom. Although a small part of atoms gets cooled down and does not contribute to the lasing process, the majority of atoms display the lasing we are interested in. In figure 6.7(b) one can

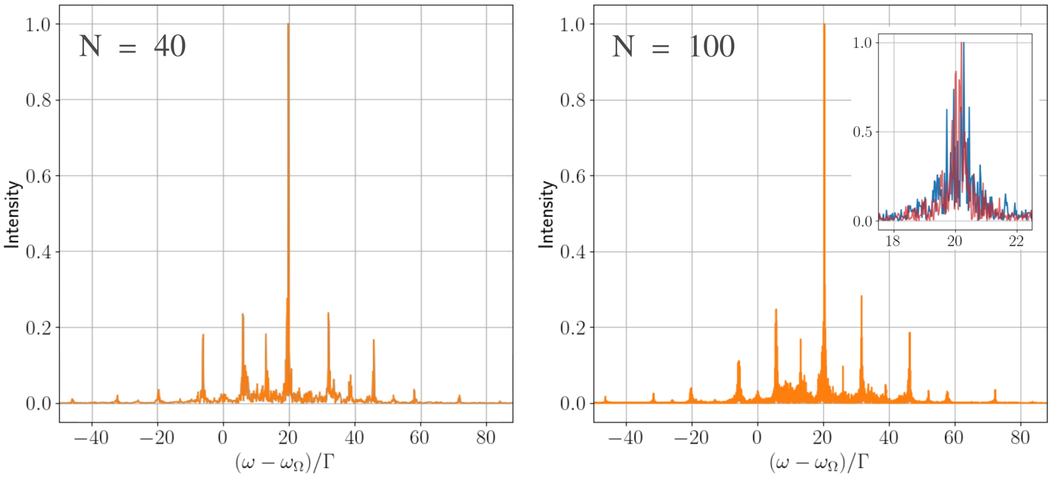

Figure 6.8: Spectrum of the cavity light for the ensemble of $N = 40$ (left panel) and $N = 100$ atoms (right panel) presented in figure 6.7. The emission intensity is normalized and the inset shows a zoom-in of the central peak profile (blue line). The red line in the inset shows the spectrum under cavity dephasing with the rate $\xi = 10\Gamma$.

see continuous lasing from the atoms reaching the order of one photon on average in the cavity. We expect fluctuations in the photon number to be mitigated in the case of significantly larger atomic ensembles, where each atom only weakly contributes to the emission process. However, due to the number of equations growing as $\mathcal{O}(N^2)$ we are limited to a system of a few hundred atoms.

Let us calculate the spectrum of the light in the cavity. According to the Wiener-Khinchin theorem [58] the spectrum can be found as a Fourier transform of the first-order correlation function $g^{(1)}(\tau) = \langle a^\dagger(t_0+\tau)a(t_0)\rangle$,

$$S(\omega) = 2\Re\left\{\int_0^\infty d\tau e^{-i\omega\tau} g^{(1)}(\tau)\right\}. \tag{6.13}$$

Here, we use the quantum regression theorem [124] to write down a set of differential equations for the first-order correlation function, where t_0 is normally given by the time the system reaches its steady state. However, since in our case the dynamics does not have a steady state, we have to include these equations in the full system of equations (6.12) and average it over a set of equidistant initial conditions $g^1(0) = \langle a^\dagger a\rangle(t_0)|_{t_0=t_{end}}$ chosen from the final stage of the dynamics.

After the averaging process one can see the resulting spectrum, as presented in figure 6.8 for $N = 40$ and $N = 100$ atoms. The spectrum averages quite well already after several averaging steps and reveals the main spectral peak coming from the atoms at the frequency close to the bare atomic transition, which linewidth is below the natural linewidth of the atomic transition Γ. The inset shows a zoom-in of the central peak profile which broadening can be attributed to the emission from different atoms at slightly different frequencies (blue line). The red line shows that the resulting spectrum is robust to cavity fluctuations in the presence of moderate cavity noise with the dephasing rate $\xi = 10\Gamma$.

Additionally to the central peak, there are numerous sidebands located left and right from the atomic transition frequency. They appear to be independent of the number of atoms, coupling constant, and Rabi frequencies of the lasers. We associate them with the motion of atoms with a constant velocity, which is observed in figure 6.7(a). One can calculate the frequency of these motional sidebands as

$$\omega_{SB} = \omega_a \pm \omega_\pm = \omega_a \pm 2\pi \frac{v}{\lambda}, \tag{6.14}$$

where $v/\lambda = \omega_r p/(\pi k)$. Since the atomic motion is linear one can write

$$\omega_\pm = \pm \frac{2\omega_r \langle p \rangle^{st}}{k}. \tag{6.15}$$

Substituting the real parameters used in figure 6.8 into equations (6.15) we calculate the frequencies $w_\pm$, which agree well with the central frequencies of the sidebands observed in the spectrum.

6.4 Conclusions and outlook

We have studied population inversion and gain within an optical cavity in a cold ensemble of coherently driven two-level atoms with an intrinsic light force generated inversion mechanism. Using numerical simulations of the coupled atom-field dynamics we have found the operating conditions producing continuous narrow-band emission close to the unperturbed atomic line. In the limit of low photon number operation, the central frequency is largely insensitive to cavity fluctuations. Note, that the driving field has to be far-detuned from the atomic resonance such that there are no pump laser photons coherently scattered into the cavity. As we have shown, adding an extra specially tuned driving field significantly improves the performance of the system.

At this point our simulations are limited to a few hundred atoms since we use a second-order cumulant expansion as a minimum model to reliably predict the laser spectrum. Much higher output laser power with a cleaner spectrum can be expected for realistic atom numbers of up to a million, where each atom only needs to contribute very weakly to the gain and thus less pump power is required for lasing. Unfortunately such system sizes are beyond our present numerical capabilities. Similarly, a reliable evaluation of the photon statistics, as for instance the calculation of the second-order correlation function $g^{(2)}(\tau)$, requires even higher-order expansions thereby limiting the tractable atom number even further.

Conceptually, the chosen example setup constitutes a minimalist implementation of a superradiant laser requiring only a single standing wave pump field and a single mode within the cavity to facilitate trapping, pumping, and lasing simultaneously. Via state-dependent light forces atoms excited at the antinodes of the pump standing wave are drawn towards its nodes, where the coupling to the cavity mode can be made maximal by a suitable mode choice. The operating principle here is reminiscent of maser implementations, where in order to implement gain one uses coherent excitation and magnetic separation of the excited state fraction. In our model, the excited state separation is facilitated by differential optical gradient forces, which typically are much stronger than magnetic gradient forces for neutral atoms.

Eventually more complex geometries involving higher-order transverse modes and special state-dependent optical guiding fields can be envisaged for better performance to increase gain and pump efficiency. As there is a large number of options here, we have restricted ourselves to only one generic implementation to exhibit the basic principle more clearly. Future more refined models need to be developed in collaboration with a specific experimental implementation.

Acknowledgements

We acknowledge funding from the L'OREAL Austria Fellowship "For Women in Science" 2023 and the European Unionâs Horizon 2020 research and innovation program under the Marie Sklodowska-Curie Grant Agreement No. 860579 (project MoSaiQC).

Data Availability

All plots were generated directly from the formulas within the paper using the Julia programming language and the open source framework QuantumOptics.jl [125]. The data are openly available at *https://doi.org/10.5281/zenodo.7950727*.

7 Publication

The author of this thesis performed the theoretical analysis as well as all analytical and numerical calculations presented in this work. L. O. co-supervised this work, and H. R. provided the idea and supervision of this publication.

arXiv:2407.16046 (2024)

Self-Ordering, Cooling and Lasing in an Ensemble of Clock Atoms

A. Bychek[1], L. Ostermann[1] and H. Ritsch[1]

[1]*Institut für Theoretische Physik, Universität Innsbruck,*
Technikerstrasse 21, A-6020 Innsbruck, Austria

Active atomic clocks are predicted to provide far better short-term stability and robustness against thermal fluctuations than typical feedback-based optical atomic clocks. However, continuous laser operation using an ensemble of clock atoms still remains an experimentally challenging task. We study spatial self-organization in a transversely driven ensemble of clock atoms inside an optical resonator and coherent light emission from the cavity. We focus on the spectral properties of the emitted light in the narrow atomic linewidth regime, where the phase coherence providing frequency stability is stored in the atomic dipoles rather than the cavity field. The atoms are off-resonantly driven by a standing-wave coherent laser transversely to the cavity axis allowing for atomic motion along the cavity axis as well as along the pump. In order to treat larger atom numbers we employ a second-order cumulant expansion which allows us to calculate the spectrum of the cavity light field. We identify the self-organization threshold where the atoms align themselves in a checkerboard pattern thus maximizing light scattering into the cavity which simultaneously induces cooling. For a larger driving intensity, more atoms are transferred to the excited state, reducing cooling but increasing light emission from the excited atoms. This can be enhanced via a second cavity mode at the atomic frequency spatially shifted by a quarter wavelength. For large enough atom numbers we observe laser-like emission close to the bare atomic transition frequency.

doi: 10.48550/arXiv.2407.16046

7.1 Introduction

Building a continuously operating superradiant laser, which constitutes the core of a next-generation active optical atomic clock, has been an integral part of developing more robust and accurate timekeeping devices in the last two decades, both theoretically and experimentally [22, 23, 40, 55, 66, 70, 75, 94, 112, 113, 126–128]. The continuous clock operation on a narrow-linewidth atomic transition is of particular interest for frequency metrology, precision measurements and quantum sensing [105, 129].

Various advances in this direction, such as pulsed superradiance [47, 71, 73], continuous lasing proof of principle experiments on kHz transitions [41, 43, 118], conveyor belt setups [42, 44, 72, 117, 120] or more complicated multi-level pumping protocols [93] have been reported in the last years. However, a continuous superradiant laser on an optical transition remains challenging and has not been realized yet.

In contrast to the conventional mechanism of self-organization operating in the far-detuned dispersive regime [15–17, 130–134], where the atoms are never excited by the pump laser but act as light scatterers into the cavity creating their own trapping potential, we excite the atoms and leverage state-dependent light forces created by the pump laser and the light scattered into the cavity mode. In this way the atoms will acquire an excited state population while subsequently moving through field minima resulting in an almost unperturbed atomic transition frequency. At this point, the atoms will serve as the gain medium for our laser by means of stimulated emission.

Methodologically expanding our previous work in ref. [135], we employ a second-order cumulant expansion [22, 56, 82] that allows for the treatment of experimentally realistic system sizes, while still capturing the essence of the involved physics as suggested by comparison to full quantum simulations for a small atom number. The

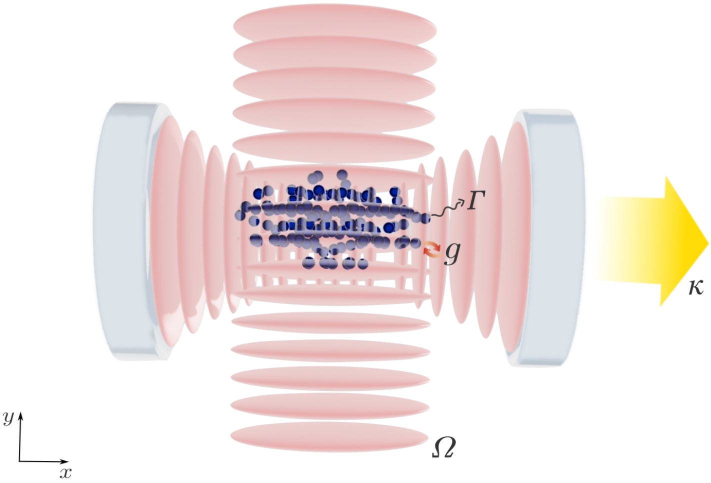

Figure 7.1: *Schematic illustration of the system.* An ensemble of clock atoms is trapped within a red-detuned standing wave transverse to a Fabry-Perot optical cavity with one mode red-detuned close to the pump field. The atomic transition couples to the cavity (g), the pump (Ω) and the environment (Γ) allowing for collective resonant scattering from the pump to the cavity mode with losses characterized by a decay rate (κ). Light forces via collective scattering will modify atomic motion in the xy-plane and eventually induce 2D atomic ordering, cooling and lasing.

spatial degrees of freedom are treated in a semi-classical phase space approach where we include atomic motion along the cavity axis as well as along the direction of the orthogonal coherent pump.

7.2 Model

We study the dynamics and self-organization of atoms having a narrow atomic linewidth in a so-called intermediate bad-cavity regime, where the cavity linewidth (κ) is bigger than the linewidth of the gain medium (Γ). In the limit of small photon numbers, the phase coherence accounting for frequency stability is stored in the atoms rather than in the cavity field. In the absence of an incoherent pumping mechanism for the atoms, we aim for conditions under which the atomic dynamics in the cavity leads to continuous lasing close to the bare atomic transition frequency.

We consider a basic model for self-organization in a linear single-mode cavity (ω_c), as depicted in fig 7.1. The two-level atoms (ω_a) are illuminated off-resonantly (ω_Ω)

by a coherent standing-wave laser drive $\Omega\cos(ky)$ transversely to the cavity axis and experience a dipole light force affecting their spatial degrees of freedom in the cavity. The phase of the scattered light is determined by the particles' position and as the driving strength surpasses the self-organization threshold one can observe the atoms arrange themselves into one of two regular checkerboard patterns thus maximizing scattering into the cavity. This can be shown from the solution of the master equation for the density matrix ($\hbar = 1$),

$$\dot{\rho} = -i\left[H,\rho\right] + \mathcal{L}_\kappa\left[\rho\right] + \mathcal{L}_\Gamma\left[\rho\right], \tag{7.1}$$

with the Hamiltonian in the rotating frame of the laser drive, which can be written as

$$H = -\Delta_a \sum_{i=1}^{N} \sigma_i^+\sigma_i^- - \Delta_c a^\dagger a + \sum_{i=1}^{N} g(x_i,y_i)(a\sigma_i^+ + a^\dagger\sigma_i^-) + \sum_{i=1}^{N} \Omega\cos(k'y_i)\left(\sigma_i^+ + \sigma_i^-\right), \tag{7.2}$$

where $\Delta_a = \omega_\Omega - \omega_a$, $\Delta_c = \omega_\Omega - \omega_c$, $\sigma_i^+ = (\sigma_i^-)^\dagger = |e\rangle_i\langle g|_i$ denote the raising (lowering) operators of the i-th atom with ground state $|g\rangle$ and excited state $|e\rangle$. The ladder operator $a^\dagger$ (a) is the photon creation (annihilation) operator of the cavity mode and atoms experience a position-dependent coupling to the cavity $g(x,y) = g\cos(kx)e^{-y^2/w_0^2}$. We describe the atomic motion in the xy-plane by semi-classical equations,

$$\begin{aligned} \dot{\langle x\rangle} &= 2\omega_r\langle p_x\rangle/k_a^2, \quad \dot{\langle y\rangle} = 2\omega_r\langle p_y\rangle/k_a^2, \\ \dot{\langle p_x\rangle} &= -\Big\langle \frac{\partial H}{\partial x}\Big\rangle, \quad \dot{\langle p_y\rangle} = -\Big\langle \frac{\partial H}{\partial y}\Big\rangle, \end{aligned} \tag{7.3}$$

where $\omega_r = k_a^2/(2m)$ is the atomic recoil frequency given by the atomic mass m and wave number $k_a = \omega_a/c$ of the atomic transition. Since the laser is not very far detuned from both the cavity and the atomic transition frequency we suppose that $k \approx k' \approx k_a$ and measure the distances in units of the atomic transition wavelength λ.

The Liouvillian in the standard Lindblad form represents the decay processes

$$\begin{aligned} \mathcal{L}_\kappa[\rho] &= \frac{\kappa}{2}(2a\rho a^\dagger - a^\dagger a\rho - \rho a^\dagger a) \\ \mathcal{L}_\Gamma[\rho] &= \frac{\Gamma}{2}\sum_{i=1}^{N}(2\sigma_i^-\rho\sigma_i^+ - \sigma_i^+\sigma_i^-\rho - \rho\sigma_i^+\sigma_i^-) \end{aligned} \tag{7.4}$$

describing individual spontaneous atomic emission with the rate Γ and cavity losses with the rate κ.

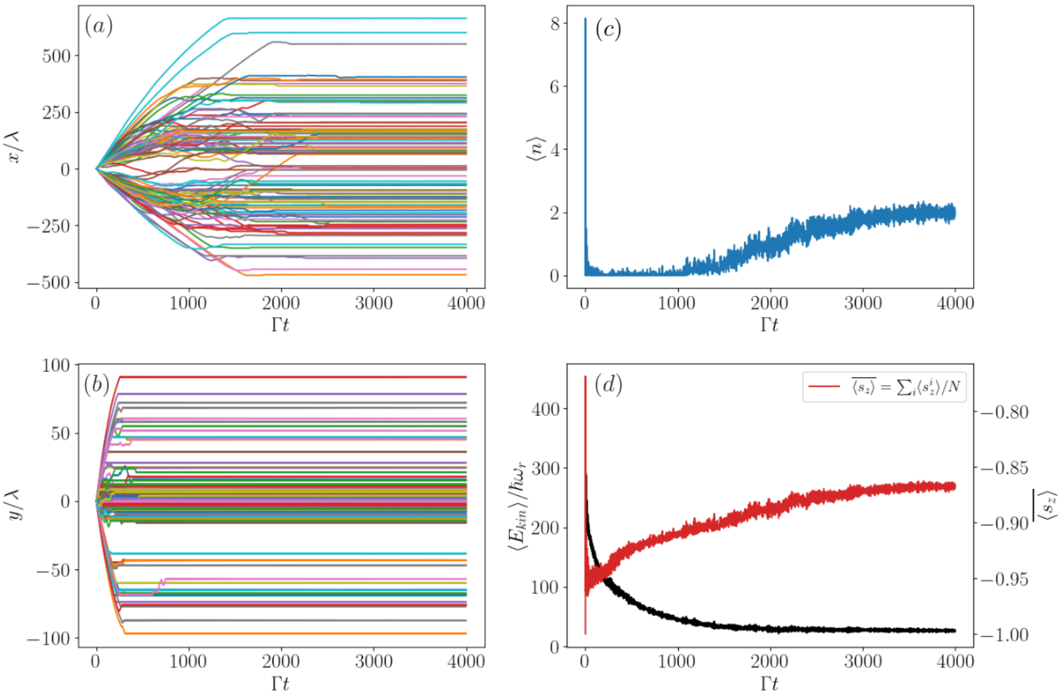

Figure 7.2: *Dynamics.* (a-b) (x,y) motion of $N = 100$ atoms in the parameter regime of self-organization, (c) mean intracavity photon number in the coarse of time, (d) mean kinetic energy (black line) and inversion averaged over the atomic ensemble (red line) depending on time. Parameters: $g = 1\Gamma$, $\kappa = 10\Gamma$, $\Omega = 5\Gamma$, $\Delta_a = -20\Gamma$, $\Delta_c = -10\Gamma$, $w_0 = 1000\lambda$, $\omega_r = 1\Gamma$. The curves show concurrent trapping, cooling and self-ordering via collective light scattering into the cavity mode.

In the self-organization regime, atoms scatter light into the cavity in such a way that the resulting field simultaneously traps and cools the atoms keeping them in an organized pattern, which is stable on a long time scale. More precisely, in the dispersive regime the following two conditions have to be met [17],

$$\delta = \Delta_c - \frac{1}{\Delta_a}\sum_{i=1}^{N} g^2(x_i, y_i) < 0, \tag{7.5}$$

stemming from the effective cavity frequency due to the presence of the atoms. Cavity cooling is ensured when the effective cavity detuning δ is negative. In the case of positive detuning, the atoms acquire kinetic energy from the driving light resulting in

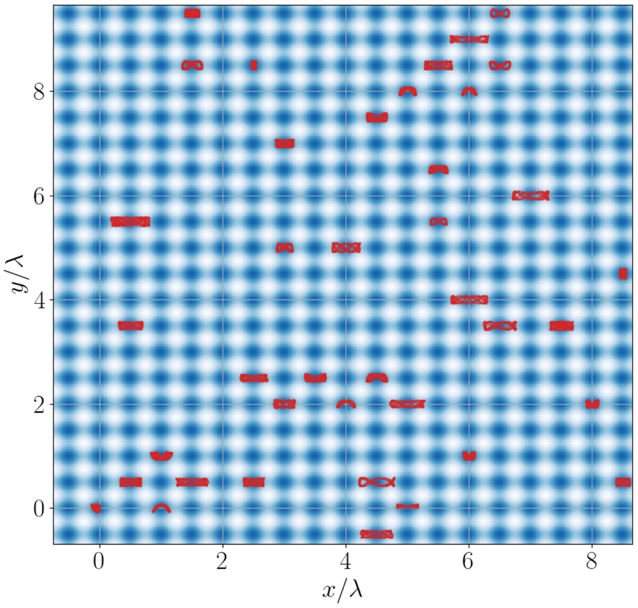

Figure 7.3: *Self-Organization.* Atomic trajectories in the xy-plane (red color) during the final stage of the dynamics in the regime of self-organization presented in fig. 7.2 plotted on top of the light intensity distribution. A checkerboard pattern of trapped atoms emerges in the xy-plane.

cavity heating. The second condition [130],

$$\frac{2\sqrt{N}g'\Omega}{|\Delta_a|} > \frac{(\kappa/2)^2 + \delta^2}{2|\delta|}, \tag{7.6}$$

with $g' = \sqrt{\sum_i g^2(x_i, y_i)/N}$ the averaged atom-field coupling over the ensemble, corresponds to the pumping threshold above which the atoms tend to self-organize in order to minimize their energy in the potential resulting from the interference between the cavity and the pump field. In this work, we will examine these conditions as we move away from the dispersive regime towards the saturation of the atomic transition.

The full master equation description does not allow to numerically calculate many atoms due to the exponential growth of the Hilbert space with the atom number. Hence, in order to simulate the system dynamics and spectrum of the light field in the cavity for an ensemble of many atoms we use a cumulant expansion approach [22, 56, 82]. We restrict ourselves to the second-order cumulant expansion and assume that the higher-order correlations are negligible, i. e. $\langle ABC\rangle_C \approx \langle A\rangle\langle BC\rangle + \langle B\rangle\langle AC\rangle + \langle C\rangle\langle AB\rangle - 2\langle A\rangle\langle B\rangle\langle C\rangle$. Thus, we start from the Heisenberg equations for operator averages describing our system, which for a given operator $\mathcal{O}$ reads

$$\frac{d}{dt}\langle\mathcal{O}\rangle = i\langle[H,\mathcal{O}]\rangle + \kappa\langle\mathcal{D}[a]\mathcal{O}\rangle + \Gamma\sum_i\langle\mathcal{D}[\sigma_i^-]\mathcal{O}\rangle, \tag{7.7}$$

where $\mathcal{D}[c]\mathcal{O} = \left(2c^\dagger\mathcal{O}c - c^\dagger c\mathcal{O} - \mathcal{O}c^\dagger c\right)/2$. Using the second-order cumulant expansion we obtain a closed set of equations describing our system,

$$\begin{aligned}
\frac{d}{dt}\langle a\rangle &= -(\kappa/2 - i\Delta_c)\langle a\rangle - i\sum_j g(x_j,y_j)\langle\sigma_j^-\rangle \\
\frac{d}{dt}\langle\sigma_m^-\rangle &= -(\Gamma/2 - i\Delta_a)\langle\sigma_m^-\rangle + ig(x_m,y_m)\langle a\rangle(2\langle\sigma_m^+\sigma_m^-\rangle - 1) + i\Omega\cos(ky_m)(2\langle\sigma_m^+\sigma_m^-\rangle - 1) \\
\frac{d}{dt}\langle a^\dagger a\rangle &= -\kappa\langle a^\dagger a\rangle + i\sum_j g(x_j,y_j)(\langle a\sigma_j^+\rangle - \langle a^\dagger\sigma_j^-\rangle) \\
\frac{d}{dt}\langle a\sigma_m^+\rangle &= -(\frac{\kappa+\Gamma}{2} + i\Delta_a - i\Delta_c)\langle a\sigma_m^+\rangle + ig(x_m,y_m)(\langle a^\dagger a\rangle - 2\langle a^\dagger a\rangle\langle\sigma_m^+\sigma_m^-\rangle - \langle\sigma_m^+\sigma_m^-\rangle) \\
&\quad - i\sum_{j;m\neq j} g(x_j,y_j)\langle\sigma_m^+\sigma_j^-\rangle - i\Omega\cos(ky_m)\langle a\rangle(2\langle\sigma_m^+\sigma_m^-\rangle - 1) \\
\frac{d}{dt}\langle\sigma_m^+\sigma_m^-\rangle &= -\Gamma\langle\sigma_m^+\sigma_m^-\rangle - ig(x_m,y_m)(\langle a\sigma_m^+\rangle - \langle a^\dagger\sigma_m^-\rangle) - i\Omega\cos(ky_m)(\langle\sigma_m^+\rangle - \langle\sigma_m^-\rangle) \\
\frac{d}{dt}\langle\sigma_m^+\sigma_j^-\rangle &= -\Gamma\langle\sigma_m^+\sigma_j^-\rangle - ig(x_m,y_m)\langle a^\dagger\sigma_j^-\rangle(2\langle\sigma_m^+\sigma_m^-\rangle - 1) + ig(x_j,y_j)\langle a\sigma_m^+\rangle(2\langle\sigma_j^+\sigma_j^-\rangle - 1) \\
&\quad + i\Omega\cos(ky_j)\langle\sigma_m^+\rangle(2\langle\sigma_j^+\sigma_j^-\rangle - 1) - i\Omega\cos(ky_m)\langle\sigma_j^-\rangle(2\langle\sigma_m^+\sigma_m^-\rangle - 1) \\
\frac{d}{dt}\langle x_m\rangle &= 2\omega_r\langle p_{xm}\rangle/k^2 \\
\frac{d}{dt}\langle y_m\rangle &= 2\omega_r\langle p_{ym}\rangle/k^2 \\
\frac{d}{dt}\langle p_{xm}\rangle &= 2gk\sin(kx_m)e^{-y_m^2/w_0^2}\Re\{\langle a\sigma_m^+\rangle\} \\
\frac{d}{dt}\langle p_{ym}\rangle &= \frac{4g}{w_0^2}\cos(kx_m)y_m e^{-y_m^2/w_0^2}\Re\{\langle a\sigma_m^+\rangle\} + 2k\Omega\sin(ky_m)\Re\{\langle\sigma_m^+\rangle\},
\end{aligned} \tag{7.8}$$

where $m = 1..N$, $g(x_m,y_m) = g\cos\left(k\langle x_m\rangle\right)e^{-\langle y_m\rangle^2/w_0^2}$, and $\Re\{\langle\mathcal{O}\rangle\}$ is used to denote the real part of an expectation value of an operator. The resulting solution gives us the time evolution of the atomic positions and momenta, as well as the mean intracavity photon number $\langle a^\dagger a\rangle$ and the population inversion $\langle\sigma_z\rangle = \langle\sigma^+\sigma^-\rangle - \langle\sigma^-\sigma^+\rangle$, which are shown in fig. 7.2 for $N = 100$ atoms. We can plot the atomic trajectories in the final stage of the dynamics to show the emerging checkerboard pattern in the self-organization regime, as presented in fig. 7.3.

In fig. 7.4 we calculate the time-averaged order parameter and mean photon number

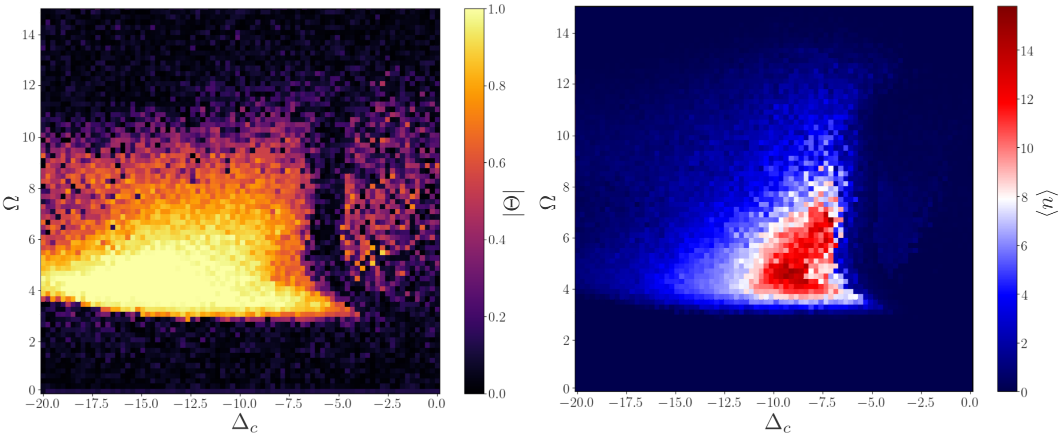

Figure 7.4: *Self-Organization (Laser Drive).* Absolute value of the order parameter (left) and mean photon number (right) scans for $N = 100$ atoms depending on the cavity detuning (Δ_c) and driving strength (Ω). Parameters: $\kappa = 10\Gamma$, $g = 1.5\Gamma$, $\Delta_a = -20\Gamma$, $w_0 = 1000\lambda$, $\omega_r = 1\Gamma$.

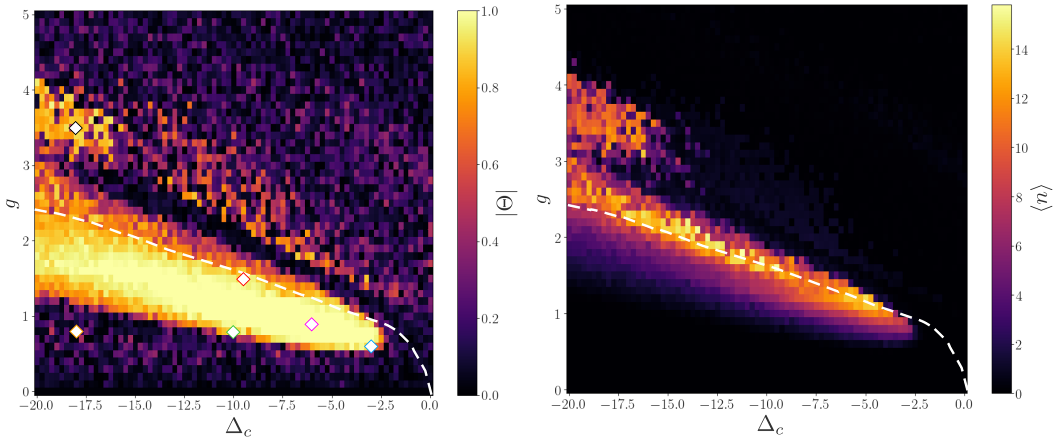

Figure 7.5: *Self-Organization (Cavity Coupling).* Absolute value of the order parameter (left) and mean photon number (right) for $N = 100$ atoms depending on the cavity detuning (Δ_c) and atom-cavity coupling strength (g). Parameters: $\kappa = 10\Gamma$, $\Omega = 5\Gamma$, $\Delta_a = -20\Gamma$, $w_0 = 1000\lambda$, $\omega_r = 1\Gamma$. The white dashed line indicates the zeros of the effective cavity detuning calculated at each point according to eq. (7.5). White rhombus markers show different parameter sets used in fig. 7.7 for the calculation of the cavity field spectra.

in the cavity mode during the final stage of the dynamics as a function of the cavity detuning and the driving strength. In order to obtain a comprehensive parameter scan we restrict ourselves to the first-order cumulant expansion (mean-field solution), which does not allow for calculating the spectral properties of the light field but substantially reduces the number of equations in eqs. (7.8). Both the second-order and the mean-field solution are in good agreement with each other as well as with the full master equation solution for small atom numbers. Above the pumping threshold one can observe self-ordering, where particles organize in a regular checkerboard pattern characterized by the order parameter

$$\Theta = \frac{1}{N} \sum_{i=1}^{N} \cos(\langle kx_i \rangle) \cos(\langle ky_i \rangle) \longrightarrow \pm 1 \tag{7.9}$$

corresponding to one of the two possible realizations of the checkerboard. Increasing the driving strength further towards saturation leads to cavity heating and the expulsion of atoms from the cavity. Therefore, in the following we choose an intermediate optimal value of the driving Rabi frequency and present the scan over the atom-cavity coupling strength for $\Omega = 5\Gamma$ in fig. 7.5. The white dashed line indicates the zeros of the effective cavity detuning in eq. (7.5) calculated at each point of the parameter scan. Across the line, the effective cavity detuning changes its sign and becomes positive resulting in cavity heating. White rhombus markers indicate different parameter choices used for the calculation of the cavity field spectra shown in fig. 7.7, which is discussed in the following section.

In fig. 7.6 we present the expectation value of the kinetic energy per atom,

$$\langle E_{kin} \rangle = \frac{1}{N} \sum_{i=1}^{N} \frac{\langle p_{xi} \rangle^2}{2m} + \frac{\langle p_{yi} \rangle^2}{2m} \tag{7.10}$$

averaged over time during the final stage of the atomic dynamics. One can clearly see the sharp transition between the atomic cooling and heating regimes. However, this transition happens significantly further away than one would expect from the zeroes of the effective cavity detuning indicated by the white dashed line. In the upper left region of the plot, where the cavity frequency approaches the atomic frequency, one can observe an extended region of cavity cooling and self-organization. Here, the cavity field as well as the atomic dynamics become more noisy but ordering persists.

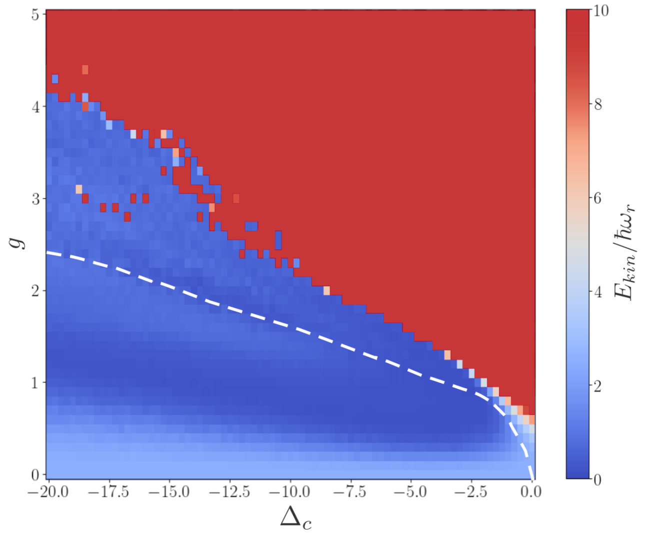

Figure 7.6: *Cavity Cooling.* Kinetic energy in eq. (7.10) presented as a function of the cavity detuning (Δ_c) and atom-cavity coupling strength (g). The kinetic energy upper limit is set to $10\hbar\omega_r$ for a better resolution in the cooling region. The parameters are the same as in fig. 7.5 with the white dashed line indicating the zeros of the effective cavity detuning.

7.3 Cavity output spectrum

Even in the regime when the system dynamics has stabilized to a quasi-stationary state, the atomic motion creates additional fluctuations of the photon number around its average value. These fluctuations are significant for a small number of particles in the simulation but become less pronounced the larger the atom number is. In order to find the spectrum we make use of the quantum regression theorem [57] and calculate the first-order correlation function $g^{(1)}(\tau) = \langle a^\dagger(t_0+\tau)a(t_0)\rangle$. According to the Wiener-Khinchin theorem [58] the spectrum can be found as the Fourier transform of the first-order correlation function,

$$S(\omega) = 2\Re\left\{\int_0^\infty d\tau e^{-i\omega\tau} g^{(1)}(\tau)\right\}. \tag{7.11}$$

We examine the cavity output spectrum at each point of the scan in fig. 7.5 searching for narrow emission or lasing close to the bare atomic transition frequency with a particular interest in the region around self-organization. We use the second-order cumulant approach in eqs. (7.8) combined with the equations for the dynamics of the

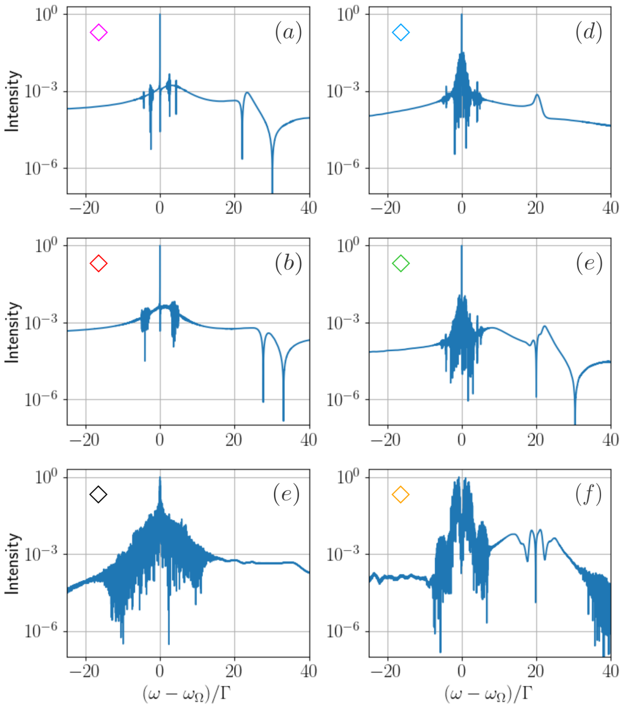

Figure 7.7: *Spectra.* Normalized spectral distribution of the cavity output field for $N = 100$ atoms in different parameter regions depicted by white rhombus markers in fig. 7.5. An increased spectral intensity and a very narrow dip in the spectrum appear in the vicinity of the bare atomic transition frequency close to the self-organization threshold. Parameters: (a) $\Delta_c = -6\Gamma$, $g = 0.9\Gamma$; (b) $\Delta_c = -9.5\Gamma$, $g = 1.5\Gamma$; (c) $\Delta_c = -18\Gamma$, $g = 3.5\Gamma$; (d) $\Delta_c = -3\Gamma$, $g = 0.6\Gamma$; (e) $\Delta_c = -10\Gamma$, $g = 0.8\Gamma$; (f) $\Delta_c = -18\Gamma$, $g = 0.8\Gamma$, $\kappa = 10\Gamma$, $\Omega = 5\Gamma$, $\Delta_a = -20\Gamma$, $w_0 = 1000\lambda$, $\omega_r = 1\Gamma$.

first-order correlation function in order to compute the spectrum [94]. In fig. 7.7 we present the spectra of the cavity light field for an ensemble of $N = 100$ atoms obtained for different parameter sets indicated by white rhombus markers in fig. 7.5.

In the ordered regime, a coherent peak at the pump frequency is dominant in the spectra, accompanied by motional broadening. In the case of perfect ordering presented in the spectrum in fig. 7.7(a), one can resolve the motional sideband peaks as all atoms in the ensemble oscillate around their trapping positions in the same way. Additionally, in fig. 7.7(b) we present the spectrum in the area of the maximal photon number given in fig. 7.4 for $g = 1.5\Gamma$. Above the main region of the self-organization, both the cavity field and atomic dynamics become rather noisy. Here, we do not

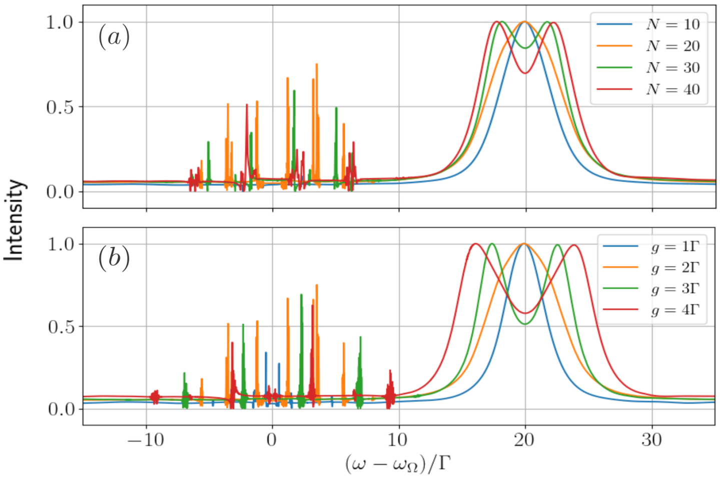

Figure 7.8: *Filter Cavity Mode Spectra.* (a) Spectra of the filter cavity mode output for a coupling strength $g = 2\Gamma$ and different atom numbers N. (b) Same as above for varying coupling strength g and $N = 20$ atoms. The operating parameters are: $\kappa = 10\Gamma$, $\Omega = 5\Gamma$, $\Delta_a = \Delta_{c2} = -20\Gamma$, $\Delta_c = -10\Gamma$, $w_0 = 1000\lambda$, $\omega_r = 1\Gamma$.

observe any spectral features close to the atomic frequency even in the extended region of self-organization, as shown in fig. 7.7(c).

Of particular interest are the spectra in the parameter region where the self-ordering threshold has not been fully reached. In fig. 7.7(d)-(f) we observe an increased spectral intensity close to the atomic transition frequency, which we associate with the emission from the excited atomic fraction. Because the atoms in this region are not perfectly ordered, they undergo complex dynamics as they continue to move, oscillate, and jump from one field antinode to another. Note, that the dipole light force has the opposite sign depending on the atomic state. Thus, in case of the red-detuned laser drive, the ground-state atoms are drawn to the field maxima whereas the excited-state atoms are expelled from these regions. In this case, the excited atoms can subsequently move through the field minima and emit photons that will be visible in the spectrum near the bare atomic frequency. Moreover, in fig. 7.7(e)-(f), we find that the spectra reveal a narrow absorption minimum at the atomic frequency, which can be associated with the atomic antiresonance [136, 137]. In the self-organization regime, the position of this minimum becomes shifted above the bare atomic frequency. We attribute this to the energy light shifts that atoms experience being trapped around the field antinodes.

Along with the main cosine mode of the cavity it is interesting to study the spectra when we introduce an additional sine mode into the system resonant to the atomic transition frequency. This sine mode will play the role of a filter for the light coming from the atoms. Interesting behavior occurs when the atoms are close to but not quite in the self-organization regime as they not only oscillate around their position as in fig. 7.3 but can jump from one antinode of the field to another, thereby increasing the emission probability into the sine mode. Of course, there is much less light going into the filter mode than there is light in the main mode of the cavity.

The second mode makes the simulation for the spectra much more computationally demanding substantially increasing the amount of equations in the system described by the Hamiltonian

$$H' = H - \Delta_{c2} b^\dagger b + \sum_{i=1}^{N} g \sin(kx_i) e^{-y_i^2/w_0^2} (b\sigma_i^+ + b^\dagger \sigma_i^-), \tag{7.12}$$

where $\Delta_{c2} = \omega_\Omega - \omega_{c2}$ and $b^\dagger$, b are the photon creation and annihilation operators in the second cavity mode. In fig. 7.8(a) we fix the cavity coupling strength to $g = 2\Gamma$ and increase the atom number up to $N = 40$ atoms. One can observe the normal mode splitting when the condition $g\sqrt{N} > \kappa$ is fulfilled. Similarly, fixing the number of atoms and changing the coupling constant leads to a splitting in spectra depicted in fig. 7.8(b).

7.4 Conclusions

In this work, we have studied spatial self-organization and spectral properties of the emitted light in a transversely driven clock atom ensemble coupled to a linear Fabry-Perot optical cavity. Our simulations demonstrate that cavity cooling and atomic self-ordering via collective scattering also appear in the bad-cavity limit where the atomic linewidth is much smaller than the cavity linewidth and of the order of the recoil frequency. Under a strong drive, state-dependent light forces induced by the driving laser and the light scattered into the cavity allow for the atoms to acquire excited state population while subsequently moving through the field's minima. In the self-organization regime, a dominant spectral peak in the cavity output stems from coherent light scattering at the pump frequency and is surrounded by motional sidebands. When the self-organization threshold has not been fully reached, we observe an increased spectral intensity as well as a narrow antiresonance close to the unperturbed atomic transition frequency, which can be useful for clock spectroscopy. Finally, in order to provide for a continuous frequency reference, the light coming from the excited atomic fraction can be filtered via a second cavity mode spatially shifted by a quarter wavelength and tuned to the bare atomic transition frequency. We anticipate that this will lead to laser-like emission for sufficiently large ensembles, which, unfortunately, goes beyond our simulation capabilities, but is readily available in experiment [44].

Data availability

Numerical simulations were performed with the open-source framework Differentialequations.jl [81] and QuantumOptics.jl [125] in the Julia programming language. The graphs were produced using the Matplotlib library [83]. All raw data are openly available at *https://doi.org/10.5281/zenodo.12796758*.

Acknowledgments

We would like to thank Vera Schäfer for helpful discussions and her comments on the manuscript. We acknowledge funding from the L'ORÃAL Austria Fellowship "For Women in Science" 2023 (A.B.) and the FET OPEN Network Cryst3 funded by the European Union (EU) via Horizon 2020 (L.O., H.R.). This work was also financed with funds from the state of Tyrol (A.B., L.O.).

8 Conclusions and Outlook

In this thesis, I theoretically investigated collective dynamics and lasing in active optical atomic clocks based on two-level quantum emitters interacting with quantized light fields in a planar optical cavity.

The first two projects of my thesis focused on the collective superradiant emission of coherent light in an ensemble of clock atoms subjected to inhomogeneous broadening effects. The inhomogeneity is primarily associated with a distribution of the atomic resonance frequencies among the ensemble. This effect can lead to a disruption of the collective interaction between the atoms. Here, we showed that strong optical pumping can induce synchronization of the atomic dipoles over a large bandwidth, provided that the critical atom number is reached. We saw that including a variation of the atom-cavity coupling among the ensemble only presented itself as a scaling factor in the effective coupling strength and did not show a substantial difference compared to the homogeneous coupling case. We developed an extensive numerical model of clusters with various atomic parameters using the second-order cumulant expansion method, which allowed us to simulate realistic systems with a large number of atoms beyond the mean-field approach. In the following, this model provided a basis for the investigation of the spectral properties and stability of active clocks in realistic systems with inhomogeneous broadening. In this study, we identified optimal operational parameters for achieving the ultimate frequency stability of active optical clocks in the superradiant lasing regime. We showed that the spectral linewidth under optimized conditions can be smaller than the natural linewidth of the atomic transition even in the presence of moderate inhomogeneous broadening and dephasing processes.

In order to ensure continuous-wave operation in superradiant clocks, it is necessary to realize a continuous population inversion mechanism which excites the atoms. We proposed a new scenario for creating an intrinsic light force generated inversion and gain in the ensemble of coherently driven atoms inside an optical cavity. In this part, we performed extensive numerical simulations in an ensemble of a few hundred atoms, where we used the cumulant expansion approach together with the semi-classical equations of motion to investigate the atomic dynamics and spectra of the cavity light field. Here, tailored state-dependent forces were used to gather and concentrate excited-state atoms in regions of strong atom-cavity coupling while ground-state atoms were repelled. We found the optimal operating conditions between the external atomic dynamics and driving fields that provide continuous narrow-band emission close to the unperturbed atomic line, which central frequency is largely insensitive to cavity fluctuations.

Next, we extended the developed framework to study self-organization, cooling and lasing in an ensemble of clock atoms. In the bad-cavity regime, we analyzed the self-organization behavior and cavity output spectra as functions of the laser-cavity detuning and the driving strength. Of particular interest to us were the spectra in the regime where the self-ordering threshold has not been fully reached. While the atoms can jump there from one field antinode to another, we presented the conditions for the laser-like emission in the vicinity of the self-organization threshold. In the future, it could be interesting to extend this study to large atomic ensembles, which goes beyond our simulation capabilities, but is readily achievable in experiment.

Future research questions could involve the effects of dipole-dipole interactions and collisions in a dense atomic ensemble, which could lead to frequency noise and mutual interaction forces heating up the system. The quantum mechanical description of atomic motion could provide further insights into the many-body quantum dynamics. However, this would substantially increase the complexity of the problem as the Hilbert space would grow drastically. As we did not focus on a particular superradiant laser experiment, further investigations with more refined models have to be developed in collaboration with a specific experimental setup.

Bibliography

[1] N. Bohr, "I. on the constitution of atoms and molecules," *The London, Edinburgh, and Dublin Philosophical Magazine and Journal of Science*, vol. 26, no. 151, pp. 1–25, 1913.

[2] A. Einstein, "Emission and absorption of radiation in quantum theory," *Verhandlungen der Deutschen Physikalischen Gesellschaft*, vol. 18, pp. 318–323, 1916.

[3] A. Einstein, "Zur quantentheorie der strahlung," *Phys Zeit*, vol. 18, p. 121, 1917.

[4] L. d. Broglie, "Xxxv. a tentative theory of light quanta," *The London, Edinburgh, and Dublin Philosophical Magazine and Journal of Science*, vol. 47, no. 278, pp. 446–458, 1924.

[5] M. Born and P. Jordan, "Zur quantenmechanik," *Zeitschrift für Physik*, vol. 34, no. 1, pp. 858–888, 1925.

[6] W. Heisenberg, *Über quantentheoretische Umdeutung kinematischer und mechanischer Beziehungen.* Springer, 1985.

[7] E. Schrödinger, "Quantisierung als eigenwertproblem," *Annalen der physik*, vol. 385, no. 13, pp. 437–490, 1926.

[8] W. Pauli Jr, "Über das wasserstoffspektrum vom standpunkt der neuen quantenmechanik," *Zeitschrift für Physik A Hadrons and nuclei*, vol. 36, no. 5, pp. 336–363, 1926.

[9] P. A. M. Dirac, "The quantum theory of the emission and absorption of radiation," *Proceedings of the Royal Society of London. Series A, Containing Papers of a Mathematical and Physical Character*, vol. 114, no. 767, pp. 243–265, 1927.

[10] F. J. Dyson, "The radiation theories of tomonaga, schwinger, and feynman," *Physical Review*, vol. 75, no. 3, p. 486, 1949.

[11] C. Cohen-Tannoudji, J. Dupont-Roc, and G. Grynberg, *Atom-photon interactions: basic processes and applications.* John Wiley & Sons, 1998.

[12] P. Domokos, P. Horak, and H. Ritsch, "Semiclassical theory of cavity-assisted atom cooling," *Journal of Physics B: Atomic, Molecular and Optical Physics*, vol. 34, no. 2, p. 187, 2001.

[13] P. Maunz, T. Puppe, I. Schuster, N. Syassen, P. W. Pinkse, and G. Rempe, "Cavity cooling of a single atom," *Nature*, vol. 428, no. 6978, pp. 50–52, 2004.

[14] C. Genes, D. Vitali, P. Tombesi, S. Gigan, and M. Aspelmeyer, "Ground-state cooling of a micromechanical oscillator: Comparing cold damping and cavity-assisted cooling schemes," *Physical Review AâAtomic, Molecular, and Optical Physics*, vol. 77, no. 3, p. 033804, 2008.

[15] P. Domokos and H. Ritsch, "Collective cooling and self-organization of atoms in a cavity," *Physical review letters*, vol. 89, no. 25, p. 253003, 2002.

[16] H. W. Chan, A. T. Black, and V. Vuletić, "Observation of collective-emission-induced cooling of atoms in an optical cavity," *Physical review letters*, vol. 90, no. 6, p. 063003, 2003.

[17] J. Asbóth, P. Domokos, H. Ritsch, and A. Vukics, "Self-organization of atoms in a cavity field: Threshold, bistability, and scaling laws," *Physical Review A*, vol. 72, no. 5, p. 053417, 2005.

[18] M. Gross and S. Haroche, "Superradiance: An essay on the theory of collective spontaneous emission," *Physics reports*, vol. 93, no. 5, pp. 301–396, 1982.

[19] F. Mivehvar, F. Piazza, T. Donner, and H. Ritsch, "Cavity qed with quantum gases: new paradigms in many-body physics," *Advances in Physics*, vol. 70, no. 1, pp. 1–153, 2021.

[20] P. Michler, A. Kiraz, C. Becher, W. Schoenfeld, P. Petroff, L. Zhang, E. Hu, and A. Imamoglu, "A quantum dot single-photon turnstile device," *science*, vol. 290, no. 5500, pp. 2282–2285, 2000.

[21] D. Meschede, "Radiating atoms in confined space: From spontaneous emission to micromasers," *Physics Reports*, vol. 211, no. 5, pp. 201–250, 1992.

[22] D. Meiser, J. Ye, D. Carlson, and M. Holland, "Prospects for a millihertz-linewidth laser," *Physical review letters*, vol. 102, no. 16, p. 163601, 2009.

[23] T. Maier, S. Kraemer, L. Ostermann, and H. Ritsch, “A superradiant clock laser on a magic wavelength optical lattice,” *Optics express*, vol. 22, no. 11, pp. 13269–13279, 2014.

[24] J. D. Prestage, S. K. Chung, R. J. Thompson, and P. MacNeal, “Progress on small mercury ion clock for space applications,” in *2009 IEEE International Frequency Control Symposium Joint with the 22nd European Frequency and Time Forum*, pp. 54–57, IEEE, 2009.

[25] S. Reynaud, C. Salomon, and P. Wolf, “Testing general relativity with atomic clocks,” *Space science reviews*, vol. 148, pp. 233–247, 2009.

[26] A. Derevianko, K. Gibble, L. Hollberg, N. R. Newbury, C. Oates, M. S. Safronova, L. C. Sinclair, and N. Yu, “Fundamental physics with a state-of-the-art optical clock in space,” *Quantum Science and Technology*, vol. 7, no. 4, p. 044002, 2022.

[27] J. D. Prestage and G. L. Weaver, “Atomic clocks and oscillators for deep-space navigation and radio science,” *Proceedings of the IEEE*, vol. 95, no. 11, pp. 2235–2247, 2007.

[28] C. J. Kennedy, E. Oelker, J. M. Robinson, T. Bothwell, D. Kedar, W. R. Milner, G. E. Marti, A. Derevianko, and J. Ye, “Precision metrology meets cosmology: improved constraints on ultralight dark matter from atom-cavity frequency comparisons,” *Physical Review Letters*, vol. 125, no. 20, p. 201302, 2020.

[29] S. Lea, “Limits to time variation of fundamental constants from comparisons of atomic frequency standards,” *Reports on Progress in Physics*, vol. 70, no. 9, p. 1473, 2007.

[30] R. Bondarescu, M. Bondarescu, G. Hetényi, L. Boschi, P. Jetzer, and J. Balakrishna, “Geophysical applicability of atomic clocks: direct continental geoid mapping,” *Geophysical Journal International*, vol. 191, no. 1, pp. 78–82, 2012.

[31] T. Mehlstäubler, G. Grosche, C. Lisdat, P. Schmidt, and H. Denker, “Atomic clocks for geodesy,” *arXiv preprint arXiv:1803.01585*, 2018.

[32] D. B. Newell, E. Tiesinga, *et al.*, “The international system of units (si),” *NIST Special Publication*, vol. 330, pp. 1–138, 2019.

[33] F. Riehle, *Frequency standards: basics and applications.* John Wiley & Sons, 2006.

[34] H. Katori, M. Takamoto, V. PalâChikov, and V. Ovsiannikov, "Ultrastable optical clock with neutral atoms in an engineered light shift trap," *Physical Review Letters*, vol. 91, no. 17, p. 173005, 2003.

[35] E. D. Black, "An introduction to pound–drever–hall laser frequency stabilization," *American journal of physics*, vol. 69, no. 1, pp. 79–87, 2001.

[36] N. Picqué and T. W. Hänsch, "Frequency comb spectroscopy," *Nature Photonics*, vol. 13, no. 3, pp. 146–157, 2019.

[37] E. Oelker, R. Hutson, C. Kennedy, L. Sonderhouse, T. Bothwell, A. Goban, D. Kedar, C. Sanner, J. Robinson, G. Marti, D. Matei, T. Legero, M. Giunta, R. Holzwarth, F. Riehle, U. Sterr, and J. Ye, "Demonstration of $4.8 \times 10^{\hat{a}17}$ stability at 1 s for two independent optical clocks," *Nature Photonics*, vol. 13, pp. 714–719, 10 2019.

[38] M. Notcutt, L.-S. Ma, A. D. Ludlow, S. M. Foreman, J. Ye, and J. L. Hall, "Contribution of thermal noise to frequency stability of rigid optical cavity via hertz-linewidth lasers," *Physical Review A*, vol. 73, no. 3, p. 031804, 2006.

[39] H. M. Goldenberg, D. Kleppner, and N. Ramsey, "Atomic hydrogen maser," *Physical Review Letters*, vol. 5, no. 8, p. 361, 1960.

[40] J. G. Bohnet, Z. Chen, J. M. Weiner, D. Meiser, M. J. Holland, and J. K. Thompson, "A steady-state superradiant laser with less than one intracavity photon," *Nature*, vol. 484, no. 7392, pp. 78–81, 2012.

[41] M. A. Norcia and J. K. Thompson, "Cold-strontium laser in the superradiant crossover regime," *Physical Review X*, vol. 6, no. 1, p. 011025, 2016.

[42] C.-C. Chen, R. González Escudero, J. Minář, B. Pasquiou, S. Bennetts, and F. Schreck, "Continuous bose–einstein condensation," *Nature*, vol. 606, no. 7915, pp. 683–687, 2022.

[43] S. L. Kristensen, E. Bohr, J. Robinson-Tait, T. Zelevinsky, J. W. Thomsen, and J. H. Müller, "Subnatural linewidth superradiant lasing with cold sr 88 atoms," *Physical Review Letters*, vol. 130, no. 22, p. 223402, 2023.

[44] V. Schäfer, Z. Niu, J. Cline, D. Young, E. Song, H. Ritsch, and J. Thompson, "Continuous momentum state lasing and cavity frequency-pinning with laser-cooled strontium atoms," *arXiv preprint arXiv:2405.20952*, 2024.

[45] F. Famà, S. Zhou, B. Heizenreder, M. Tang, S. Bennetts, S. B. Jäger, S. A. Schäffer, and F. Schreck, "Continuous cavity-qed with an atomic beam," *arXiv preprint arXiv:2407.18668*, 2024.

[46] R. H. Dicke, "Coherence in spontaneous radiation processes," *Physical review*, vol. 93, no. 1, p. 99, 1954.

[47] T. Laske, H. Winter, and A. Hemmerich, "Pulse delay time statistics in a superradiant laser with calcium atoms," *Physical review letters*, vol. 123, no. 10, p. 103601, 2019.

[48] S. A. Schäffer, M. Tang, M. R. Henriksen, A. A. Jørgensen, B. T. Christensen, and J. W. Thomsen, "Lasing on a narrow transition in a cold thermal strontium ensemble," *Physical Review A*, vol. 101, no. 1, p. 013819, 2020.

[49] D. A. Steck, "Quantum and atom optics," 2007.

[50] E. T. Jaynes and F. W. Cummings, "Comparison of quantum and semiclassical radiation theories with application to the beam maser," *Proceedings of the IEEE*, vol. 51, no. 1, pp. 89–109, 1963.

[51] H.-P. Breuer and F. Petruccione, *The theory of open quantum systems.* OUP Oxford, 2002.

[52] C. A. Brasil, F. F. Fanchini, and R. d. J. Napolitano, "A simple derivation of the lindblad equation," *Revista Brasileira de Ensino de Física*, vol. 35, pp. 01–09, 2013.

[53] C. Hotter, "Collective quantum dynamics for large ensembles of clock atoms in optical cavities," *[Doctoral thesis, University of Innsbruck]*, 2023.

[54] A. L. Schawlow and C. H. Townes, "Infrared and optical masers," *Physical review*, vol. 112, no. 6, p. 1940, 1958.

[55] G. A. Kazakov, S. Dubey, A. Bychek, U. Sterr, M. Bober, and M. Zawada, "Ultimate stability of active optical frequency standards," *Physical Review A*, vol. 106, no. 5, p. 053114, 2022.

[56] R. Kubo, "Generalized cumulant expansion method," *Journal of the Physical Society of Japan*, vol. 17, no. 7, pp. 1100–1120, 1962.

[57] H. J. Carmichael, *Statistical methods in quantum optics 1: master equations and Fokker-Planck equations.* Springer Science & Business Media, 2013.

[58] R. R. Puri, *Mathematical methods of quantum optics*, vol. 79. Springer Science & Business Media, 2001.

[59] R. Bonifacio, P. Schwendimann, and F. Haake, "Quantum statistical theory of superradiance. i," *Physical Review A*, vol. 4, no. 1, p. 302, 1971.

[60] F. Haake, M. I. Kolobov, C. Fabre, E. Giacobino, and S. Reynaud, "Superradiant laser," *Physical review letters*, vol. 71, no. 7, p. 995, 1993.

[61] M. G. Benedict, *Super-radiance: Multiatomic coherent emission.* CRC Press, 1996.

[62] M. O. Scully and A. A. Svidzinsky, "The super of superradiance," *Science*, vol. 325, no. 5947, pp. 1510–1511, 2009.

[63] J. Chen, "Active optical clock," *Chinese Science Bulletin*, vol. 54, no. 3, pp. 348–352, 2009.

[64] D. Meiser and M. Holland, "Steady-state superradiance with alkaline-earth-metal atoms," *Physical Review A*, vol. 81, no. 3, p. 033847, 2010.

[65] Y. Zhang, Y.-X. Zhang, and K. Mølmer, "Monte-carlo simulations of superradiant lasing," *New Journal of Physics*, vol. 20, no. 11, p. 112001, 2018.

[66] K. Debnath, Y. Zhang, and K. Mølmer, "Lasing in the superradiant crossover regime," *Physical Review A*, vol. 98, no. 6, p. 063837, 2018.

[67] C. Hotter, D. Plankensteiner, L. Ostermann, and H. Ritsch, "Superradiant cooling, trapping, and lasing of dipole-interacting clock atoms," *Optics express*, vol. 27, no. 22, pp. 31193–31206, 2019.

[68] A. Gogyan, G. Kazakov, M. Bober, and M. Zawada, "Characterisation and feasibility study for superradiant lasing in 40 ca atoms," *Optics express*, vol. 28, no. 5, pp. 6881–6892, 2020.

[69] A. Shankar, J. T. Reilly, S. B. Jäger, and M. J. Holland, "Subradiant-to-subradiant phase transition in the bad cavity laser," *arXiv preprint arXiv:2103.07402*, 2021.

[70] Q. Wu, Y. Zhang, X. Yang, S.-L. Su, C. Shan, and K. Mølmer, "A superradiant maser with nitrogen-vacancy center spins," *Science China Physics, Mechanics & Astronomy*, vol. 65, no. 1, p. 217311, 2022.

[71] M. A. Norcia, M. N. Winchester, J. R. Cline, and J. K. Thompson, "Superradiance on the millihertz linewidth strontium clock transition," *Science advances*, vol. 2, no. 10, p. e1601231, 2016.

[72] C.-C. Chen, S. Bennetts, R. G. Escudero, B. Pasquiou, F. Schreck, *et al.*, "Continuous guided strontium beam with high phase-space density," *Physical Review Applied*, vol. 12, no. 4, p. 044014, 2019.

[73] M. Tang, S. A. Schäffer, A. A. Jørgensen, M. R. Henriksen, B. T. Christensen, J. H. Müller, and J. W. Thomsen, "Cavity-immune features in the spectra of superradiant crossover laser pulses," *arXiv preprint arXiv:2104.13305*, 2021.

[74] K. Numata, A. Kemery, and J. Camp, "Thermal-noise limit in the frequency stabilization of lasers with rigid cavities," *Physical review letters*, vol. 93, no. 25, p. 250602, 2004.

[75] H. Liu, S. B. Jäger, X. Yu, S. Touzard, A. Shankar, M. J. Holland, and T. L. Nicholson, "Rugged mhz-linewidth superradiant laser driven by a hot atomic beam," *Physical Review Letters*, vol. 125, no. 25, p. 253602, 2020.

[76] S. B. Jäger, H. Liu, A. Shankar, J. Cooper, and M. J. Holland, "Regular and bistable steady-state superradiant phases of an atomic beam traversing an optical cavity," *Physical Review A*, vol. 103, no. 1, p. 013720, 2021.

[77] M. A. Norcia, A. W. Young, W. J. Eckner, E. Oelker, J. Ye, and A. M. Kaufman, "Seconds-scale coherence in a tweezer-array optical clock," *arXiv preprint arXiv:1904.10934*, 2019.

[78] K. Debnath, Y. Zhang, and K. Mølmer, "Collective dynamics of inhomogeneously broadened emitters coupled to an optical cavity with narrow linewidth," *Physical Review A*, vol. 100, no. 5, p. 053821, 2019.

[79] M. Xu, D. A. Tieri, E. Fine, J. K. Thompson, and M. J. Holland, "Synchronization of two ensembles of atoms," *Physical review letters*, vol. 113, no. 15, p. 154101, 2014.

[80] A. Bychek, "Clusters," *https://doi.org/10.5281/zenodo.4916393*, 2021.

[81] C. Rackauckas and Q. Nie, "Differentialequations. jl–a performant and feature-rich ecosystem for solving differential equations in julia," *Journal of Open Research Software*, vol. 5, no. 1, 2017.

[82] D. Plankensteiner, C. Hotter, and H. Ritsch, "Quantumcumulants. jl: A julia framework for generalized mean-field equations in open quantum systems," *Quantum*, vol. 6, p. 617, 2022.

[83] J. D. Hunter, "Matplotlib: A 2D graphics environment," *Computing in Science & Engineering*, vol. 9, no. 3, pp. 90–95, 2007.

[84] B. Zhu, J. Schachenmayer, M. Xu, F. Herrera, J. G. Restrepo, M. J. Holland, and A. M. Rey, "Synchronization of interacting quantum dipoles," *New Journal of Physics*, vol. 17, no. 8, p. 083063, 2015.

[85] A. Bychek, "Superradiant laser figures," *Figshare*, https://doi.org/10.6084/m9.figshare.15321819.v1, 2021.

[86] A. D. Ludlow, M. M. Boyd, J. Ye, E. Peik, and P. O. Schmidt, "Optical atomic clocks," *Rev. Mod. Phys.*, vol. 87, pp. 637–701, Jun 2015.

[87] J. Chen, "Active optical clock," *Chinese Science Bulletin*, vol. 54, pp. 348–352, Feb 2009.

[88] G. A. Kazakov and T. Schumm, "Active optical frequency standards using cold atoms: Perspectives and challenges," in *2014 European Frequency and Time Forum (EFTF)*, pp. 411–414, 2014.

[89] G. A. Kazakov and T. Schumm, "Active optical frequency standard using sequential coupling of atomic ensembles," *Phys. Rev. A*, vol. 87, p. 013821, Jan 2013.

[90] M. C. Teich and R. Y. Yen, "On the signalâtoânoise ratio for optical heterodyne detection," *J. Appl. Phys.*, vol. 43, no. 5, pp. 2480–2481, 1972.

[91] E. Rubiola, "On the measurement of frequency and of its sample variance with high-resolution counters," *Rev. Sci. Instrum.*, vol. 76, p. 054703, 2005.

[92] S. T. Dawkins, J. J. McFerran, and A. N. Luiten, "Considerations on the measurement of the stability of oscillators with frequency counters," *IEEE Trans. Ultrason. Ferroelectr. Freq. Control*, vol. 54, pp. 918–925, 2007.

[93] C. Hotter, D. Plankensteiner, G. Kazakov, and H. Ritsch, "Continuous multi-step pumping of the optical clock transition in alkaline-earth atoms with minimal perturbation," *Optics Express*, vol. 30, no. 4, pp. 5553–5568, 2022.

[94] A. Bychek, C. Hotter, D. Plankensteiner, and H. Ritsch, "Superradiant lasing in

inhomogeneously broadened ensembles with spatially varying coupling," *Open Research Europe*, vol. 1, no. 73, 2021.

[95] G. A. Kazakov and T. Schumm, "Stability analysis for bad cavity lasers using inhomogeneously broadened spin-1/2 atoms as a gain medium," *Phys. Rev. A*, vol. 95, p. 023839, Feb 2017.

[96] J. A. Muniz, D. J. Young, J. R. K. Cline, and J. K. Thompson, "Cavity-QED measurements of the ^{87}Sr millihertz optical clock transition and determination of its natural linewidth," *Phys. Rev. Research*, vol. 3, p. 023152, May 2021.

[97] S. G. Porsev and A. Derevianko, "Hyperfine quenching of the metastable $^3p_{0,2}$ states in divalent atoms," *Phys. Rev. A*, vol. 69, p. 042506, Apr 2004.

[98] A. Gogyan, G. Kazakov, M. Bober, and M. Zawada, "Characterisation and feasibility study for superradiant lasing in 40ca atoms," *Opt. Express*, vol. 28, pp. 6881–6892, Mar 2020.

[99] S. Dörscher, R. Schwarz, A. Al-Masoudi, S. Falke, U. Sterr, and C. Lisdat, "Lattice-induced photon scattering in an optical lattice clock," *Phys. Rev. A*, vol. 97, p. 063419, Feb. 2018.

[100] P. Lemonde and P. Wolf, "Optical lattice clock with atoms confined in a shallow trap," *Phys. Rev. A*, vol. 72, p. 033409, Sep 2005.

[101] R. B. Hutson, A. Goban, G. E. Marti, L. Sonderhouse, C. Sanner, and J. Ye, "Engineering quantum states of matter for atomic clocks in shallow optical lattices," *Phys. Rev. Lett.*, vol. 123, p. 123401, Sep 2019.

[102] G. J. Dick, "Local oscillator induced instabilities in trapped ion frequency standards," in *Proceedings of* 19^{th} *Annu. Precise Time and Time Interval Meeting, Redendo Beach, 1987*, (Washington, DC), pp. 133–147, U.S. Naval Observatory, 1988.

[103] M. Schioppo, R. C. Brown, W. F. McGrew, N. Hinkley, R. J. Fasano, K. Beloy, T. H. Yoon, G. Milani, D. Nicolodi, J. A. Sherman, N. B. Phillips, C. W. Oates, and A. D. Ludlow, "Ultra-stable optical clock with two cold-atom ensembles," *Nature Photonics*, vol. 11, pp. 48–52, 2017.

[104] T. Takano, M. Takamoto, I. Ushijima, N. Ohmae, T. Akatsuka, A. Yamaguchi, Y. Kuroishi, H. Munekane, B. Miyahara, and H. Katori, "Geopotential measurements with synchronously linked optical lattice clocks," *Nature Photonics*,

vol. 10, pp. 662–666, 2016.

[105] T. Bothwell, C. J. Kennedy, A. Aeppli, D. Kedar, J. M. Robinson, E. Oelker, A. Staron, and J. Ye, "Resolving the gravitational redshift across a millimetre-scale atomic sample," *Nature*, vol. 602, no. 7897, pp. 420–424, 2022.

[106] M. E. Kim, W. F. McGrew, N. V. Nardelli, E. R. Clements, Y. S. Hassan, X. Zhang, J. L. Valencia, H. Leopardi, D. B. Hume, T. M. Fortier, A. D. Ludlow, and D. R. Leibrandt, "Optical coherence between atomic species at the second scale: improved clock comparisons via differential spectroscopy." arXiv:2109.09540 [physics.atom-ph], Sep 2021.

[107] S. Dörscher, A. Al-Masoudi, M. Bober, R. Schwarz, R. Hobson, U. Sterr, and C. Lisdat, "Dynamic decoupling of laser phase noise in compound atomic clocks," *Commun. Phys.*, vol. 3, p. 185, 2020.

[108] MenloSystems, "Datasheet ORS-Cubic (D-ORS-Cubic-EN 15/12/20)." online at https://www.menlosystems.com/assets/datasheets/Ultrastable_Lasers/MENLO_ORS-Cubic-D-EN_2020-12_3w.pdf, 2020. Mentioning of company names is for technical communication only and does not represent an endorsement of certain products or manufacturers.

[109] M. M. Boyd, T. Zelevinsky, A. D. Ludlow, S. Blatt, T. Zanon-Willette, S. M. Foreman, and J. Ye, "Nuclear spin effects in optical lattice clocks," *Phys. Rev. A*, vol. 76, p. 022510, 2007.

[110] M. Xu, D. A. Tieri, E. C. Fine, J. K. Thompson, and M. J. Holland, "Synchronization of two ensembles of atoms," *Phys. Rev. Lett.*, vol. 113, p. 154101, Oct 2014.

[111] G. Kazakov, S. Dubey, and A. Bychek, "Calculation of minimal attainable linewidth of a bad-cavity laser with incoherent pumping," 2022.

[112] M. A. Norcia, J. R. Cline, J. A. Muniz, J. M. Robinson, R. B. Hutson, A. Goban, G. E. Marti, J. Ye, and J. K. Thompson, "Frequency measurements of superradiance from the strontium clock transition," *Physical Review X*, vol. 8, no. 2, p. 021036, 2018.

[113] Y. Zhang, C. Shan, and K. Mølmer, "Active frequency measurement on superradiant strontium clock transitions," *Physical Review Letters*, vol. 128, no. 1, p. 013604, 2022.

[114] M. A. Weiss and F. L. Walls, "Preliminary evaluation of time scales based on hydrogen masers," *IEEE transactions on instrumentation and measurement*, vol. 45, no. 1, pp. 265–270, 1996.

[115] A. Bauch, E. Staliuniene, and G. Gomah, "A status report on time scale generation in ptb," in *2015 Joint Conference of the IEEE International Frequency Control Symposium & the European Frequency and Time Forum*, pp. 379–383, IEEE, 2015.

[116] M. Tang, S. A. Schäffer, A. A. Jørgensen, M. R. Henriksen, B. T. Christensen, J. H. Müller, and J. W. Thomsen, "Cavity-immune spectral features in the pulsed superradiant crossover regime," *Physical Review Research*, vol. 3, no. 3, p. 033258, 2021.

[117] R. G. Escudero, C.-C. Chen, S. Bennetts, B. Pasquiou, F. Schreck, *et al.*, "Steady-state magneto-optical trap of fermionic strontium on a narrow-line transition," *Physical Review Research*, vol. 3, no. 3, p. 033159, 2021.

[118] M. Tang, S. A. Schäffer, and J. H. Müller, "Prospects of a superradiant laser based on a thermal or guided beam of sr 88," *Physical Review A*, vol. 106, no. 6, p. 063704, 2022.

[119] J. R. Cline, V. M. Schäfer, Z. Niu, D. J. Young, T. H. Yoon, and J. K. Thompson, "Continuous collective strong coupling between atoms and a high finesse optical cavity," *arXiv preprint arXiv:2211.00158*, 2022.

[120] R. Takeuchi, H. Chiba, S. Okaba, M. Takamoto, S. Tsuji, and H. Katori, "Continuous outcoupling of ultracold strontium atoms combining three different traps," *Applied Physics Express*, 2023.

[121] G. Hechenblaikner, M. Gangl, P. Horak, and H. Ritsch, "Cooling an atom in a weakly driven high-q cavity," *Physical Review A*, vol. 58, no. 4, p. 3030, 1998.

[122] J. Dalibard and C. Cohen-Tannoudji, "Dressed-atom approach to atomic motion in laser light: the dipole force revisited," *JOSA B*, vol. 2, no. 11, pp. 1707–1720, 1985.

[123] M. Fox, *Quantum optics: an introduction*, vol. 15. Oxford university press, 2006.

[124] H. J. Carmichael and M. O. Scully, "Statistical methods in quantum optics 1: Master equations and fokker-planck equations," *Physics Today*, vol. 53, no. 3, p. 78, 2000.

[125] S. Krämer, D. Plankensteiner, L. Ostermann, and H. Ritsch, "Quantumoptics. jl: A julia framework for simulating open quantum systems," *Computer Physics Communications*, vol. 227, pp. 109–116, 2018.

[126] J. Zhang, T. Shi, J. Miao, D. Yu, and J. Chen, "An extremely bad-cavity laser," *arXiv preprint arXiv:2310.14240*, 2023.

[127] E. A. Bohr, S. L. Kristensen, C. Hotter, S. A. Schäffer, J. Robinson-Tait, J. W. Thomsen, T. Zelevinsky, H. Ritsch, and J. H. Müller, "Collectively enhanced ramsey readout by cavity sub-to superradiant transition," *Nature Communications*, vol. 15, no. 1, p. 1084, 2024.

[128] D. Yu, J. Zhang, S. Zhang, and J. Chen, "Prospects for an active optical clock based on cavityless lasing," *Advanced Quantum Technologies*, vol. 7, no. 2, p. 2300308, 2024.

[129] J. Ye and P. Zoller, "Essay: Quantum sensing with atomic, molecular, and optical platforms for fundamental physics," *Physical Review Letters*, vol. 132, no. 19, p. 190001, 2024.

[130] W. Niedenzu, T. Grießer, and H. Ritsch, "Kinetic theory of cavity cooling and self-organisation of a cold gas," *Europhysics Letters*, vol. 96, no. 4, p. 43001, 2011.

[131] K. Arnold, M. Baden, and M. Barrett, "Self-organization threshold scaling for thermal atoms coupled to a cavity," *Physical review letters*, vol. 109, no. 15, p. 153002, 2012.

[132] H. Ritsch, P. Domokos, F. Brennecke, and T. Esslinger, "Cold atoms in cavity-generated dynamical optical potentials," *Reviews of Modern Physics*, vol. 85, no. 2, p. 553, 2013.

[133] S. Schütz, S. B. Jäger, and G. Morigi, "Thermodynamics and dynamics of atomic self-organization in an optical cavity," *Physical Review A*, vol. 92, no. 6, p. 063808, 2015.

[134] S. B. Jäger, S. Schütz, and G. Morigi, "Mean-field theory of atomic self-organization in optical cavities," *Physical Review A*, vol. 94, no. 2, p. 023807, 2016.

[135] A. Bychek and H. Ritsch, "A superradiant two-level laser with intrinsic light force generated gain," *New Journal of Physics*, vol. 25, no. 11, p. 113010, 2023.

[136] P. Alsing, D. Cardimona, and H. Carmichael, "Suppression of fluorescence in a lossless cavity," *Physical Review A*, vol. 45, no. 3, p. 1793, 1992.

[137] C. Sames, H. Chibani, C. Hamsen, P. A. Altin, T. Wilk, and G. Rempe, "Antiresonance phase shift in strongly coupled cavity qed," *Physical Review Letters*, vol. 112, no. 4, p. 043601, 2014.

List of Publications

Publications during PhD

- A. Bychek, L. Ostermann, and H. Ritsch, "Self-Ordering, Cooling and Lasing in an Ensemble of Clock Atoms," *arXiv preprint arXiv:2407.16046* (2024).
- A. Bychek, H. Ritsch, "A superradiant two-level laser with intrinsic light force generated gain," *New Journal of Physics*, 25, 113010 (2023).
- G. A. Kazakov, S. Dubey, A. Bychek, U. Sterr, M. Bober, and M. Zawada, "Ultimate stability of active optical frequency standards," *Physical Review A*, 106(5), 053114 (2022).
- A. Bychek, C. Hotter, D. Plankensteiner, and H. Ritsch, "Superradiant lasing in inhomogeneously broadened ensembles with spatially varying coupling," *Open Research Europe*, 1:73 (2021).

Publications before PhD

- A. A. Bychek, D. N. Maksimov, and A. R. Kolovsky, "Decay of symmetry-protected quantum states," *Physical Review A*, 102(3), 033324 (2020).
- A. A. Bychek, P. S. Muraev, D. N. Maksimov, and A. R. Kolovsky, "Open Bose-Hubbard chain: Pseudoclassical approach," *Physical Review E*, 101(1), 012208 (2020).
- A. A. Bychek, P. S. Muraev, D. N. Maksimov, and A. R. Kolovsky, "Chaotic and regular dynamics in the three-site Bose-Hubbard model," *AIP Conference Proceedings*, 2241(1), 020007 (2020).
- A. A. Bychek, P. S. Muraev, D. N. Maksimov, and A. R. Kolovsky, "Probing quantum chaos in many-body quantum systems by the induced dissipation,"

Physical Review A, 100(1), 013610 (2019).

- A. A. Bychek, D. N. Maksimov, and A. R. Kolovsky, “NOON state of Bose atoms in the double-well potential via an excited-state quantum phase transition,” *Physical Review A*, 97(6), 063624 (2018).